The development of N,N,N,N-tetradentate Fe(II) complexes for alkene and alcohol oxidation

L Swartzberg

orcid.org/0000-0002-5806-5152

Dissertation submitted in partial fulfilment of the requirements for the degree *Masters of Science in Chemistry* at the North West University

Supervisor:	Dr AJ Swarts
Co-supervisor:	Prof CGCE van Sittert

Graduation May 2018

23392878

Abstract

We developed a catalyst system capable of oxidising olefinic and alcohol substrates under ambient air and at low temperatures. Our catalyst system comprises of an iron precursor in combination with a bis-heterocyclic diamine ligand set. These ligands have different steric and electronic properties, by i) varying the substituents on the pyridyl ring, and ii) varying the *N*-heterocycle.

Firstly, we prepared a series of chiral (*R,R*) bis-heterocyclic secondary diamine ligands (**L3.6** to **L3.10**; **(*R,R*)-L3.6**, heterocycle = pyridine; **(*R,R*)-L3.7**, heterocycle = 6-methyl-2-pyridine; **(*R,R*)-L3.8**, heterocycle = 6-bromo-2-pyridine; **(*R,R*)-L3.9**, heterocycle = 1-methyl-imidazole; **(*R,R*)-L3.10**, heterocycle = quinoline) and the corresponding iron(II) complexes (**C3.1** to **C3.5**; **(*R,R*)-C3.1**, heterocycle = pyridine; **(*R,R*)-C3.2**, heterocycle = 6-methyl-2-pyridine; **(*R,R*)-C3.3**, heterocycle = 6-bromo-2-pyridine; **(*R,R*)-C3.4**, heterocycle = 1-methyl-imidazole; **(*R,R*)-C3.5**, heterocycle = quinoline). Nuclear magnetic resonance (NMR, ^{1}H, ^{13}C) spectroscopy, mass spectrometry (MS) and ultraviolet-visible (UV-Vis) spectroscopy were used to characterise these ligands and complexes. These complexes were investigated as catalysts in the oxidation of *cis*-cyclooctene. All the complexes exhibited similar catalytic activity, with turnover numbers between 9.60 and 12.70, which led us to believe that the complexes have low stability. This was confirmed with electrospray ionisation (ESI) MS, which indicated the oxidative degradation of the catalysts, which leads to lower stability and subsequently lower catalytic activity.

To improve the stability, a series of chiral (*R,R*) and (*S,S*) bis-heterocyclic tertiary diamine ligands (**L4.1** to **L4.4**; **(*R,R*)** and **(*S,S*)-L4.1**, heterocycle = pyridine; **(*R,R*)** and **(*S,S*)-L4.2**, heterocycle = 6-methyl-2-pyridine; **(*R,R*)** and **(*S,S*)-L4.3**, heterocycle = 6-bromo-2-pyridine; **(*R,R*)** and **(*S,S*)-L4.4**, heterocycle = 1-methyl-imidazole) and their Fe(II)-triflate complexes (**C4.1** to **C4.4**; **(*R,R*)** and **(*S,S*)-C4.1**, heterocycle = pyridine; **(*R,R*)** and **(*S,S*)-C4.2**, heterocycle = 6-methyl-2-pyridine; **(*R,R*)** and **(*S,S*)-C4.3**, heterocycle = 6-bromo-2-pyridine; **(*R,R*)** and **(*S,S*)-C4.4**, heterocycle = 1-methyl-imidazole) was prepared. These complexes were characterised by a variety of spectroscopic and analytical techniques. These included NMR (^{1}H, ^{13}C) spectroscopy, MS, UV-Vis spectroscopy, elemental analysis and magnetic susceptibility. With the desired complexes in hand, we commenced their evaluation as catalysts in the oxidation of *cis*-cyclooctene and benzyl alcohol. Of the series of complexes evaluated, **(*R,R*)-C4.1** was able to convert 96% of *cis*-cyclooctene to cyclooctene epoxide with 100% selectivity. The addition of substituents in the 6-position of the pyridine ring had a pronounced steric effect that resulted in the complexes favouring a high-spin configuration, which led to lower catalytic activity. Replacing the pyridine donor with an imidazole donor also

displayed a steric effect, which resulted in a complex that possesses a weaker ligand field and lower catalytic activity. The addition of acetic acid to the oxidation system resulted in up to a 30% increase in the conversion. For benzyl alcohol oxidation, the highest conversion of 73% was seen when employing **(*S,S*)-C4.1**. Different parameters of the oxidation reaction were optimised, which included oxidant concentration and catalyst loading. The catalytic activity increased as the amount of H_2O_2 increased, but also resulted in over-oxidation to benzoic acid. Using 25 µmol of catalyst resulted in the highest catalytic activity. The limitations and functional group tolerance of this catalyst system were investigated by extending the alcohol substrate scope and this system was able to oxidise allylic, benzylic as well as aliphatic primary and secondary alcohols to the corresponding aldehyde and ketone products.

Keywords: alkene, alcohol, iron, non-heme, oxidation

Acknowledgements

Firstly, I would like to thank my supervisor, Dr Andrew Swarts. The door to his office was always open whenever I had a question about my research or writing. Thank you for your continuous support, enthusiasm and motivation these two years and for always being willing to help. I've learnt so much from you and I am really thankful for everything you taught me.

I would also like to acknowledge Prof Cornie van Sittert, my co-supervisor. Thank you for motivating me, reading through my dissertation and giving valuable comments.

The NRF (grant number: 103018) and NWU for the funding and making it possible for me to do my Masters degree.

The CRB for the facilities and laboratory space.

Dr Johan Jordaan at the Laboratory for Analytical Services. Thank you for the countless NMR and MS samples and that you always went out of your way to help.

I would also like to thank the supervisors and students in the Catalysis and Synthesis group. Thank you for your help in the lab and input in my project.

My sincere thanks also goes to Mrs Hestelle Stoppel for all the admin and orders. Thank you for listening and giving good advice.

My good friends, Alma and Lindie who are also doing their Masters. Thank you for your support and encouragement and that we could start and complete this together.

I would also like to thank my family for their unfailing support and continuous encouragement throughout my years of study. My sister, Emma for being there for me and listening and understanding.

My Father in Heaven for giving me the opportunity to study and for all the blessing I receive every day.

Conference contributions

Swartzberg, L.; van Sittert, CGCE.; Swarts, AJ., The development of N,N,N,N tetradentate iron(II) complexes for alkene and alcohol oxidation. CATSA, Kwa Maritane, Pilanesberg, November 2017. Poster presentation

Swartzberg, L.; van Sittert, CGCE.; Swarts, AJ., The development of N,N,N,N tetradentate iron(II) complexes for alkene and alcohol oxidation. Third South African-Romanian Scientific Workshop, Bucaharest, Romania, January 2017. Oral presentation

Swartzberg, L.; van Sittert, CGCE.; Swarts, AJ., Fe catalysed alkane and alkene oxidation: effect of steric and electronic parameters on non-heme oxygenase activity. CATSA, Champagne Sports Resort, Drakensberg, November 2016. Poster presentation

Swartzberg, L.; van Sittert, CGCE,; Swarts, AJ. Fe gekataliseerde alkeenoksidasie: effek van steriese en elektroniese parameters op nie-heemoksigenase aktiwiteit. SAAWK Studentesimposium, Potchefstroom, Oktober 2016. Oral presentation

List of abbreviations

A/K ratio	alcohol/ketone ratio
AcOH	acetic acid
BBPC	N,N′-di(phenylmethyl)- N,N′-bis(pyridinylmethyl)-1,2-cyclohexanediamine
BPMCN	N,N′-dimethyl-N,N′-bis(2-pyridylmethyl)-cyclohexane-1,2-diamine
BPMCP	N,N′-dimethyl- N,N′-bis[(*R*)-4-tert-butylphenyl(2-pyridinylmethyl)]cyclohexane-1*R*,2*R*-diamine
BPMEN	N,N′-dimethyl-N,N′-bis(2-pyridylmethyl)-ethane-1,2-diamine
BPMPN	N,N′-dimethyl-N,N′-bis(2-pyridinylmethyl)propane-1,3-diamine
BQCN	N,N′-dimethyl-N,N′-bis(8-quinolyl)cyclohexane-diamine
BQEN	N,N′-dimethyl-N,N′-bis(8-quinolyl)ethane-1,2-diamine
$BQMe_2PN$	N,N′-dimethyl-N,N′-bis(8-quinolyl)-2,2-dimethyl-propane-1,3-diamine
BQMEN	N,N′-dimethyl-N,N′-bis(8-quinolylmethyl)ethane-1,2-diamine
BQPN	N,N′-dimethyl-N,N′-bis(8-quinolyl)propane-1,3-diamine
DCM	dichloromethane
DCTB	trans-2-[3-(4-tert-Butylphenyl)-2-methyl-2-propenylidene]malononitrile
dH_2O	distilled water
ee	enantiomeric excess
equiv	equivalent
ESI-MS	electrospray ionisation mass spectrometry
GC	gas chromatography
GC-MS	gas chromatography – mass spectrometry
indH	1,3-bis(2′-pyridylimino)isodoline
KIE	kinetic isotope effect
MALDI	matrix assisted laser desorption ionisation

List of abbreviations

MCPBA	*m*-chloroperoxybenzoic acid
Me-Im	*N*-methylimidazole
MeOH	methanol
Me-picH	6-methyl-picolinate
$MgSO_4$	magnesium sulphate
nm	nanometer
NMR	nuclear magnetic resonance
OAT	oxygen-atom transfer
OTf^-	trifluoromethanesulfonate anion
PAP	1,4-di(2′-pyridyl)aminophtalazine
PDP	({(*S*)-2-[(*S*)-1-(pyridine-2-ylmethyl)pyrrolidine-2-yl]pyrrolidin-1-yl)}methyl)-pyridine
PhIO	iodosobenzene
PMCP	N,N′-dimethyl- N,N′-bis[(*R*)-phenyl(2-pyridinylmethyl)]cyclohexane-1*R*,2*R*-diamine
ppm	parts per million
py	pyridine
r.t	room temperature
SbF_6^-	hexafluoroantimonate anion
TBHP	tert-butyl hydroperoxide
TEMPO	2,2,6,6-tetramethylpiperidine-1-oxyl
TON	turnover number
TPA	tris(2-pyridylmethyl)amine
TPP	5,10,15,20-tetraphenylporphyrinato
TTP	chloro(5,10,15,20-tetra-(*o*-tolyl-porphyrinato)
UV-Vis	ultraviolet visible

Table of contents

Table of contents

List of Figures

Chapter 2: General principles, mechanism and development of various iron-based oxidation systems

Chapter 4: Evaluating (*R,R*) and (*S,S*) bis-heterocyclic tertiary diamine Fe(II) complexes in the oxidation of alkene and alcohol substrates

List of Figures

List of Schemes

Chapter 2: General principles, mechanism and development of various iron-based oxidation systems

Chapter 3: Evaluation of (*R,R*) bis-heterocyclic secondary diamine Fe(II) complexes in the oxidation of *cis*-cyclooctene

Chapter 4: Evaluating (*R,R*) and (*S,S*) bis-heterocyclic tertiary diamine Fe(II) complexes in the oxidation of alkene and alcohol substrates

List of Tables

Chapter 1

Importance and application of the oxidation of various substrates

1.1 Literature background

Carbon-heteroatom (C-X) bonds are common in organic compounds that are used as building blocks in the chemical, pharmaceutical, biological and material sciences industry.[1] Coupled to this is the need for methods to synthesise these building blocks. Currently, the focus is on transforming hydrocarbons from various sources such as petrochemicals, natural gas and oil.[2] The hydrocarbons that have encountered the most attention are alkanes and alkenes.[3] Alkanes are not that susceptible towards different chemical reactions, while alkenes show high reactivity. By transforming these alkanes and alkenes, new paths to more valuable products may emerge and these products can then be used as feedstock in different chemical processes. Products that can be formed include aldehydes, alcohols, ketones, epoxides and *cis*-diols.[4] Of particular interest are epoxides because they are a versatile class of compounds and an important building block for organic synthesis. The 1,2-diols also have a variety of applications. They are used in the fine chemical industry as a building block and in the pharmaceutical and agrochemical industry these compounds are used as intermediates.[5] Another important transformation is the oxidation of alcohols to produce the corresponding aldehydes or ketones. These products are important intermediates in different industries such as plastic additives, flavouring compounds, perfumes, pharmaceuticals and dyes.[6] Due to the different applications of these products, the focus is on finding a catalyst system capable of oxidising and functionalising a range of organic substrates.

Nature has solved the problem of selective oxidation of C-H bonds under mild conditions by using enzymes and metallo-enzymes. Metallo-enzymes are enzymes that contain transition metal ions in their active sites. Although these enzymes are very effective for oxidising substrates in the human body, they are inactive towards non-natural substrates.[7] To oxidise non-natural substrates, chemists use enzymes as a blueprint and attempt to synthesise new and efficient catalyst systems. Examples of these catalyst systems are heme and non-heme oxygenases, which are capable of selectively oxidising alkane and alkene C-H bonds and that have resulted in the development of numerous synthetic equivalents. Over the years, various metals have been investigated. Catalysts that employ precious metals such as palladium, ruthenium and rhodium were found to be effective in different applications.[8] The problems with these metals are their high price, toxicity and they are not readily available. These drawbacks resulted in a search for alternative metal catalysts that are environmentally and economically friendly. A solution may be the first row transition metals. An ideal metal to use is iron. Iron is found in large quantities in the earth's crust, it is environmentally benign and it also exists in a variety of oxidation states.[9] The combination of these characteristics makes iron a compelling candidate for use in catalysis.

Catalysts are employed for the synthesis of approximately 80% of pharmaceutical and chemical products and therefore it is important to consider all the different aspects that may have an influence on the catalyst system.[8] The central metal used as well as the structure of the surrounding ligand will have an effect on the selectivity and reactivity of the catalyst. There is an increasing need to use more environmentally friendly reaction conditions and therefore the development of an atom-, energy- and chemical-efficient oxidation process for the transformation of these alkanes, alkenes and alcohols is of utmost importance.[10] This will in turn have a positive economic influence and result in an increased supply of chemical feedstock. The current focus is on constructing new and straightforward catalyst systems that can perform these transformations. The goal is also to utilise environmentally friendly conditions, which include the use of readily available substrates and mild oxidants. Oxidants such as ambient air and hydrogen peroxide are particularly attractive because the only by-product when using hydrogen peroxide is water.[11]

Over the years, a variety of non-heme complexes have been synthesised and investigated. A problem with non-heme catalyst systems that are used in combination with H_2O_2 is low conversions and poor product selectivities. This resembles Fenton-type chemistry.[12] When highly reactive oxidants are used, this can lead to a large amount of side reactions and the formation of radicals, which influences the selectivity of the products formed. As such, the focus is on developing catalyst systems that operate via a metal-based mechanism thereby ensuring better product selectivity.

1.2 Aim of the study

As part of our research programme that is focused on the development of iron-catalysed organic transformations under benign conditions, we propose a catalyst system capable of oxidising olefinic and alcohol substrates under ambient air and at low temperatures. Our catalyst system will comprise of an iron precursor in combination with a bis-heterocyclic diamine ligand set. This will be tetradentate ligands with pyridine donors, as well as substituents on the pyridine ring. The pyridine will also be replaced with quinoline and imidazole donors. These modifications will allow for the investigation of substituent as well as heterocycle effects on the catalytic activity of the catalysts. We aim to determine what the effect different steric and electronic properties on the ligand will have on the activity seen for the catalysts as well as the effect of the ligand topology.

1.3 Objectives

The first objective is the synthesis of bis-heterocyclic diamine ligand sets, in which the diamines are both secondary and tertiary. These ligands will have different steric and

electronic properties, by i) varying the substituents on the pyridyl ring and ii) varying the *N*-heterocycle.

Thereafter, the focus will be on developing iron(II) complexes bearing these bis-heterocyclic diamine ligands. The bis-heterocyclic diamine ligand sets and their resulting iron(II) complexes will also be fully characterised by employing different spectroscopic and analytical techniques.

The next objective is to evaluate these complexes in alkene and alcohol oxidation. We will also attempt to optimise various parameters of the oxidation reaction. These include evaluating the effect of oxidant concentration, substrate concentration and carboxylic acid additives. Another goal is to evaluate how the different steric and electronic properties of the ligand affects the catalysis. The substrate scope of alcohol oxidation will also be extended and investigated to determine the efficiency of this catalyst system.

1.4 Outline of the dissertation

Chapter 2 describes the evolution of iron-based oxidation systems. This includes the enzymes that are used as mimics and heme and non-heme oxygenases that developed from these enzymes. The mechanistic aspects of heme and non-heme oxygenases will be discussed and the importance of the ligand topology will be highlighted. Different examples of these catalyst systems for the oxidation of alkane, alkene and alcohol substrates will be discussed and finally the drawbacks and selectivity issues of these non-heme complexes will be described.

In Chapter 3, the synthesis of a (*R,R*) bis-heterocyclic secondary diamine ligand set and the corresponding iron(II) complexes will be described. The iron(II) complexes, containing secondary diamines in the ligand backbone, were investigated in the oxidation of *cis*-cyclooctene. This chapter will also examine the stability of these secondary diamine-containing catalysts and the effect that the stability of the catalyst has on the catalytic activity.

Chapter 4 will focus on the synthesis and characterisation of a (*R,R*) and (*S,S*) bis-heterocyclic tertiary diamine ligand set and the corresponding iron(II) complex set. These complexes were evaluated as catalysts in the oxidation of *cis*-cyclooctene and benzyl alcohol. This chapter will describe the impact of the ligand topology as well as the influence of substituents present in the catalyst on the catalytic activity. Different reaction parameters for alcohol oxidation will be optimised and described in this chapter. The oxidation of a range of primary and secondary alcohol substrates will also be evaluated and reported.

Chapter 5 will provide concluding remarks related to the study as well as recommendations for future work.

1.5 References

1. Correa, A.; Mancheño, O. G.; Bolm, C., *Chem. Soc. Rev.*, **2008,** *37* (6), 1108-1117.
2. Derouane, E. G.; Parmon, V.; Lemos, F.; Ribeiro, F. R., *Sustainable Strategies for the Upgrading of Natural Gas: Fundamentals, Challenges, and Opportunities: Proceedings of the NATO Advanced Study Institute, held in Vilamoura, Portugal, July 6-18, 2003*. Springer Science & Business Media: 2006; Vol. 191.
3. Bordeaux, M.; Galarneau, A.; Drone, J., *Angew. Chem. Int. Ed.*, **2012,** *51* (43), 10712-10723.
4. Mac Leod, T. C.; Kirillova, M. V.; Pombeiro, A. J.; Schiavon, M. A.; Assis, M. D., *Appl. Catal., A*, **2010,** *372* (2), 191-198.
5. Bäckvall, J.E., *Modern oxidation methods*. John Wiley & Sons: 2011.
6. Zhang, S.; Miao, C.; Xu, D.; Sun, W.; Xia, C., *Chin. J. Cat.*, **2014,** *35* (11), 1864-1870.
7. Farinas, E. T.; Schwaneberg, U.; Glieder, A.; Arnold, F. H., *Adv. Synth. Catal.*, **2001,** *343* (6-7), 601-606.
8. Enthaler, S.; Junge, K.; Beller, M., *Angew. Chem. Int. Ed.*, **2008,** *47* (18), 3317-3321.
9. Haslinger, S. Bioinspired Iron N-Heterocyclic Carbene Complexes in C–H Bond Oxidation: Reactivity, Electronic Properties, and Catalytic Activity. Universität München, 2015.
10. Fernandes, R. R.; Lasri, J.; da Silva, M. F. C. G.; Da Silva, J. A.; da Silva, J. J. F.; Pombeiro, A. J., *Appl. Catal., A*, **2011,** *402* (1), 110-120.
11. Piera, J.; Bäckvall, J. E., *Angew. Chem. Int. Ed.*, **2008,** *47* (19), 3506-3523.
12. England, J.; Davies, C. R.; Banaru, M.; White, A. J.; Britovsek, G. J., *Adv. Synth. Catal.*, **2008,** *350* (6), 883-897.

Chapter 2

General principles, mechanism and development of various iron-based oxidation systems

2.1 Background

The chemical industry is constantly growing, which causes an increase in the demand for feedstock materials. To synthesise different feedstocks, the focus is on the selective transformations of hydrocarbons. The most abundant and cheapest hydrocarbons available are alkanes and alkenes, typically found in natural gas, oil as well as in biogas.[1] However, in the chemical industry, alkanes have a limited use because these hydrocarbons are relatively inert towards chemical reactions. For this reason alkane transformation reactions have received a great deal of attention to develop new routes from hydrocarbons to more valuable products. These valuable products include alcohols, aldehydes, ketones, acids and peroxides.[2] These oxygenates find widespread application as feedstocks in the pharmaceutical and chemical industry.[3] Economical and practical issues have made investigations into the oxidation of alkanes a significant research enterprise with the goal being the selective oxidative transformation of hydrocarbons.[4, 5]

In biological systems, the oxidation of alkane and alkene C-H bonds as well as O-H bonds in alcohols is a fundamental transformation required for the biosynthesis of metabolites as well as drug metabolism.[6] These oxidations are effectively and selectively carried out in nature by means of enzymes, which serves as an inspiration for chemists to be able to perform these reactions in the laboratory.

When investigating hydrocarbon oxidation, chemists use enzymes as a blueprint for the development of different catalysts. Enzymes that contain iron have an important role in electron transfer reactions and in the transport and activation of a variety of molecules.[7] These favourable features resulted in significant interest in developing oxidation catalysts that contain iron. The most well-known metallo-enzyme for oxidation reactions is Cytochrome P-450.[8] Cytochrome P-450 is classified as a heme-containing monooxygenase, capable of activating the C-H bonds of an alkane to form the corresponding alcohol or ketone product.[9] As a result of Cytochrome P-450 and other heme oxygenases being able to hydroxylate alkanes, their structural features have served as inspiration to synthesise catalysts that mimic the coordination environment of the native enzyme active site, which could reproduce this oxidation reaction. Heme oxygenase is the first class of catalysts that was investigated and is based on the active site of the Cytochrome P-450 enzyme. An important structural property of these types of catalysts is a porphyrin ring in their structure. The insight gained from Cytochrome P-450 and heme oxygenases led to the development of non-heme oxygenases that do not have a porphyrin ring in their structure. Figure 2.1 depicts the timeline of the development of different iron oxidation of substrates.

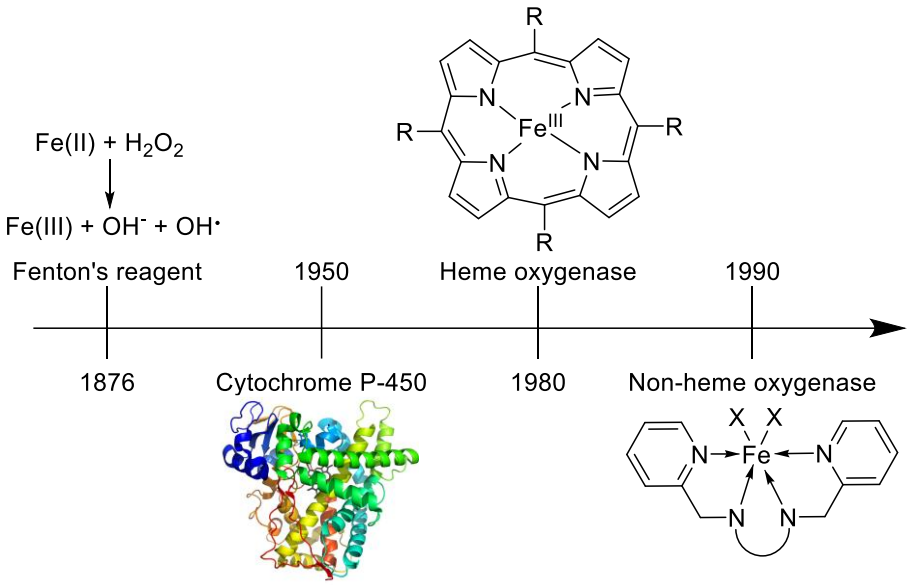

Figure 2.1: Timeline of the development of different catalyst systems for C-H oxidation.

However, before investigating catalysts for the oxidation of hydrocarbons in detail, it is important to understand the reasons for the inertness of the aliphatic C-H bond.

2.2 Factors governing the reactivity of aliphatic C-H bonds

The inertness of the aliphatic C-H bond is related to the activation energy required to break the bond. The unactivated C-H bond is a strong covalent bond, with a bond activation energy of 400 kJ.mol^{-1}.[1]

The strength of the C-H bond is mostly influenced by electronic effects and without the presence of directing groups, the electronic effects will dominate the selectivity of the oxidation reaction. Figure 2.2 indicates the effect of electron-withdrawing and other functional groups on the C-H bond. The rate of C-H bond oxidation is influenced by the presence of electron-withdrawing groups on a substrate. If there is an electron-withdrawing group on the α- or β-carbon, the reactivity of the C-H bond will decrease. As such, oxidation will take place at the position that is the most electron rich.[10, 11]

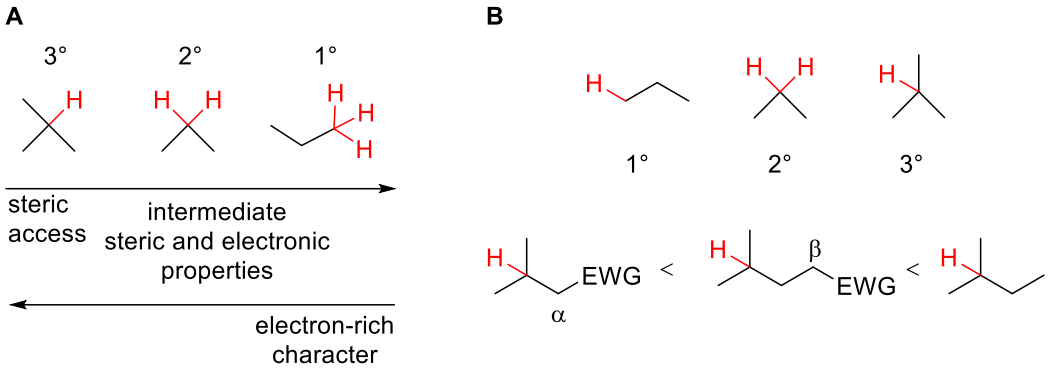

Figure 2.2: Steric and electronic properties of C-H bonds. The more electron-rich bond is more easily oxidised.[6, 11]

Additionally, directing groups may be employed to override the reactive site preference of certain substrates. This entails that the most sterically accessible and electron-rich C-H bonds are the most easily oxidised and will therefore have an influence on the selectivity of the oxidation reaction.[12] A drawback of this approach is the installation and removal of directing groups, which increases the number of synthetic manipulations that have to be done. Despite this drawback, using directing groups is a successful strategy to improve the regioselectivity of C-H oxidation reactions.[10, 13]

2.3. Evolution of iron catalysed oxidation systems

2.3.1 Fenton's reagent and related chemistry

The first system capable of oxidising organic hydrocarbons was reported by Fenton in 1876.[14] He could oxidise alkanes by using iron(II) salts with dihydrogen peroxide as oxidant in an acidic aqueous solution. Different mechanistic scenarios were proposed for this reaction, but most involved the formation of an OH• or OOH• radical (Scheme 2.1). It was also found that the course of the reaction mechanism would depend on the specific reaction conditions employed and may therefore vary from one reaction to the next.[15] Due to the high reactivity of these hydroxyl radicals, they immediately undergo several possible reactions in the presence of an organic substrate (e.g. cyclohexane), which leads to the oxidation of the substrate.[16, 17] The first reaction to take place is H_2O_2 decomposition with the formation of hydroxyl and hydroperoxo radicals, which are the active species. These radicals are usually long-lived and react with the alkane substrate to produce the oxidised product. If dioxygen is present, alkyl peroxide radicals can be formed. When two alkyl peroxide radicals combine, it results in either the formation of an equimolar amount of alcohol and ketone, through Russel-type termination,[18] as final product or the formation of alkyl hydroperoxides as the final product. An equimolar amount of alcohol and ketone is usually indicative of a Fenton-type pathway being followed.

$Fe(II) + H_2O_2 \rightarrow Fe(III) + OH^- + OH\bullet$

$Fe(III) + H_2O_2 \rightarrow Fe(II) + HOO\bullet + H^+$

H_2O_2 decomposition

$RH + OH\bullet \rightarrow H_2O + R\bullet$

$R\bullet + OH\bullet \rightarrow R\text{-}OH$

$R\bullet + HOO\bullet \rightarrow R\text{-}OOH$

Radical reactions

$R\bullet + O_2 \rightarrow ROO\bullet$

$ROO\bullet + H_2O \rightarrow R\text{-}OOH + OH\bullet$

$2\ ROO\bullet \rightarrow R\text{-}OH + R{=}O + O_2$

Termination by O_2

Scheme 2.1: Fenton-type reaction pathway. Highly reactive radicals are formed when hydrogen peroxide decomposes in the presence of Fe(II) or Fe(III). Equal amounts of ketone and alcohol can be formed in the presence of dioxygen due to the fact that a termination step of the radical reactions takes place.[16]

The presence of highly reactive hydroxyl radicals in Fenton's reagent leads to low product selectivity and this resulted in changes being made to this system so as to improve these drawbacks.[19] Researchers started to investigate enzymes that are able to oxidise C-H bonds in an attempt to improve product selectivity and be able to perform the oxidation reactions under mild reaction conditions.

2.3.2 Cytochrome P-450 and heme oxygenases

Cytochrome P-450 are a group of enzymes coordinated to iron and catalyse a wide range of important processes with high stereo- and regioselectivity in the human body and other life forms. Examples of these processes are hydrocarbon hydroxylation, alkene epoxidation, aromatic hydroxylation and many more.[1, 20] The part of the enzyme responsible for the oxidation is the active site. The active site of these enzymes is a well-defined coordination environment consisting of an iron(III) centre coordinated by a tetradentate porphyrin ligand (Figure 2.3). This iron active centre can form complexes with molecular oxygen and subsequently insert one oxygen atom from O_2 into a wide range of hydrophobic substrates with high stereo- and regioselectivity.

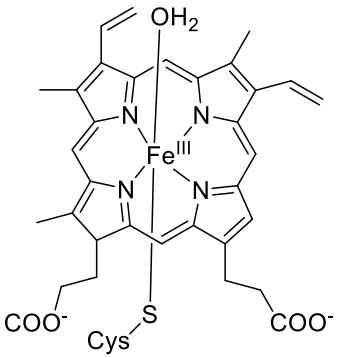

Figure 2.3: Active site of Cytochrome P-450 enzyme.[21]

Scheme 2.2 depicts the catalytic cycle of hydrocarbon oxidation for Cytochrome P-450 enzymes. When the enzyme is in rest, it is in the ferric state (**1**) with thiolate and water occupying the proximal and distal positions, respectively. The water ligand is replaced when the substrate binds to the enzyme (**2**). The ferric Cytochrome P-450 is reduced to ferrous Cytochrome P-450 (**3**). A dioxygen complex is formed upon binding of molecular oxygen (**4**). The next step is protonation and one-electron reduction, which produces a Fe(III)-hydroperoxo complex (**5**). The following step involves protonation as well as heterolytic cleavage of the O-O bond to produce a water molecule as well as a reactive iron-oxo intermediate (**6**). The instability of the Fe(III) hydroperoxo complex results in the formation of a radical cation Fe(IV) species (**6a**), or an Fe(V) species (**6b**). The oxidised product is formed through oxygen-atom transfer (OAT) from the iron complex to the bound substrate (**7**). The final step is product dissociation and the cycle is complete (**8**).[22, 23]

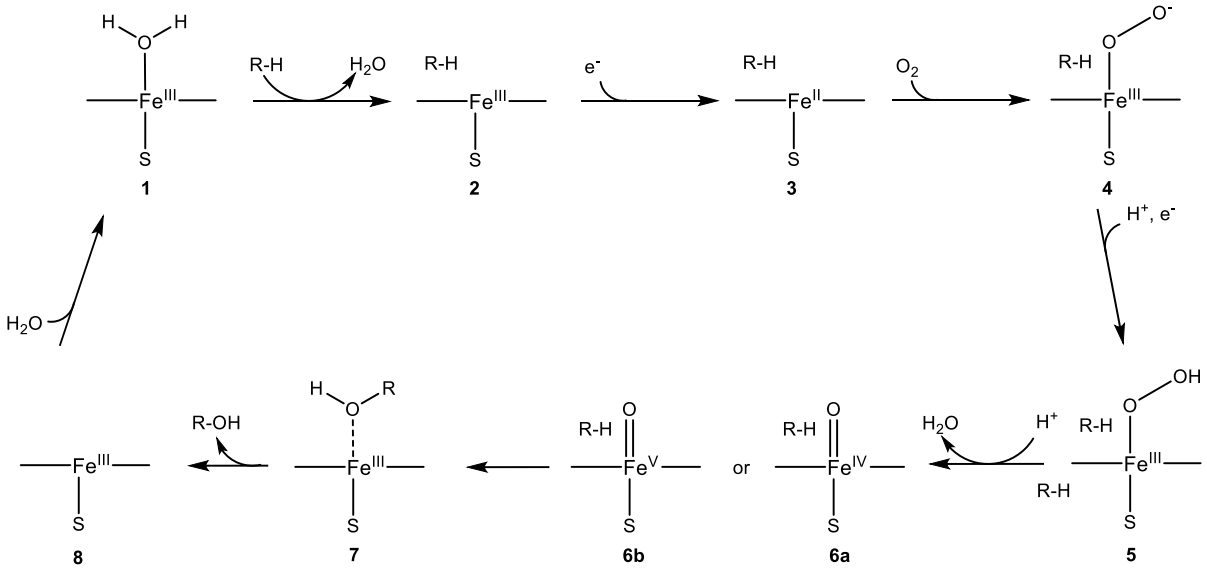

Scheme 2.2: Catalytic cycle of Cytochrome P-450. R-H indicates a hydrocarbon substrate and R-OH the resulting oxidised product. The S represents the cysteine thiolate ligand.[23]

Cytochrome P-450 shows incomparable activity towards different substrates in living organisms, but these enzymes are poorly active towards non-natural substrates.[24] This is because Cytochrome P-450 enzymes have extremely low stability under normal catalysis conditions utilised in the laboratory. As such, the structure of these enzymes and different reaction conditions had to be changed for oxidation of non-natural substrates. Understanding the mechanism of Cytochrome P-450 oxidation resulted in the development of porphyrin based ligands (Figure 2.4), which were used to create artificial heme catalyst systems.[16] The goal was to synthesise bioinspired catalysts to oxidise specific substrates with the desired selectivity as well as mimic the catalytic activity of native Cytochrome P-450 enzymes. Synthetic metalloporphyrins are similar to heme-containing enzymes, which are active towards oxidation of various substrates.[25] The porphyrin ring can act as an electron donor and is able to generate the Fe(IV) radical cation intermediate. The four coordinate structure of these ligands is stable and they are able to withstand degradation.

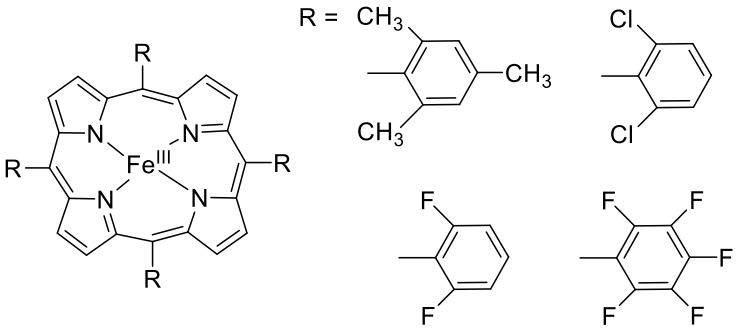

Figure 2.4: Examples of porphyrin based catalysts and different substituents that can be used.[26]

The mechanism by which heme complexes oxidise hydrocarbon substrates is similar to that of Cytochrome P-450. Scheme 2.3 indicates the formation of the reactive species that are responsible for the oxidation of the substrate. The reactive species are iron(IV)-oxo porphyrin π-cation radicals (**2**) and are formed by O-O bond heterolysis of the iron(III)-hydroperoxo species (**1**). Homolytic cleavage of the O-O bond is also possible and results in the formation of Fe^{IV}-oxo species (**3**) as well as a hydroxyl radical. Evidence suggests that different conditions determine the way the O-O bond will be cleaved. This includes factors such as the electronic properties of the axial and porphyrin ligands that influence the electronic nature of the complexes as well as the type of solvent used. Aprotic solvents are more likely to cause homolysis, while protic solvents result in heterolysis.[27]

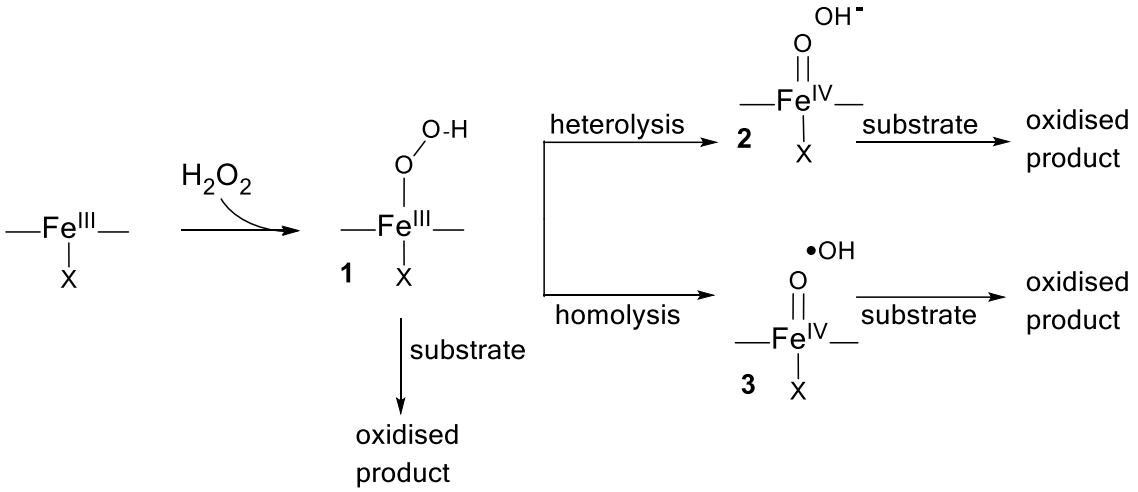

Scheme 2.3: Mechanism of the reaction of iron porphyrin complexes with H_2O_2. Adapted from Nam.[27]

The first example of these porphyrin-based heme mimics was reported by Groves and co-workers in 1979.[28] They prepared a Fe(TPP)Cl (TPP = 5,10,15,20-tetraphenylporphyrinato) porphyrin-based complex (Figure 2.5) and employed it as a catalyst precursor to oxidise alkanes and alkenes to alcohols and epoxides. For the oxidation of cyclohexene, the yield was 55% for cyclohexene epoxide, with 15% for cyclohexenol and this reaction also produced trace amounts of cyclohexenone. A major drawback of the system is rapid catalyst decomposition. In an extension of their work, Groves and co-workers employed the [Fe(TPP)Cl] as catalyst with iodosylbenzene as oxidant in the presence of an excess amount of cyclohexane as substrate at room temperature.[29] This reaction produced cyclohexanone and cyclohexanol in a 1:15 ratio and a combined yield of 8%. They also investigated *m*-chloroperoxybenzoic acid as oxidant and only achieved a 2% yield of cyclohexanol. Although this reaction appeared inefficient, it indicated that an aliphatic C-H bond could be hydroxylated under mild conditions. Different modifications were made to this system in an attempt to improve the product yield.[30]

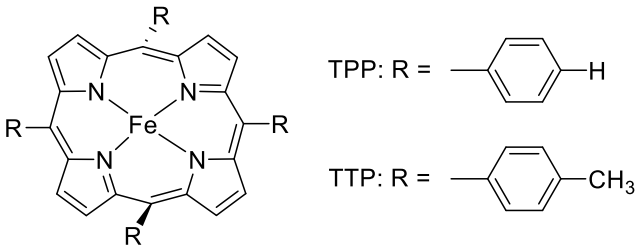

Figure 2.5: [Fe(TTP)] and [Fe(TPP)] heme-based complexes used for cycloalkane and cycloalkene oxidation.[29]

The [Fe(TPP)Cl] catalyst was replaced with a chloro(5,10,15,20-tetra-(*o*-tolyl-porphyrinato)) iron(III) [Fe(TTP)Cl] catalyst. These catalysts are depicted in Figure 2.5. When this catalyst was used in combination with iodosylbenzene as oxidant to oxidise cyclohexane, the amount of oxidised products increased three-fold. They also used this catalyst in combination with iodosylbenzene and bromotrichloromethane to oxidise cycloheptane.

In this reaction, 24% cycloheptanol, 3.6% cycloheptanone and 18% cycloheptyl bromide were produced.[29] Heterolysis of the O-O bond of the iron(III)-hydroperoxo species leads to the formation of iron(IV)-oxo porphyrin π-cation radicals, which are the active species in this oxidation reaction. The formation of these species is influenced by the electron richness of the porphyrin ring as well as the electron donating ability of the axial ligands. The type of solvent used will also have an effect on the catalytic activity of these porphyrin complexes.[27] In the case of the [Fe(TTP)Cl] and [Fe(TPP)Cl] catalysts, the more electron rich [Fe(TTP)Cl] resulted in better stabilisation of the high-valent iron-oxo species and led to better catalytic activity. These examples indicated that iron porphyrin complexes are able to oxidise C-H bonds, but the conversion and product selectivities are low. This highlighted the fact that heme ligands possess limitations when it comes to electronic and steric modifications. The drawbacks associated with heme oxygenase mimics in terms of activity, selectivity and stability resulted in a shift to a novel class of oxygenases, i.e. non-heme oxygenases.[16]

2.3.3 Non-heme oxygenases

Since the 1990s, there have been numerous examples of non-heme iron complexes catalysing a variety of different C-H bond activation reactions.[31] Figure 2.6 shows only a few examples of reactions catalysed by non-heme oxygenases.

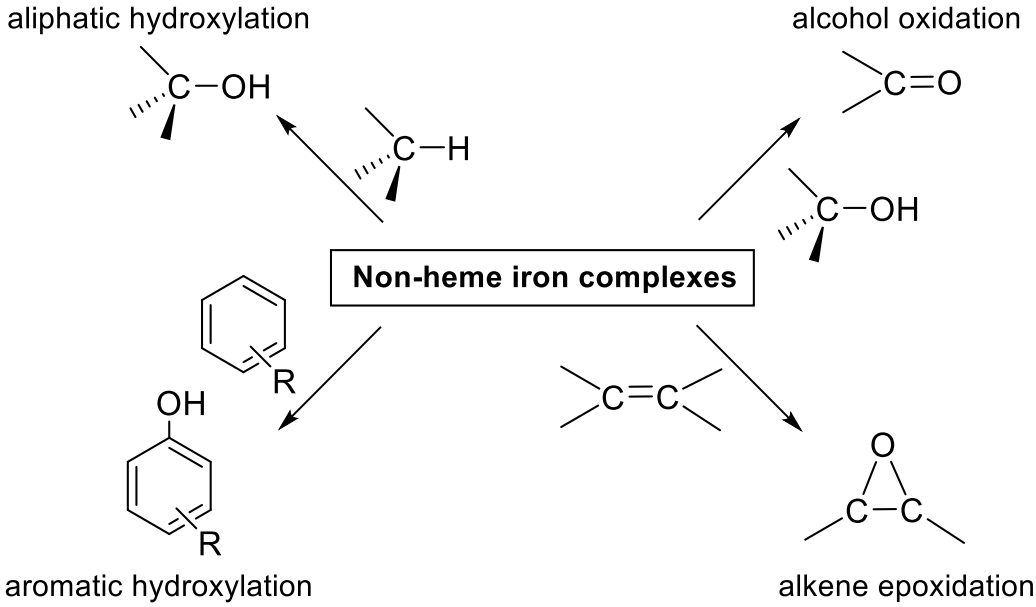

Figure 2.6: Examples of reaction catalysed by non-heme iron complexes.[32]

These non-heme iron complexes usually feature a polydentate N-donor ligand and use H_2O_2 as oxidant. It is also important to understand the mechanism by which these complexes operate to develop catalyst systems that possess high activity and selectivity.

2.3.3.1 Mechanistic aspects of non-heme complexes

Even though oxidation reactions occur in abundance in nature, there is still little information on the mechanistic details of these reactions, but it is important to consider the mechanistic aspects of the alkane oxidation reaction.[33] The type of mechanistic pathway that the catalyst follows will determine the selectivity and product distribution of the reaction.[34]

The key species in the oxidation of hydrocarbons with non-heme iron complexes is the Fe^{III}-OOH intermediate, formed during the reaction of the catalyst precursor with H_2O_2.[21, 35] The Fe^{III}-OOH intermediate itself can be an oxidant or cleavage of the O-O bond result in the subsequent formation of high-valent Fe-oxo species (Scheme 2.4).[36] Heterolysis of the O-O bond produces a Fe^{V}=O and OH^- species and homolysis produces a Fe^{IV}=O and short lived highly reactive HO• species.[12] HO• of RO• active species result in a radical pathway that has high activity, but causes low selectivity in the oxidised products. Metal-based oxidants such as Fe^{V}=O, Fe^{IV}=O or Fe^{III}-OOH provide better product selectivity, but show lower catalytic activity. The reactive species that are formed depend on the nature of the ligands, substrates and solvents.[17] For heterolytic cleavage to occur, it is necessary to have two *cis* labile sites on the iron centre. These labile sites are responsible for H_2O_2 activation and the subsequent formation of metal-based oxidants. Pentadentate ligands cause homolytic cleavage of the O-O bond. It is therefore necessary to optimise the electronic structure of the iron(II) precursor and to balance the reaction conditions in such a way that it will restrain Fenton-type decomposition, but prolong the reactivity of the high-valent iron oxo intermediates.[16]

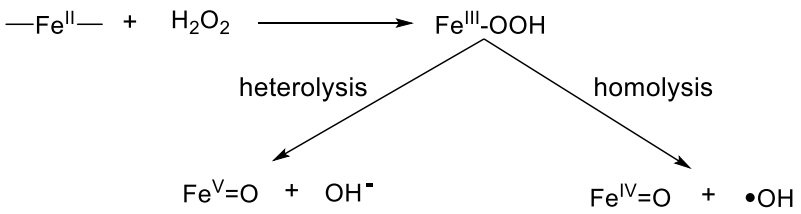

Scheme 2.4: The reaction of an iron complex with H_2O_2 leads to the formation of a Fe^{III}-OOH intermediate and thereafter two different reactive species. Adapted from Lee, et al.[37]

The metal centre in the Fe^{III}-OOH intermediate can exist in either low- or high-spin state and is dependent on the specific ligand present in the complex.[38] The effect of the spin state was investigated by Chen and co-workers,[39] and they found that low-spin intermediates integrate one oxygen atom from H_2O_2 and one from H_2O, while for high-spin intermediates both oxygen atoms originate from H_2O_2. The spin state and the Fe-oxo intermediates have an influence on the final oxidised products.

The oxidation products formed are influenced by the specific mechanistic pathway that the reaction followed. This led to the development of different tools that are used to investigate the mechanism for a specific reaction.[35, 40] Some of these tools are:

Alcohol/Ketone ratio

Alkylperoxyl radicals are formed when the freely diffusing alkyl radicals are trapped by O_2. An equimolar amount of ketone and alcohol is formed through the Russel-type termination of these intermediates. This is independent of the oxidant/substrate ratio. A radical chain mechanism usually lead to an A/K ratio of close to 1. It is believed that metal-based oxidants (Fe^{V}=O and Fe^{IV}=O) leads to high stereoselectivity in the product and generate alcohols as products, whereas, if HO• radicals are responsible for the oxidation, an equimolar amount of ketone and alcohol is formed.[41, 42]

Kinetic isotope effect

C-H and C-D bonds are equally oxidised by highly reactive radicals and result in a KIE value of 1 to 2. These radicals are strong oxidising agents and do not discriminate between the different bonds present in the substrates. For selective, metal-based oxidants, the KIE values are significantly higher, due to the different bond activation energies of C-H and C-D bonds. This results in KIE values in the range of 3 to 5.

Reaction under air/argon

The presence of O_2 leads to the trapping of the radicals and the subsequent formation of the oxidised product. In the absence of O_2, a reaction that proceeds through a free-radical mechanism will produce lower oxidation yields. When the results are similar in the presence or absence of O_2, this usually indicates a metal-based mechanism.

In the last decade, different oxidising systems that are based on transition metal complexes as catalysts, were discovered and investigated. The next section will look at the influence of ligand structure on the catalytic activity as well as the development of these non-heme-based oxidation systems.

2.3.3.2 Effect of ligand topology on the reactivity of iron complexes

To design catalysts that have high reactivity and selectivity, it is important to recognise the factors that regulate the reactivity of non-heme iron complexes. A principal factor to consider is the structure of the ligand around the iron centre. Different ways that linear tetradentate N4 ligands can coordinate to an octahedral iron centre have been described by Bosnich (2002).[43] The different topologies are: *cis*-α, *cis*-β and *trans* (Figure 2.7) and are determined by the absolute chirality of the internal diamine donors. Three chelate rings are formed by these

ligands and the bite angle strain regulates the preference for the three possible topologies. Each of these topologies has a different effect on the reactivity of the resultant complex.

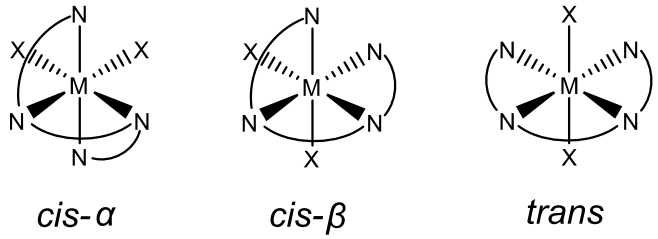

Figure 2.7: Different topologies exhibited by the complexes as a result of the chirality of the internal diamine donors.[44]

When the ligand coordinates to the metal, the two internal amine donors become chiral. If we assume that the internal donors do not change then five pairs of enantiomers are possible: *cis*-α (*S,S* or *R,R*), *cis*-β (*S,S* or *R,R*), *cis*-β (*S,R* or *R,S*), *trans* (*S,S* or *R,R*) and *trans* (*S,R* or *R,S*). The *cis*-α (S,R or R,S) geometry is not possible because the complex experiences intense bite-angle strain.[45]

H_2O_2 activation takes place at the labile coordination sites and the chemical environment of these sites is influenced by the way that the N4 ligand coordinates to the Fe^{II}-centre. The *cis*-α topology causes the labile sites to be *trans* to the amine nitrogen atom of the ligand, resulting in the labile sites being chemically equivalent. On the other hand, these labile sites are *trans* to a pyridine and an aliphatic amine in the *cis*-β topology, which causes the labile sites to be chemically inequivalent.[46] The labile sites are needed for H_2O_2 activation and control the catalytic activity of the complexes and will therefore be influenced by their chemical equivalence. Chemical equivalence of the labile sites results in higher activity, whereas, if the labile sites are chemically inequivalent, the catalytic activity is lower. Figure 2.8 shows a few of the most common tetradentate ligands and their preferred topology.

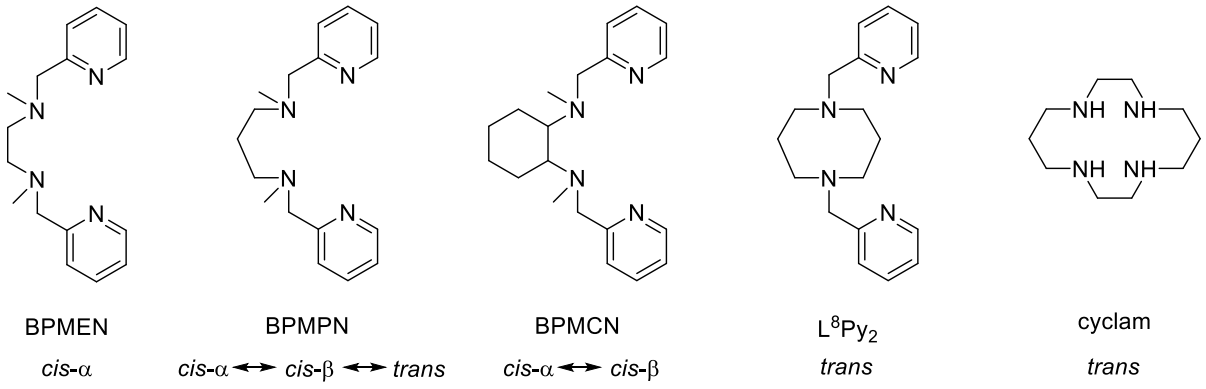

Figure 2.8: Different ligands and the topologies exhibited when these ligands coordinate to iron.[46]

Predicting the solution geometry of the ligated metal complex is not straightforward. The reason for this is that the geometry is influenced by a range of different factors, which include the solvent, temperature, concentration and the number of atoms between the donor atoms of the ligand. There is also a possibility that an equilibrium exists in solution between the geometries. This may happen when the co-ligands are labile, such as triflate or acetonitrile.[36]

A range of iron(II) bistriflate complexes with bis(pyridylmethyl)diamine ligands (Figure 2.9) that vary in the flexibility of the ligand backbone was investigated by England and co-workers.[47] Only one of these complexes displayed *cis*-α ligand topology and also had the strongest ligand field, which resulted in higher stability and lifetime for this complex, when applied in oxidation catalysis. It was found that the complexes that exhibit *cis*-β coordination show rapid deactivation because these complexes are high-spin complexes at room temperature and are kinetically labile. The *cis*-α complex is a kinetically inert low-spin complex and therefore deactivation does not occur as rapidly as for the other coordination topologies. The goal is to synthesise complexes that exhibit *cis*-α topology and higher stability, which may have a significant influence on the rate of oxidation.

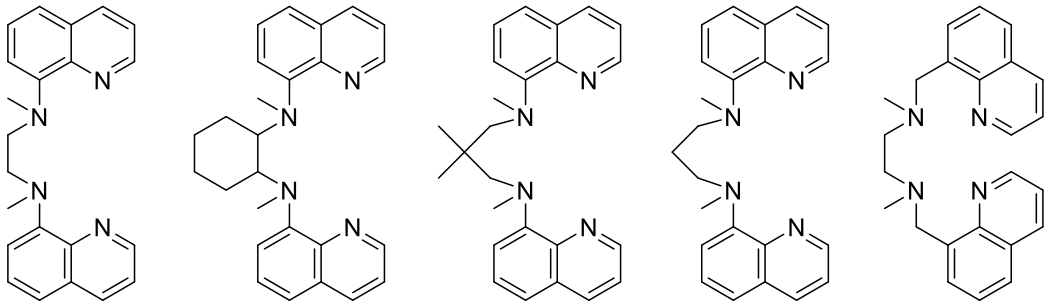

Figure 2.9: Bis(pyridylmethyl)diamine ligands used to form iron(II) bistriflate complexes with *cis*-α and *cis*-β configuration investigated by England and co-workers.[47]

Que and co-workers synthesised two [Fe^{II}(BPMCN)] (BPMCN = N,N′-dimethyl-N,N′-bis (2-pyridylmethyl)-cyclohexane-1,2-diamine) catalysts that differed in the ligand topology: *cis*-α and cis-β (Figure 2.10). α-[Fe^{II}(BPMCN)] was employed in the oxidation of cyclohexane and was converted into cyclohexanol and cyclohexanone with high stereoselectivity and a high alcohol/ketone (A/K) ratio of 5.9. This result indicates that if there is formation of radicals, they are short lived. For β-[Fe^{II}(BPMCN)], there was a difference in the oxidation behaviour. They found a loss of stereochemistry in the oxidation products of *cis*-1,2-dimethylcyclohexane and *cis*-2-heptene as well as a low A/K ratio of 1.9 for cyclohexane oxidation, which is indicative of the presence of longer-lived radicals. These observations provided further evidence that the ligand has a noteworthy role in the oxidation of hydrocarbons.[48]

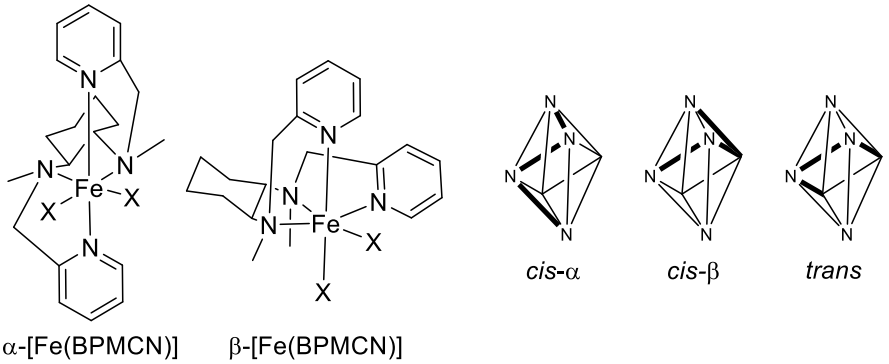

Figure 2.10: The structure of the *cis*-α and *cis*-β topology of the [Fe(BPMCN)] complex.[48]

2.3.3.3 Development of non-heme iron oxidation systems: Alkane and alkene oxidation

The initial investigation into the application of non-heme iron complexes in hydrocarbon oxidation was reported by Que and co-workers (1990).[49] They introduced tris(2-pyridylmethyl)amine (TPA) as supporting ligands for iron(III) complexes (Figure 2.11). A $[Fe^{III}(TPA)Cl_2](ClO_4)$ complex, with *cis* labile coordination sites, was evaluated in the oxidation of cyclohexane in the presence of TBHP (TBHP = *tert*-butyl hydroperoxide) as oxidant. Turnover numbers of 56 were obtained after 2 h of reaction, generating cyclohexanone, cyclohexane, chlorocyclohexane and (*tert*-butylperoxy)cyclohexane as products. They also conducted various mechanistic studies on these non-heme iron complexes and found initial evidence for a mechanism that differed from the Fenton type of chemistry. $[Fe(TPA)(CH_3CN)_2]^{2+}$ complexes and the α- and β-topological counterparts were synthesised and reacted with H_2O_2. The different electronic and steric properties of the ligand have an influence on the reactivity pattern for these Fe(TPA) catalysts. The production of a highly reactive, as well as selective oxidant was seen, which was different from the formation of hydroxyl radicals. The results of the oxidation of cyclohexane displayed a high cyclohexanol/cyclohexanone (A/K) ratio and a high kinetic isotope effect (KIE > 3). In adamantane oxidation, high regioselectivity toward the tertiary C-H bond was observed and for *cis*-1,2-dimethylcyclohexane hydroxylation they found good retention of configuration. Isotopic labelling experiments were also conducted and indicated that H_2O_2 and H_2O provided the O-atom that is incorporated in the substrates. This data provided evidence that the mechanism responsible for the oxidation of these substrates is not based on the production of free-diffusing radicals. The reaction of H_2O_2 with these complexes does not follow the Fenton-type chemistry but rather a metal-based oxidant, such as high-valent iron-oxo species (Fe^{V}=O or Fe^{IV}=O) and is able to selectively oxidise substrates.[38, 50]

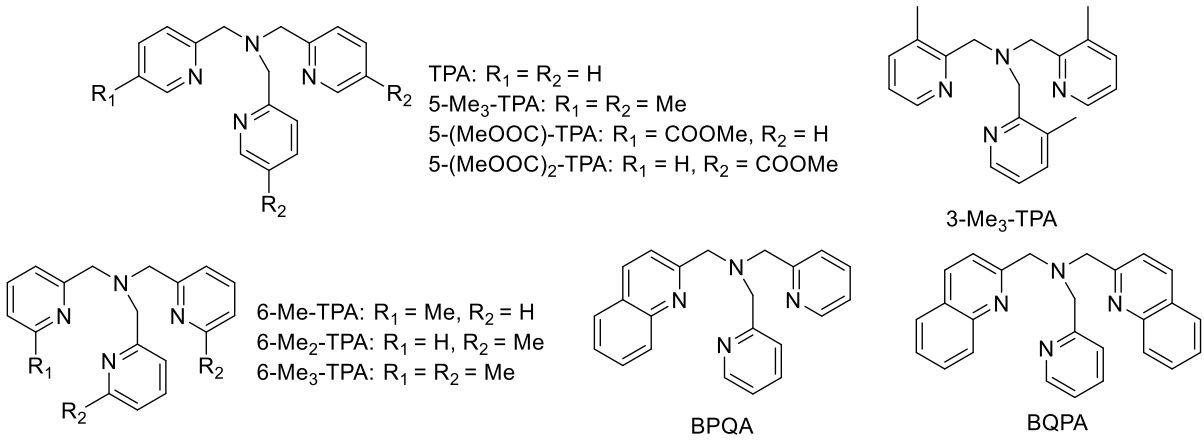

Figure 2.11: A family of TPA ligands used for hydrocarbon oxidation and the investigation into mechanistic pathways.[38]

A [Fe(II)(BPMEN)$(CH_3CN)_2$]$(SbF_6)_2$ complex (Scheme 2.5) (BPMEN = N,N′-dimethyl-N,N′-bis(2-pyridylmethyl)-ethane, 1,2-diamine) was used in an attempt to oxidise a pivalate derivative under substrate-limiting conditions with H_2O_2 as oxidant. A 7% yield, 12% conversion and 56% selectivity for the formation of the oxidised product were seen for these reactions. Because unselective oxidations are usually attributed to catalyst degradation, which results in Fenton-type chemistry, the researchers hypothesised that increased selectivity may be seen when increasing the rigidity of the BPMEN ligand. The updated catalyst was a [Fe(*S,S*-PDP)$(CH_3CN)_2$]$(SbF_6)_2$ complex (PDP = 2-({(*S*)-2-[(*S*)-1-(pyridine-2-ylmethyl) pyrrolidine-2-yl]pyrrolidin-1-yl)}methyl)-pyridine) (Scheme 2.5, complex on the right). In this catalyst, the methyl-amines were incorporated into pyrrolidine rings and also had *cis* labile coordination sites. When used in combination with H_2O_2 under substrate-limiting conditions, the selectivity increased to 92% and the yield to 14%. Adding AcOH to both catalysts caused an increase in catalytic activities for both, but not a large change in selectivity. The steric and electronic properties of the C-H bonds were responsible for the selectivity of the reaction and there was no need for directing groups; the most electron-rich C-H bond was oxidised. This observation could be applied to the oxidation of highly functionalised substrates. They also continued their studies by investigating the oxidation of secondary C-H bonds to ketones and the site selectivity and chemoselectivity of these reactions.[6, 51]

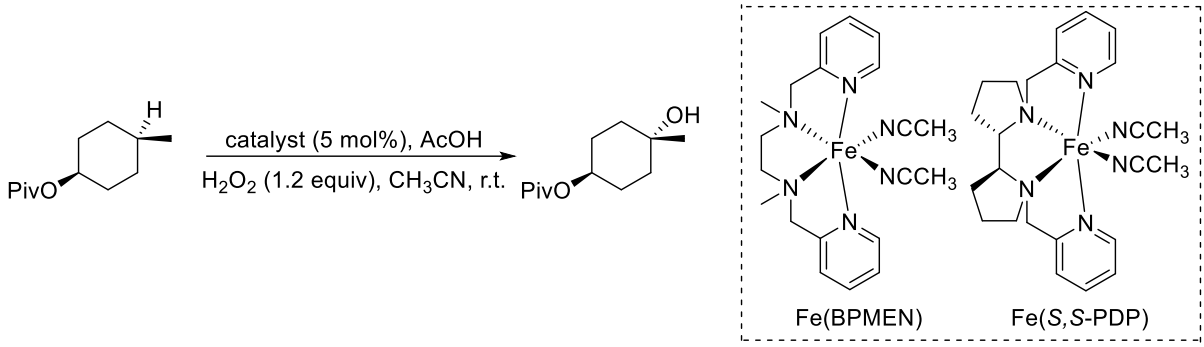

Scheme 2.5: The Fe(BPMEN) and Fe(PDP) complex employed in the oxidation of pivalate.[6]

Non-heme iron(II) bistriflate complexes that contained pyridyl and amine donors were investigated by Britovsek and co-workers (Figure 2.12).[5] They found that ligands that contain at least two pyridine donors show reactivity which differs from Fenton-like chemistry. They concluded that these pyridine donors are necessary for high catalytic activity and selectivity by causing a stronger ligand field that is able to stabilise the intermediates that are responsible for metal-based oxidation. They also reported that the catalysts containing more amine donors are less stable and degrade quickly. In addition, they found that the catalytic activity is influenced by the two *cis* coordination sites at the metal centre and therefore a six-coordinate geometry is favourable. The ligands that have more amine than pyridine donors do not have *cis* coordination labile sites because these ligands favour a five-coordinate geometry.

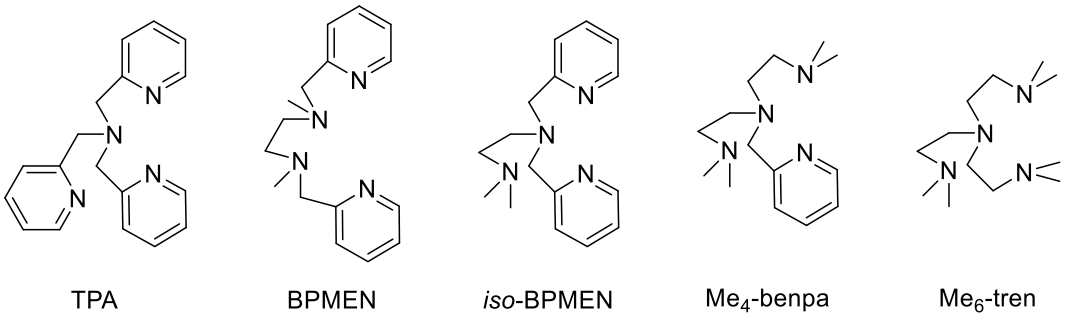

Figure 2.12: Tetradentate ligands with amine and pyridine donors evaluated by Britovsek and co-workers.[5]

England and co-workers wanted to determine which factors contribute to the catalytic activity that non-heme iron complexes display. The Fe(II) complex containing the BPMEN ligand was used as a benchmark and compared with catalysts bearing quinolyl or quinolylmethyl groups in the oxidation of cyclohexane (Figure 2.13). For [Fe(BPMEN)$(OTf)_2$], the conversion of added H_2O_2 to cyclohexanol and cyclohexanone was 65%. They found that the bis(quinolyl)diamine complexes are not as effective as [Fe(BPMEN)$(OTf)_2$]. [Fe(BQEN)$(OTf)_2$] was the most active and selective with a 51% conversion of H_2O_2 when 10 equiv of H_2O_2 was used, but when 100 equiv of H_2O_2 was used, the H_2O_2 conversion decreased to 30%. This trend was the same for Fe(II) complexes with $BQMe_2PN$ and BQPN ligands, which showed

good activity and selectivity at 10 equiv, but at 100 equiv there is a big decrease in activity, which may be an indicator that the catalyst degrades quickly. [Fe(BQCN)(OTf)$_2$] had a low conversion of only 16% and the analogous complex [Fe(BQMEN)(OTf)$_2$] had a conversion of 5%. When evaluating the ligand topologies of these complexes, they found that [Fe(BQEN)(OTf)$_2$] is in the *cis*-α conformation, [Fe(BQCN)(OTf)$_2$] was in the *cis*-β conformation and that the Fe(II) complexes with BQMe$_2$PN, BQPN and BQMEN ligands fluctuate between the *cis*-α, *cis*-*β* and *trans* configuration when they are in solution. They concluded that [Fe(BQEN)(OTf)$_2$], which has the best activity, has the strongest ligand field. The backbone of this ligand is small and results in the formation of three five-membered chelate rings, which favour the *cis*-α conformation. The other ligands have a larger backbone and increased flexibility, which results in a weaker ligand field and lower catalytic activity exhibited by their Fe(II) complexes.[47]

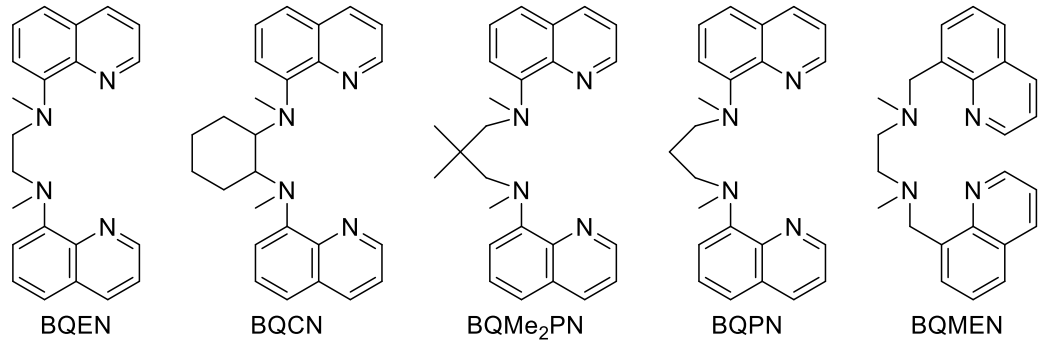

Figure 2.13: Ligand set with quinolylmethyl or quinolyl groups.[47]

These examples indicate that the stability of the ligands plays a major role in the performance of the catalyst. If the ligand and the complex are stable against degradation, the catalyst will display good catalytic activity.[47] Another factor that will influence the catalytic activity is the *cis* labile sites. The presence of two *cis* labile sites is necessary for H_2O_2 activation as well as the formation of high valent oxo species and the absence of *cis* labile sites will most likely result in Fenton-type chemistry.[52]

Different catalyst systems have also been investigated for alkene epoxidation. [Fe(II)(BPMEN)(CH$_3$CN)$_2$](ClO$_4$)$_2$ complexes were evaluated for the epoxidation of 1-decene with varying amounts of H_2O_2 as oxidant (Scheme 2.6). The alkene was completely converted when employing 4 equiv of the oxidant. A yield of 40% was observed for the epoxide product and different over-oxidised by-products were formed also. When employing the SbF_6 complex (counter-ion replaced), the reaction was more efficient. Complete conversion was found with only 1.5 equiv of the oxidant and selectivity for the epoxide increased to 71%. Further improvement to 82% in selectivity for epoxide formation was seen when adding 1 equiv of acetic acid. It was concluded that the catalytic activities of the iron compounds are inversely

proportional to the binding affinities of the anions: ClO_4^- possesses a stronger binding affinity *vs* SbF_6^-. This example demonstrates the influence of the different catalyst structures on activity as well as the effect of using acetic acid as additive.[53]

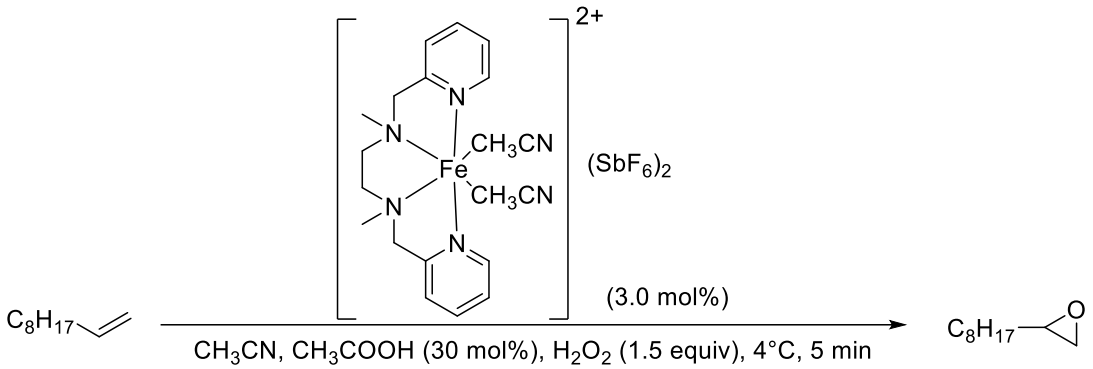

Scheme 2.6: Reaction pathway for the epoxidation of 1-decene with a Fe(II)(BPMEN) catalyst system.[53]

Que and co-workers investigated tetradentate ligands and their 6-methyl derivatives in the oxidation of various substrates (Figure 2.14). The $[Fe(BPMEN)(CH_3CN)_2](ClO_4)$ and 6-methyl substituted complexes were investigated in cyclooctene oxidation with 10 equiv of H_2O_2 as oxidant. Cyclooctene epoxide and *cis*-diols were obtained as products with yields of 75% and 9%, respectively, relative to H_2O_2. In contrast, the 6-methyl substituted analogue provided yields of 15% and 64%, respectively, for the epoxide and *cis*-diol. This result demonstrated a complete inversion in product selectivity. When using the $[Fe(BPMCN)(CF_3SO_3)_2]$ complex and the 6-methyl derivative of this complex for the oxidation of *trans*-2-heptene, the (*R,R*) configuration provided 29% *ee* (*ee* = enantiomeric excess) for the *cis*-diol and 12% *ee* for the epoxide. The (*S,S*) configuration afforded the *cis*-diol with 79% *ee*. The 6-methyl substituent that was introduced onto the ligands had a clear influence on the product selectivity of the reaction: favouring *cis*-dihydroxylation rather than epoxidation.[54]

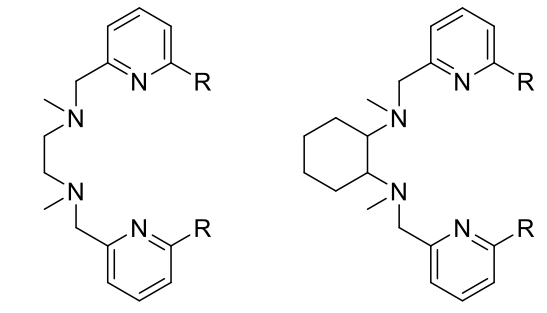

R=H: BPMEN
R=Me: 6-Me_2-BPMEN
R=H: BPMCN
R=Me: 6-Me_2-BPMCN

Figure 2.14: BPMEN and BPMCN ligands and their derivatives used in the oxidation of cyclooctene.[54]

An important consideration is also the structural properties of the catalyst. The inherent reactivity preference of the C-H bond can be overcome by increasing the steric bulk of the catalyst and therefore decreasing the accessibility of the substrate to the active iron-oxo species. He and co-workers described the effect that steric modifications may have on the regioselectivity of alkane oxidation catalysed by non-heme iron complexes.[12] They hypothesised that substrate access to the reactive part of the metal oxidant could be inhibited by introducing steric bulk onto the catalyst. They based their catalyst on the BPMCN structure and used benzyl groups to replace the methyl substituents on the amine nitrogens (Figure 2.15). This ligand was reacted with three iron(II) precursors to furnish three complexes: $Fe(SbF_6)_2$, $Fe(OTf)_2$ and $FeCl_2$. In the oxidation of cyclohexane with H_2O_2 as oxidant, the complex with the hexafluoroantimonate counter-ion, $[Fe(BBPC)(CH_3CN)_2](SbF_6)_2$, had the best reactivity (TON = 27.4) compared to $[Fe(BBPC)(Cl)_2]$, which had a TON of 12.4 and $[Fe(BBPC)(OTf)_2]$ with a TON of 12.8. $[Fe(BBPC)(CH_3CN)_2](SbF_6)_2$ also produced more cyclohexanol than cyclohexanone. These examples also indicated the effect of the counter-ion on the catalytic activity of the complex. There is competition between the counter-ions and the terminal oxidant for coordination sites on the metal and this causes the metal oxidation step to be slower, which leads to lower catalytic activity. The presence of an anionic ligand on the iron centre may also destabilise high-valent iron species. A stoichiometric amount of acetic acid was added to the $[Fe(BBPC)(CH_3CN)_2](SbF_6)_2$ system and resulted in a decrease in activity, but the selectivity for cyclohexanol increased. The $[Fe(BBPC)(CH_3CN)_2](SbF_6)_2$ was used to oxidise *cis*- and *trans*-1,2-dimethylcyclohexanes. The oxidation of these substrates will determine whether the catalyst has a preference for secondary or tertiary carbons. The results indicated that the oxidation of the sterically crowded C-H bonds is reduced by the cyclohexane ring and benzyl groups on the catalyst. The C-H bonds on the tertiary carbon atoms are oxidised less and the C-H bonds on secondary carbons are still activated.[55]

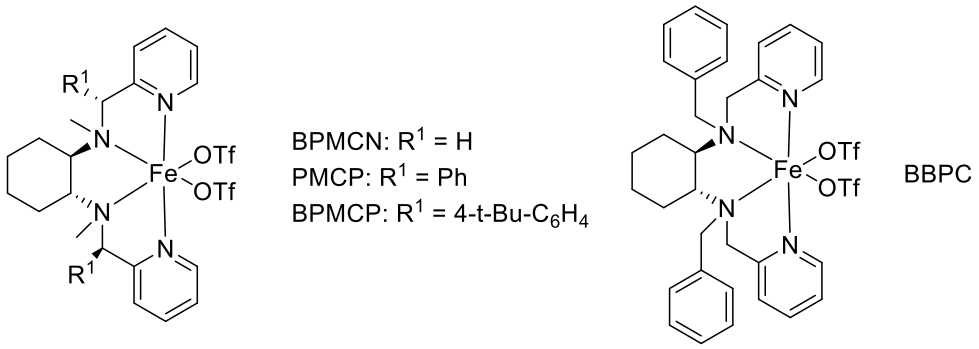

Figure 2.15: $[Fe(BPMCN)(OTf)_2]$ and $[Fe(BBPC)(OTf)_2]$ complexes with different substituents used in the oxidation of different hydrocarbons as well as the epoxidation of α,β-substituted enones.[55, 56]

Sun and co-workers investigated Fe(II) chiral complexes with BPMCN ligands (Figure 2.15) in the epoxidation of α,β-enones. Chalcone was oxidised in the presence of H_2O_2 as oxidant and AcOH as additive (Scheme 2.7). A yield of 33% and an *ee* of 66% for chalcone epoxide was found when 1 mol% of the catalyst was used. The best activity was seen for [Fe(BPMCP)$(OTf)_2$]: 77% *ee* when 2 mol% of catalyst was used at -15°C. Substituted chloro-, bromo-, and trifluoro-acetic acid, formic acid and benzoic acid were also investigated as alternative additives, but provided poorer *ee*'s and product yields than acetic acid. They also found that using H_2O_2 as oxidant provides better *ee* compared to when peracetic acid is used as oxidant. This system is limited because only *trans*-α,β-enones can be epoxidised.[56]

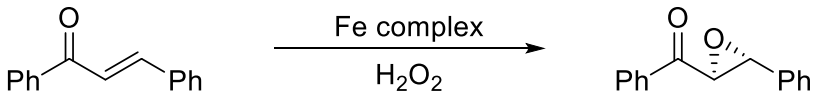

Scheme 2.7: Oxidation of α,β-enones with H_2O_2 as oxidant.[56]

In Cytochrome P-450 there are different electronic effects that influence the ability to catalyse different reactions. The electron-donating thiolate group assists in the heterolytic O-O cleavage step and results in higher catalytic activity. Costas and co-workers attempted to design non-heme iron catalysts for epoxidation, which resembles the electronic properties found in Cytochrome P-450. They synthesised a family of bipyrrolidine-based complexes (Figure 2.16) that were employed in the epoxidation of *cis*-β-methylstyrene in the hope that these catalysts in combination with H_2O_2 will produce epoxides with good enantioselectivity and high yields in a short reaction time. These complexes showed a relationship between the electron-donating ability of the ligand and product enantioselectivities and yield. An increase in the electron-donating nature of the ligand, showed an improvement in the enantioselectivity from 16% *ee* to 62% *ee* and the yield increased from 13 to 87%. They also investigated the impact of the carboxylic acid additive. When the acetic acid was absent, a decrease was seen for both the stereoselectivity and yield. [57]

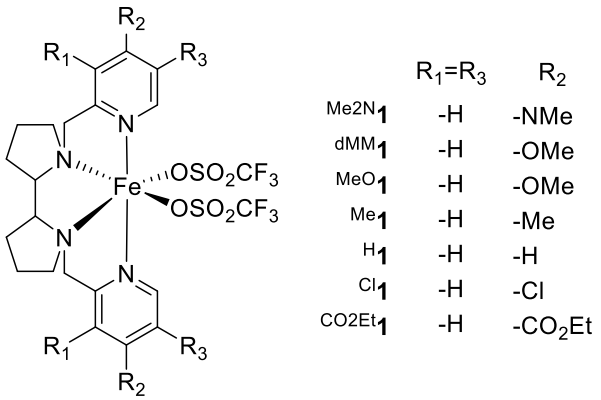

Figure 2.16: Fe(PDP) family of complexes, with different substituents on the ligand, synthesised for the epoxidation of *cis*-β-methylstyrene.[58]

They concluded that the combination of a metal, a good electron-donating ligand and carboxylic acid as co-ligand will allow heterolytic O-O bond cleavage and the electrophilic high-valent iron-oxo species will be stabilised. This also indicates that it is not always necessary to have elaborate catalysts and that fine-tuning of the electronic and steric properties of the catalyst may lead to a significant difference in catalytic activity.

2.3.3.4 Development of non-heme iron oxidation systems: Alcohol oxidation

Different iron systems have been employed for the oxidation of alcohols, but the investigation into non-heme iron complexes for alcohol oxidation is not very extensive. A few of the iron systems described in literature will be highlighted.

Sato and co-workers used a combination of picolinate, 6-methyl-picolinate (Me-picH) and $Fe(OAc)_2$ with H_2O_2 as oxidant for the oxidation of various alcohol substrates (Scheme 2.8). The optimal reaction conditions for the oxidation of cinnamyl alcohol was a 1:3 ratio of $Fe(OAc)_2$:Me-picH and 1.25 equiv of H_2O_2. This reaction afforded cinnamaldehyde as product with 95% conversion, 89% yield and 94% selectivity for the aldehyde. They also extended their scope to include different allylic and benzylic alcohols. For benzyl alcohol as substrate, this system provided 50% yield and 91% selectivity. Good selectivity toward the aldehyde was also seen for the rest of the substrates investigated.[59]

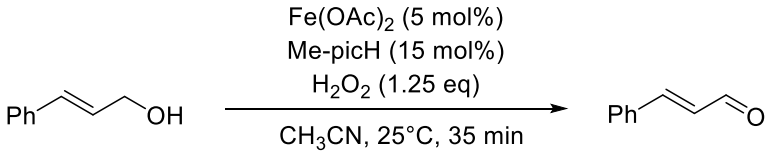

Scheme 2.8: Oxidation of alcohols with a system of $Fe(OAc)_2$, 6-methyl-picolinate and H_2O_2.[59]

Iron-catalysed alcohol oxidation was also investigated by Beller and co-workers. Iron(II) and iron(III) precursors, in combination with ligands featuring carboxylic acid and imidazole moieties, were evaluated in the presence of Na_2CO_3 as base and H_2O_2 as oxidant. The best activity was seen for 6-(*N*-phenylbenzimidazoyl)-2-pyridinecarboxylic acid as ligand, which provided a conversion of 78% and chemoselectivity of 97% for benzyl alcohol oxidation (Scheme 2.9). When using 2 equiv of H_2O_2, the conversion increased to 83%. $FeCl_3.6H_2O$ and $FeCl_2$ were found to be the best iron sources to use. They extended the scope of the aromatic alcohols and found that adding substituents on the aromatic moiety did not have a significant influence on the activity of the system. They also used this system for the oxidation of secondary alcohols and were able to efficiently oxidise secondary alcohols to the corresponding ketones when increasing the reaction time to one hour. The oxidation of allylic alcohols could also be performed with this system and gave conversions higher than 80% for a range of substrates.[60]

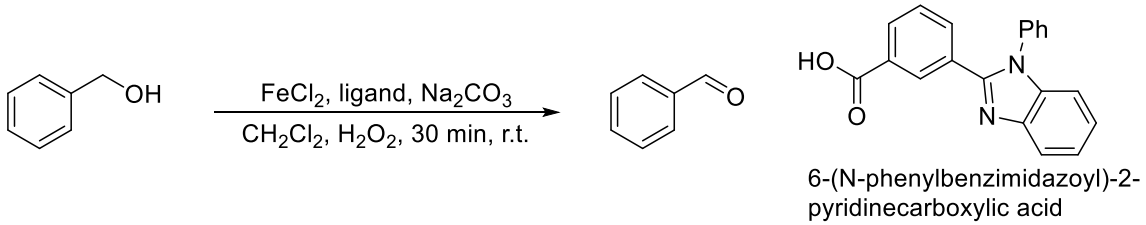

Scheme 2.9: Benzyl alcohol oxidation with a combination of iron, H_2O_2 and a ligand with carboxylic acid and imidazole moieties.[60]

Metalloporphyrins catalyse a host of oxidation reactions, including alcohol oxidation. Kim and co-workers investigated [(F_{20}TPP)FeCl] (tetrakis(pentafluorophenyl)porphyrinatoiron chloride) as the catalyst and *m*-chloroperoxybenzoic acid (MCPBA) as oxidant. They obtained high catalytic activity for a range of primary alcohol substrates. For benzyl alcohol, a conversion of 65% and yield of 6% for benzaldehyde and 36% for benzoic acid were reported. They also conducted a mechanistic investigation and concluded that an α-hydroxyalkyl radical intermediate is responsible for the oxidation of the different alcohol substrates.[61]

Speier and co-workers investigated the oxidation of primary as well as secondary alcohols catalysed by non-heme dinuclear iron complexes with H_2O_2 as oxidant. The complexes were [Fe(indH)Cl]$_2$O (indH = 1,3-bis(2′-pyridylimino)isodoline) and [$Fe_2(OMe)_2(PAP)Cl_4$] (PAP = 1,4-di(2′-pyridyl)aminophtalazine) (Figure 2.17).

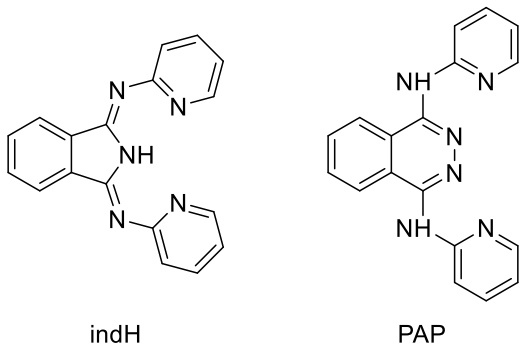

Figure 2.17: Ligands used for the formation of dinuclear iron complexes for alcohol oxidation.[62]

The reaction conditions that gave the best activity were 3.5 mmol substrate, 35 µmol catalyst and 3.5 mmol H_2O_2 in acetone under an argon atmosphere. Using [Fe(indH)Cl]$_2$O under these conditions with benzyl alcohol as substrate resulted in a 53% conversion with 98% selectivity toward benzaldehyde and 2% benzoic acid after 30 minutes. Increasing the reaction time to 60 minutes had no significant effect on the conversion. For [$Fe_2(OMe)_2(PAP)Cl_4$], after 30 minutes, the conversion was 15% with the product distribution 99% benzaldehyde and 1% benzoic acid. The conversion increased to 22% when the reaction time was increased to 120 minutes. They extended the oxidation to include various primary and secondary, aliphatic, aromatic as well as cyclic and acyclic alcohols. Of these different substrates, the highest yield

(29%) was seen for 1-phenylethanol, with $[Fe(ind)Cl]_2O$ as catalyst and a reaction time of 30 minutes.[62]

The nature of these iron tetradentate complexes makes it possible to easily manipulate the structure, as highlighted above. These catalyst systems can then be refined for a range of oxidation reactions.

2.3.3.5 Drawbacks and selectivity issues of non-heme catalyst systems

Over the years, extensive research has been conducted on non-heme catalyst systems and a great deal of progress has been made. Early on, some of the most common drawbacks of these systems were the need for harsh oxidants in high concentrations or high purity oxygen at high pressures. These drawbacks were further exacerbated by the use of expensive chemicals and the need for long reaction times. These systems also used organic peracids (PhlO, TBHP) as oxidants, which produced large amounts of waste.[1, 63] There was an urgent need for oxidation processes that use non-toxic metals and green oxidants and these systems have evolved into catalysts that use iron and hydrogen peroxide as oxidant.[64, 65]

Important and common problems of these catalytic oxidation reactions are the low product selectivity, as well as low regioselectivity and stereoselectivity.[2, 65] A challenge that still remains is producing a catalyst that will be able to oxidise a wide range of substrates and exhibit predictable and good selectivity. The substrate scope for alkane oxidation reactions is limited because the local chemical environment dictates the selectivity of the reaction. To functionalise isolated, unactivated C-H bonds with good selectivity is still a major area of investigation.[6]

The ideal catalyst will therefore be produced from renewable and less expensive sources; it should be highly selective for a particular product; and function with large turnover numbers. Mild temperatures and pressures should be needed for this catalyst and it is important that this catalyst produces a minimum amount of waste.[1] The availability of only a few methods for the oxidation of C-H bonds emphasises the fact that this is considered a very challenging chemical bond to functionalise.

Chapter 3 details the synthesis and characterisation of (*R,R*) bis-heterocyclic secondary diamine ligands and their Fe^{II}-triflate complexes. The evaluation of these complexes as catalyst precursors in the oxidation of *cis*-cyclooctene is described. The effect of water and acetic acid as additives will also be reported. The stability of these complexes was also investigated and the effect of the ligand topology will be described.

The synthesis and characterisation of (*R,R*) and (*S,S*) bis-heterocyclic tertiary diamine ligands and their Fe^{II}-triflate complexes are described in Chapter 4. These catalysts were also investigated in oxidation reactions with *cis*-cyclooctene and this data was used to investigate the effect of the ligand topology as well as different steric and electronic properties of the complex. This ability of this system to oxidise alcohols will also be evaluated. Benzyl alcohol was used as model substrate to optimise various reaction parameters. Finally, the substrate scope of the alcohols was extended to determine the efficiency of this oxidation system.

2.4. References

1. Bordeaux, M.; Galarneau, A.; Drone, J., *Angew. Chem. Int. Ed.*, **2012,** *51* (43), 10712-10723.

2. Mac Leod, T. C.; Kirillova, M. V.; Pombeiro, A. J.; Schiavon, M. A.; Assis, M. D., *Appl. Catal., A*, **2010,** *372* (2), 191-198.

3. Shul'pin, G. B., *C.R. Chim.*, **2003,** *6* (2), 163-178.

4. da Silva, V. S.; Idemori, Y. M.; De Freitas-Silva, G., *Appl. Catal., A*, **2015,** *498*, 54-62.

5. Britovsek, G. J.; England, J.; White, A. J., *Inorg. Chem.*, **2005,** *44* (22), 8125-8134.

6. Chen, M. S.; White, M. C., *Science*, **2010,** *327* (5965), 566-571.

7. Mirkhani, V.; Moghadam, M.; Tangestaninejad, S.; Mohammadpoor-Baltork, I.; Rasouli, N., *Catal. Commun.*, **2008,** *9* (13), 2171-2174.

8. Silva, A. R.; Botelho, J., *J. Mol. Catal. A: Chem.*, **2014,** *381*, 171-178.

9. De Montellano, P. R. O., *Cytochrome P450: structure, mechanism, and biochemistry*. Springer Science & Business Media: 2005.

10. Newhouse, T.; Baran, P. S., *Angew. Chem. Int. Ed.*, **2011,** *50* (15), 3362-3374.

11. Sun, C. L.; Li, B. J.; Shi, Z. J., *Chem. Rev.*, **2010,** *111* (3), 1293-1314.

12. Olivo, G.; Nardi, M.; Vìdal, D.; Barbieri, A.; Lapi, A.; Gómez, L.; Lanzalunga, O.; Costas, M.; Di Stefano, S., *Inorg. Chem.*, **2015,** *54* (21), 10141-10152.

13. Gómez, L.; Garcia-Bosch, I.; Company, A.; Benet-Buchholz, J.; Polo, A.; Sala, X.; Ribas, X.; Costas, M., *Angew. Chem.*, **2009,** *121* (31), 5830-5833.

14. Fenton, H., *Chem News*, **1876,** *33* (190), 190.

15. Retcher, B.; Costa, J. S.; Tang, J.; Hage, R.; Gamez, P.; Reedijk, J., *J. Mol. Catal. A: Chem.*, **2008,** *286* (1), 1-5.

16. Haslinger, S. Bioinspired Iron N-Heterocyclic Carbene Complexes in C–H Bond Oxidation: Reactivity, Electronic Properties, and Catalytic Activity. Universität München, 2015.

17. Gozzo, F., *J. Mol. Catal. A: Chem.*, **2001,** *171* (1), 1-22.

18. Russell, G. A., *J. Am. Chem. Soc.*, **1957,** *79* (14), 3871-3877.

19. Ensing, B.; Buda, F.; Baerends, E. J., *J. Phys. Chem. A*, **2003,** *107* (30), 5722-5731.

20. Sono, M.; Roach, M. P.; Coulter, E. D.; Dawson, J. H., *Chem. Rev.*, **1996,** *96* (7), 2841-2888.

21. Bryliakov, K. P.; Talsi, E. P., *Coord. Chem. Rev.*, **2014,** *276*, 73-96.

22. Meunier, B.; De Visser, S. P.; Shaik, S., *Chem. Rev.*, **2004,** *104* (9), 3947-3980.

23. Ortiz de Montellano, P. R., *Chem. Rev.*, **2009,** *110* (2), 932-948.

24. Farinas, E. T.; Schwaneberg, U.; Glieder, A.; Arnold, F. H., *Adv. Synth. Catal.*, **2001,** *343* (6-7), 601-606.

25. Meunier, B., *Chem. Rev.*, **1992,** *92* (6), 1411-1456.

26. Nam, W.; Lee, H. J.; Oh, S. Y.; Kim, C.; Jang, H. G., *J. Inorg. Biochem.*, **2000,** *80* (3), 219-225.

27. Nam, W., *Acc. Chem. Res.*, **2007,** *40* (7), 522-531.

28. Groves, J. T.; Kruper, W. J.; Nemo, T. E.; Myers, R. S., *J. Mol. Catal.*, **1980,** *7* (2), 169-177.

29. Groves, J. T.; Nemo, T. E., *J. Am. Chem. Soc.*, **1983,** *105* (20), 6243-6248.

30. Nappa, M. J.; Tolman, C. A., *Inorg. Chem.*, **1985,** *24* (26), 4711-4719.

31. Talsi, E. P.; Bryliakov, K. P., *Coord. Chem. Rev.*, **2012,** *256* (13), 1418-1434.

32. Nam, W.; Lee, Y.-M.; Fukuzumi, S., *Acc. Chem. Res.*, **2014,** *47* (4), 1146-1154.

33. Allpress, C. J.; Berreau, L. M., *Coord. Chem. Rev.*, **2013,** *257* (21), 3005-3029.

34. Haslinger, S.; Raba, A.; Cokoja, M.; Pöthig, A.; Kühn, F. E., *J. Catal.*, **2015,** *331*, 147-153.

35. Costas, M.; Chen, K.; Que, L., *Coord. Chem. Rev.*, **2000,** *200*, 517-544.

36. Bilis, G.; Christoforidis, K.; Deligiannakis, Y.; Louloudi, M., *Catal. Today*, **2010,** *157* (1), 101-106.

37. Lee, S. H.; Han, J. H.; Kwak, H.; Lee, S. J.; Lee, E. Y.; Kim, H. J.; Lee, J. H.; Bae, C.; Lee, S. N.; Kim, Y., *Chem. Eur. J.*, **2007,** *13* (33), 9393-9398.

38. Chen, K.; Que, L., *J. Am. Chem. Soc.*, **2001,** *123* (26), 6327-6337.

39. Chen, K.; Costas, M.; Kim, J.; Tipton, A. K.; Que, L., *J. Am. Chem. Soc.*, **2002,** *124* (12), 3026-3035.

40. Olivo, G.; Lanzalunga, O.; Di Stefano, S., *Adv. Synth. Catal.*, **2016,** *358* (6), 843-863.

41. Mekmouche, Y.; Ménage, S.; Toia-Duboc, C.; Fontecave, M.; Galey, J. B.; Lebrun, C.; Pécaut, J., *Angew. Chem. Int. Ed.*, **2001,** *40* (5), 949-952.

42. Comba, P.; Maurer, M.; Vadivelu, P., *Inorg. Chem.*, **2009,** *48* (21), 10389-10396.

43. Gavrilova, A. L.; Bosnich, B., *Chem. Rev.*, **2004,** *104* (2), 349-384.

44. Hong, S.; Lee, Y. M.; Cho, K. B.; Sundaravel, K.; Cho, J.; Kim, M. J.; Shin, W.; Nam, W., *J. Am. Chem. Soc.*, **2011,** *133* (31), 11876-11879.

45. England, J.; Davies, C. R.; Banaru, M.; White, A. J.; Britovsek, G. J., *Adv. Synth. Catal.*, **2008,** *350* (6), 883-897.

46. Mas-Ballesté, R.; Costas, M.; van den Berg, T.; Que, L., *Chem. Eur. J.*, **2006,** *12* (28), 7489-7500.

47. England, J.; Britovsek, G. J.; Rabadia, N.; White, A. J., *Inorg. Chem.*, **2007,** *46* (9), 3752-3767.

48. Costas, M.; Que Jr, L., *Angew. Chem.*, **2002,** *114* (12), 2283-2285.

49. Leising, R. A.; Norman, R. E.; Que Jr, L., *Inorg. Chem.*, **1990,** *29* (14), 2553-2555.

50. Kojima, T.; Leising, R. A.; Shiping, Y.; Que Jr, L., *J. Am. Chem. Soc.*, **1993,** *115* (24), 11328-11335.

51. Chen, M. S.; White, M. C., *Science*, **2007,** *318* (5851), 783-787.

52. Olivo, G.; Cussó, O.; Borrell, M.; Costas, M., *J. Biol. Inorg. Chem.*, **2017,** *22* (2-3), 425-452.

53. White, M. C.; Doyle, A. G.; Jacobsen, E. N., *J. Am. Chem. Soc.*, **2001,** *123* (29), 7194-7195.

54. Costas, M.; Tipton, A. K.; Chen, K.; Jo, D. H.; Que, L., *J. Am. Chem. Soc.*, **2001,** *123* (27), 6722-6723.

55. He, Y.; Gorden, J. D.; Goldsmith, C. R., *Inorg. Chem.*, **2011,** *50* (24), 12651-12660.

56. Wu, M.; Miao, C. X.; Wang, S.; Hu, X.; Xia, C.; Kühn, F. E.; Sun, W., *Adv. Synth. Catal.*, **2011,** *353* (16), 3014-3022.

57. Cussó, O.; Garcia-Bosch, I.; Ribas, X.; Lloret-Fillol, J.; Costas, M., *J. Am. Chem. Soc.*, **2013,** *135* (39), 14871-14878.

58. Cussó, O.; Ribas, X.; Lloret-Fillol, J.; Costas, M., *Angew. Chem. Int. Ed.*, **2015,** *54* (9), 2729-2733.

59. Tanaka, S.; Kon, Y.; Nakashima, T.; Sato, K., *RSC Adv.*, **2014,** *4* (71), 37674-37678.

60. Join, B.; Möller, K.; Ziebart, C.; Schröder, K.; Gördes, D.; Thurow, K.; Spannenberg, A.; Junge, K.; Beller, M., *Adv. Synth. Catal.*, **2011,** *353* (16), 3023-3030.

61. Han, J. H.; Yoo, S.K.; Seo, J. S.; Hong, S. J.; Kim, S. K.; Kim, C., *Dalton Trans.*, **2005,** (2), 402-406.

62. Balogh-Hergovich, É.; Speier, G., *J. Mol. Catal. A: Chem.*, **2005,** *230* (1), 79-83.

63. Bose, S.; Pariyar, A.; Biswas, A. N.; Das, P.; Bandyopadhyay, P., *Catal. Commun.*, **2011,** *12* (6), 446-449.

64. Pavan, C.; Legros, J.; Bolm, C., *Adv. Synth. Catal.*, **2005,** *347* (5), 703-705.

65. Fernandes, R. R.; Lasri, J.; da Silva, M. F. C. G.; Da Silva, J. A.; da Silva, J. J. F.; Pombeiro, A. J., *Appl. Catal., A*, **2011,** *402* (1), 110-120.

Chapter 3

Evaluation of (*R,R*) bis-heterocyclic secondary diamine Fe(II) complexes in the oxidation of *cis*-cyclooctene

3.1 Introduction

In the chemical industry, an important goal is the development of methods for the formation of carbon-heteroatom bonds from unfunctionalised substrates. These oxidised products have various applications in biological, chemical, pharmaceutical and agrochemical industries.[1] The products formed are also used as intermediates for flavouring compounds, dyes, perfumes and plastic additives.[2] There has been extensive research on the use of non-heme iron complexes for the oxidation of various alkane and alkene substrates.[3, 4, 5] Most of the ligands investigated possess tetradentate nitrogen donor atoms, but differ in the structure of the ligand backbone as well as the substituents present in the ligand framework. The structure of these ligands plays a significant role in the catalytic activity seen for the resulting complexes. The best activity have been observed for complexes bearing ligands that have a strong ligand field and are stable against degradation. In most cases, these are ligands that have pyridine donors and no substituents on the pyridine ring.[6, 7] The investigation into diimine and secondary diamine ligands is not very extensive, due to the belief that these bonds are not robust enough to withstand the oxidising environment.[8] It is believed that the imine bond is prone to hydrolysis and the Lewis acid character of the metal can accelerate this process. This leads to ligand degradation and causes the metal cation to be released into the solution.[8] There has been a great deal of investigation into non-heme iron complexes and from most of the research it is evident that a crucial point is ligand design. An efficient ligand design process will result in good activity as well as selectivity.

This chapter details the synthesis of diimine and secondary diamine non-heme ligands and their iron(II)-triflate complexes. The ability of these complexes to catalyse the oxidation of *cis*-cyclooctene will also be investigated. Lastly, the investigation into the stability of the complexes during catalysis will be described.

3.2 Synthesis of ligands and complexes

The first step in synthesising the ligands was the isolation of (*R,R*)-1,2-diaminocyclohexane from a mixture of *cis* and *trans* 1,2-diaminocyclohexane. This specific conformer can be isolated by the reaction with L-(+)-tartaric acid. The product was isolated as the (*R,R*)-1,2-diaminocyclohexane mono-(+)-tartrate salt (Scheme 3.1).

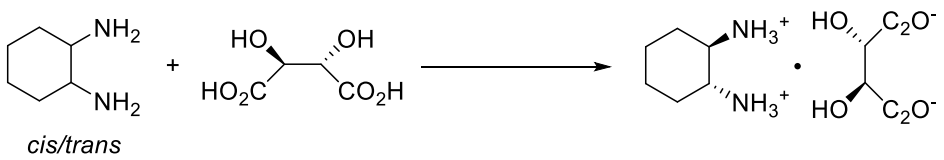

Scheme 3.1: Isolation of (*R,R*)-1,2-diaminocyclohexane by using L-(+)-tartaric acid.

For the synthesis of the diimine ligands, the (*R,R*)-1,2-diaminocyclohexane mono-(+)-tartrate salt was reacted with different carboxaldehydes. Research has found that ligands that have pyridine donors are the most active in oxidation reactions,[6] and therefore we employed 2-pyridinecarboxaldehyde, as well as 6-methyl and 6-bromo-2-pyridinecarboxaldehyde. The effect of electron-donating and electron-withdrawing substituents on the catalytic activity can then be investigated. We also decided to replace the pyridine donor with imidazole and quinoline donors to investigate the effect that structural changes in the donor would have on the catalytic activity of the complexes. Scheme 3.2 shows the reaction scheme for the synthesis of the ligands and Figure 3.1 depicts the five different diimine ligands synthesised.

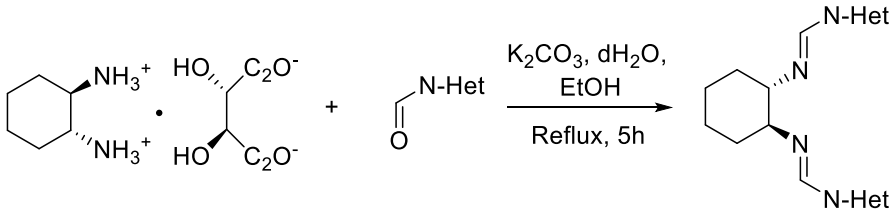

Scheme 3.2: Synthesis of diimine ligands from (*R,R*)-1,2-diaminecyclohexane mono-(+)-tartrate salt and a carboxaldehyde.

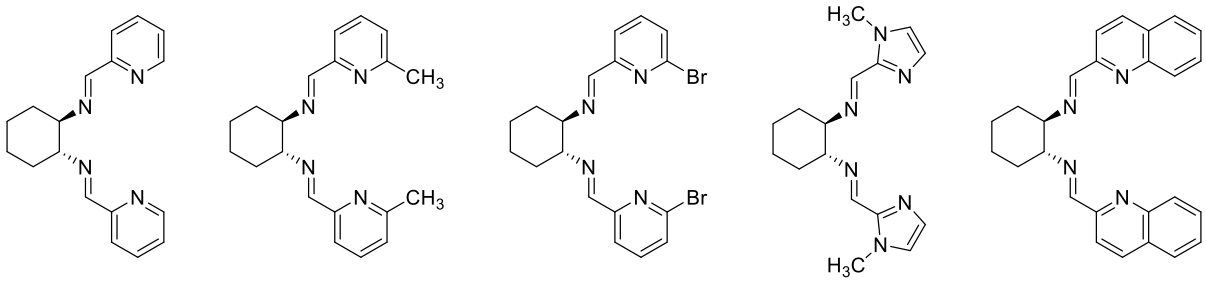

(*R,R*)-L3.1 **(*R,R*)-L3.2** **(*R,R*)-L3.3** **(*R,R*)-L3.4** **(*R,R*)-L3.5**

Figure 3.1: Set of diimine ligands synthesised by reacting (*R,R*)-1,2-diaminocyclohexane mono-(+)-tartrate salt with the corresponding carboxaldehyde.

(*R,R*)-L3.3 and **(*R,R*)-L3.5** precipitated after the addition of H_2O to the reaction mixture and were isolated as white solids. **(*R,R*)-L3.1**, **(*R,R*)-L3.2** and **(*R,R*)-L3.4** did not precipitate and had to be extracted with dichloromethane. The products were obtained as yellow oils. These ligands were isolated in poor to good yields (20 to 80%) and characterised by FT-IR and NMR spectroscopy.

3.2.1 FT-IR spectroscopic data of (*R,R*) diimine ligands, L3.1 to L3.5

The FT-IR spectra of the isolated diimine ligands, **(*R,R*)-L3.1** to **(*R,R*)-L3.5**, showed a characteristic $\nu_{C=N}$ absorption band in the range of 1640 to 1650 cm^{-1}.[9] In addition, no aldehyde absorption was observed, confirming complete condensation (Figure 3.2). In the FT-IR spectra, two absorption bands are visible in the range of 2860 to 2930 cm^{-1}, which represent the C-H stretching vibrations of cyclohexane. The C=N stretch absorption band of the pyridine

and quinoline rings is visible as an intense peak in the range of 1590 to 1610 cm^{-1}. The FT-IR spectroscopic data corresponds well with reported data.[10] The characteristic $\nu_{C=N}$ absorption band value for **(*R,R*)-L3.1** to **(*R,R*)-L3.5** is provided in Table 3.1.

Table 3.1: Absorption bands of $\nu_{C=N}$ for **(*R,R*)-L3.1** to **(*R,R*)-L3.5**.

Entry	Ligand	FT-IR ($\nu_{C=N}$)[a]
1	**(*R,R*)-L3.1**	1643
2	**(*R,R*)-L3.2**	1640
3	**(*R,R*)-L3.3**	1646
4	**(*R,R*)-L3.4**	1646
5	**(*R,R*)-L3.5**	1649

[a] Unit in cm^{-1}. Absorption band represents the acyclic $\nu_{C=N}$.

3.2.2 ^{1}H NMR spectroscopic data of (*R,R*) diimine ligands, L3.1 to L3.5

The imine proton resonance is observed as a singlet in the range of δ 8.10 to 8.40 ppm. The ligands are symmetrical, which results in all the peaks in the aromatic region integrating for two protons. The number of signals and the splitting pattern in the aromatic region corresponds to the expected ^{1}H NMR spectrum for the desired diimine ligand. For example, the aromatic region of **(*R,R*)-L3.1** integrates for a total of eight protons, the expected number for two pyridine donors (Figure 3.3).

The cyclohexyl proton resonances for **(*R,R*)-L3.1** to **(*R,R*)-L3.5** are poorly resolved and observed as broad multiplets (Figure 3.4). The integration values correspond to the number of protons (ten) that are present in the aliphatic region of the ligand.

The ^{1}H NMR spectral data of the diimine ligands, **(*R,R*)-L3.1** to **(*R,R*)-L3.5**, confirm that the correct product was formed and correlate well with data previously reported in literature.[10]

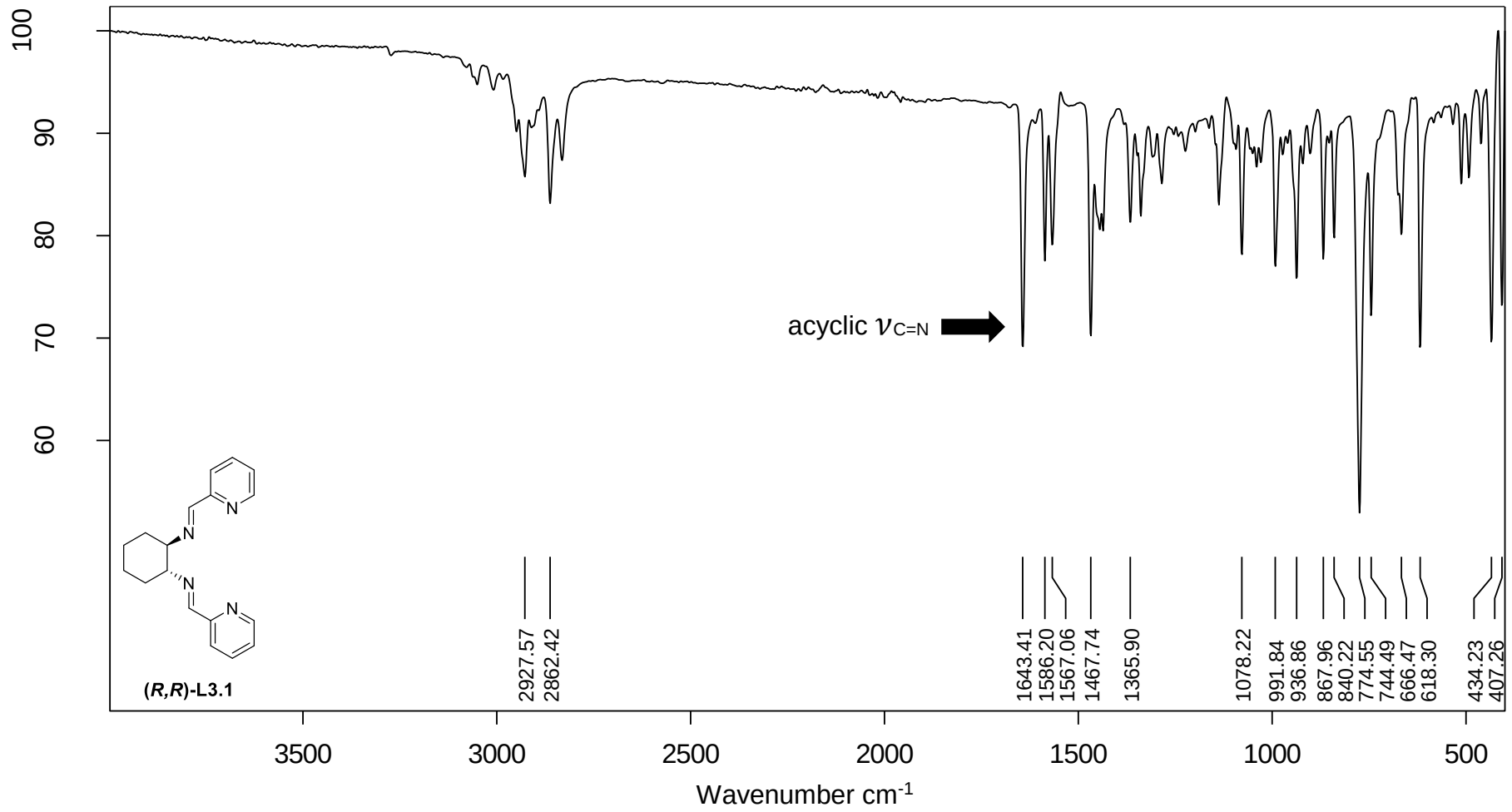

Figure 3.2: IR spectrum of **(*R*,*R*)-L3.1**.

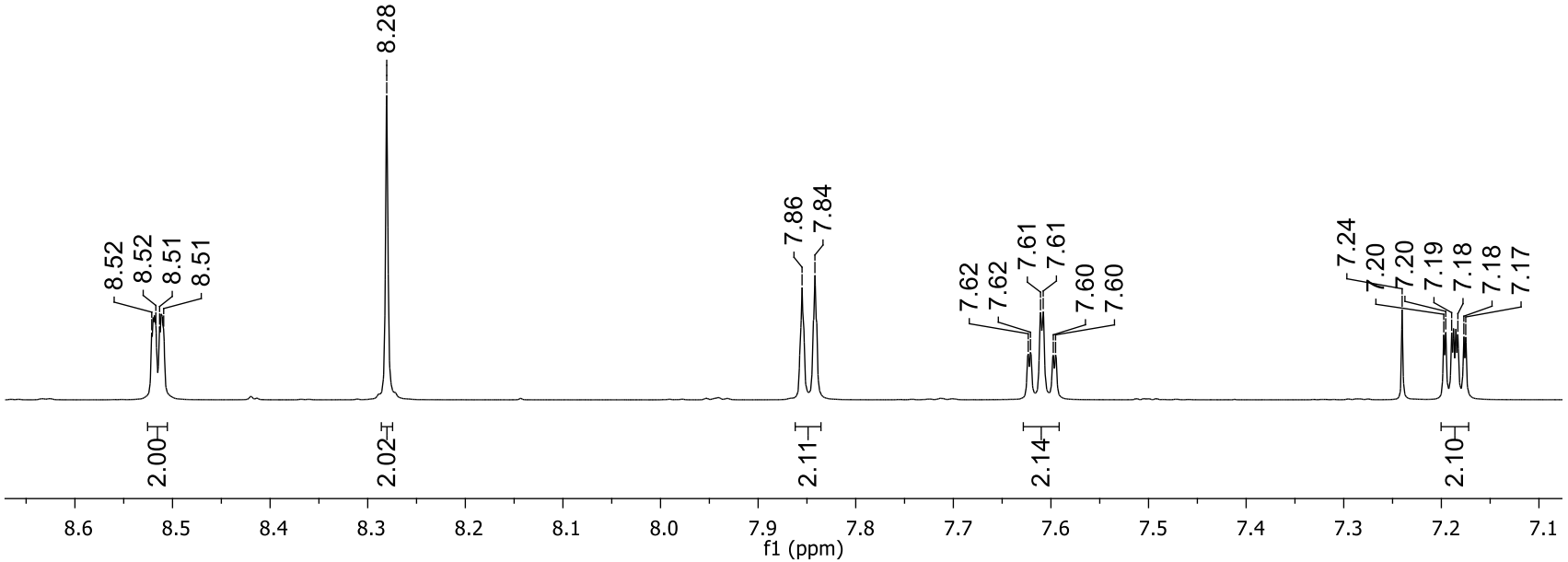

Figure 3.3: ^{1}H NMR spectrum of the aromatic region of **(*R*,*R*)-L3.1**.

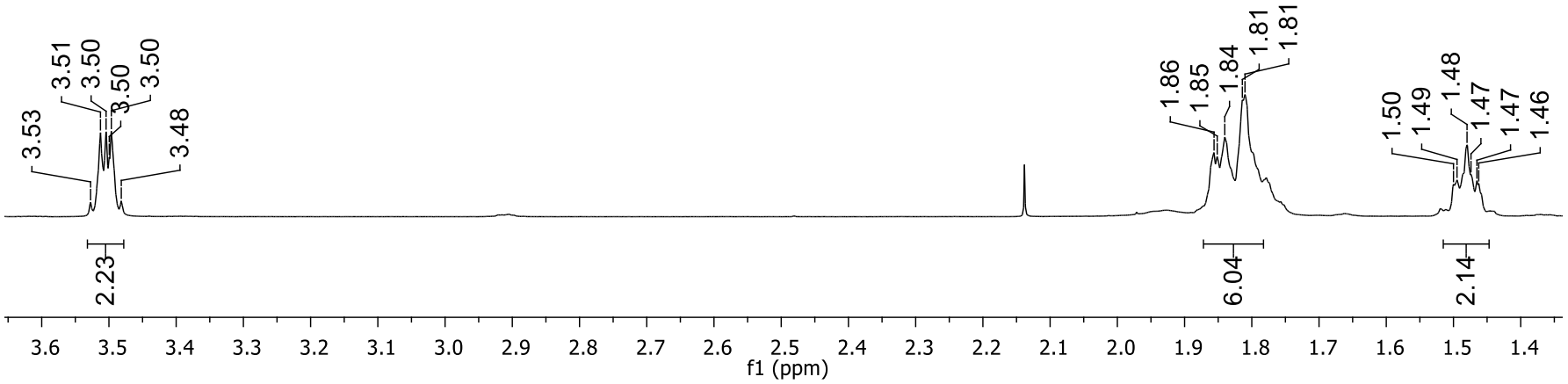

Figure 3.4: ^{1}H NMR spectrum of the aliphatic region of **(*R*,*R*)-L3.1**.

3.2.3 Complex synthesis with diimine ligands: Reaction of (*R,R*)-L3.1 with $FeCl_3$.

The diimine ligands are relatively easy to prepare and are less investigated in iron oxidation catalysis than the analogous amine ligands, so it was decided to react **(*R,R*)-L3.1** with $FeCl_3$ to synthesise the corresponding complex, **C3.1a**. The ligand and $FeCl_3$ were each dissolved in acetonitrile, added together and refluxed for 1 hour. A yellow product precipitated and was filtered off. This product was characterised by elemental analysis and the experimental results were C, 39.18; H, 4.33; N, 11.31. The calculated data for this complex is C, 51.58; H, 4.81; N, 13.37. The experimental and calculated data do not correlate. The experimental data corresponds with the calculated elemental analysis data of the hydrolysed ligand, complexing with $FeCl_3$. This means that during the reaction, one of the CH=N bonds break and the resulting complex is only coordinated to three nitrogen donor atoms (Scheme 3.3).

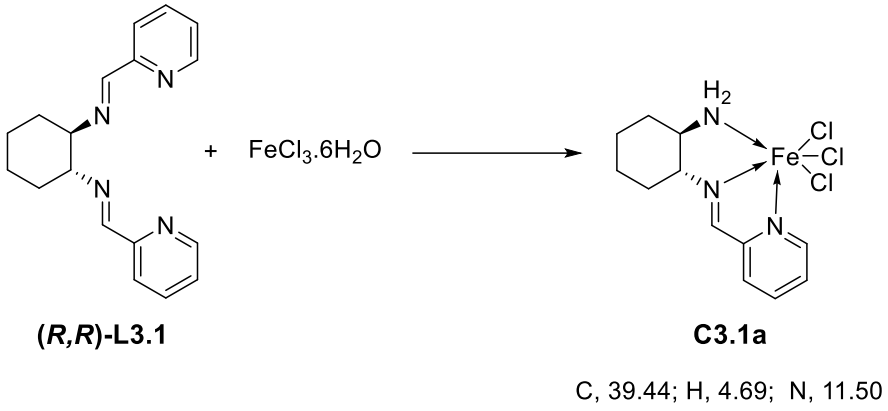

Scheme 3.3: Reacting **(*R,R*)-L3.1** with $FeCl_3.6H_2O$ results in the hydrolysis of one of the CH=N bonds. % Calculated: C, 39.44; H, 4.69; N, 11.50. Elemental analysis found C, 39.18; H, 4.33; N, 11.31.

This provides experimental evidence that the CH=N bond has lower stability and is prone to hydrolysis. Due to these results, it was decided to reduce the ligands to the more stable secondary diamine derivatives (Figure 3.5). The diimine ligands were reduced with $NaBH_4$ and were isolated as light to dark yellow oils. The reduced ligands were characterised with FT-IR and NMR spectroscopy. All of the below ligands have been reported previously, but have not been used to prepare complexes with $Fe(OTf)_2$ as catalysts for the oxidation of hydrocarbons.

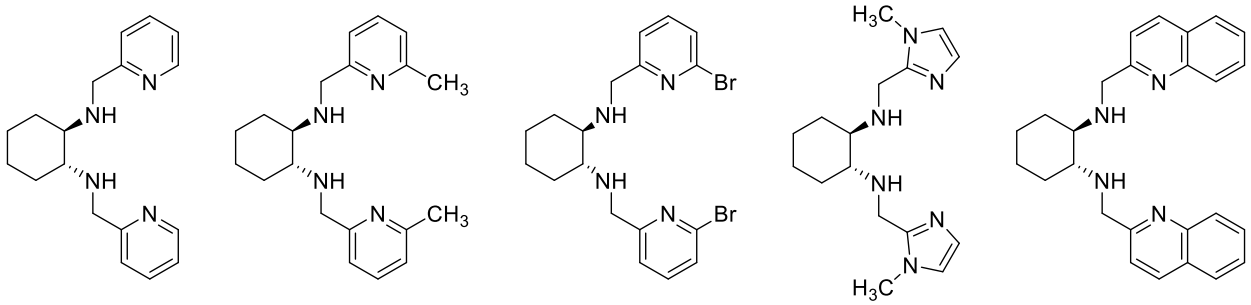

Figure 3.5: Secondary diamine ligand set resulting from the reduction of **(*R,R*)-L3.1** to **(*R,R*)-L3.5**.

3.2.4 FT-IR spectroscopic data of (*R,R*) secondary diamine ligands, L3.6 to L3.10

The FT-IR spectra of **(*R,R*)-L3.6** to **(*R,R*)-L3.10** do not show the characteristic $\nu_{C=N}$ absorption band as well as no aldehyde absorption band. The secondary diamine absorption bands are represented by a small, broad peak at ~3200 cm^{-1} and the absorption band at ~1590 cm^{-1} is due to the cyclic imine stretch (Figure 3.6).

3.2.5 ^{1}H NMR spectroscopic data of (*R,R*) secondary diamine ligands, L3.6 to L3.10

For **(*R,R*)-L3.6** to **(*R,R*)-L3.10**, no imine proton resonance in the range of δ 8.10 to 8.40 ppm is observed (Figure 3.7). The aliphatic region of **(*R,R*)-L3.6** to **(*R,R*)-L3.10** is characterised by two doublets in the range of δ 3.80 to 4.10 ppm that integrate for two protons each. These resonances may be assigned to the NH-CH_2 groups, which are now present after the diimine ligand was reduced (Figure 3.8). The broad peak observed at 2.65 ppm is assigned to the N-*H* resonance. The peaks for the cyclohexane ring are more defined compared to the diimine ligands and the integration values correspond with the number of protons that are expected in the aliphatic region. The ^{1}H NMR data reported here correspond to literature data reported for these ligands.[11]

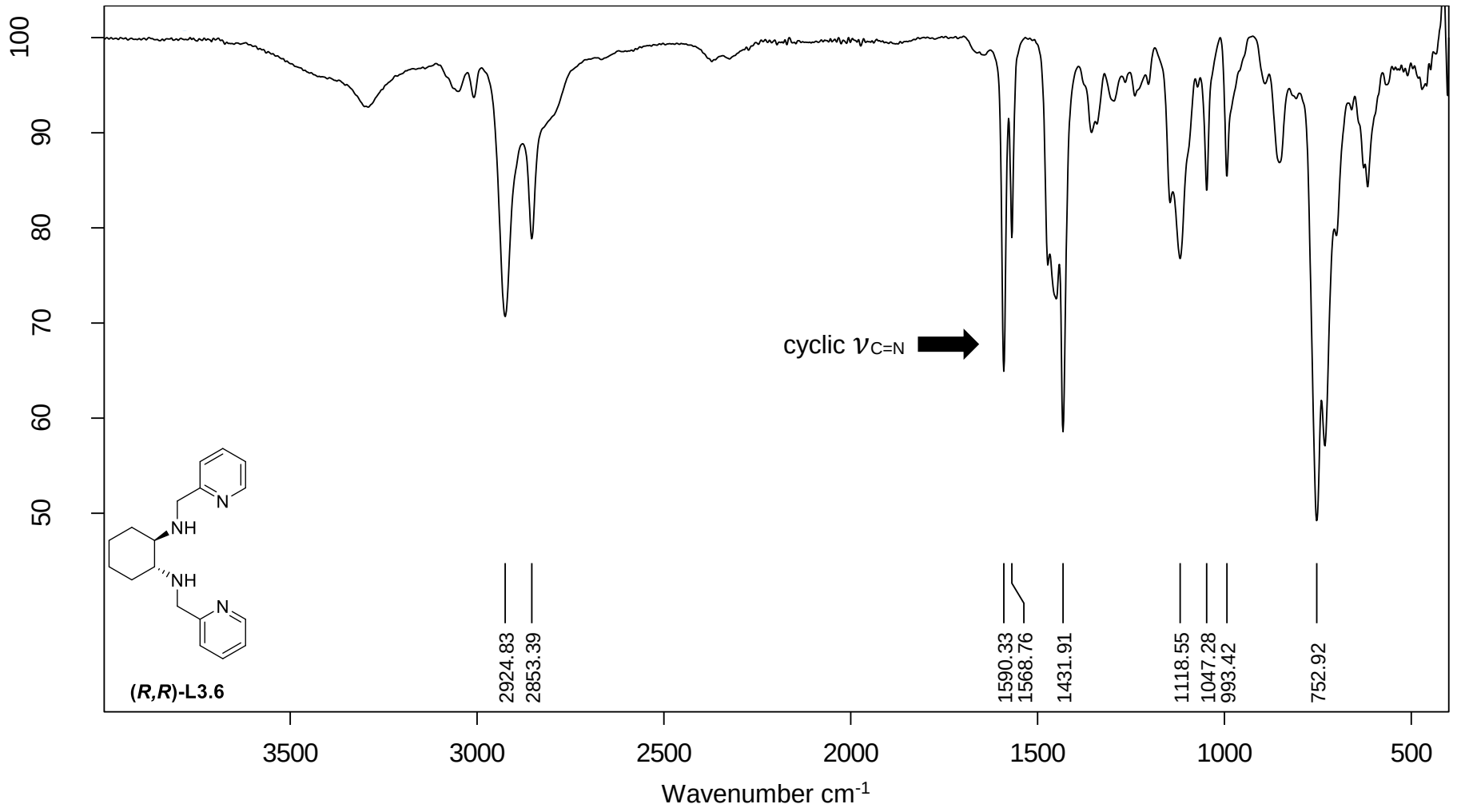

Figure 3.6: FT-IR spectrum of **(*R,R*)-L3.6**.

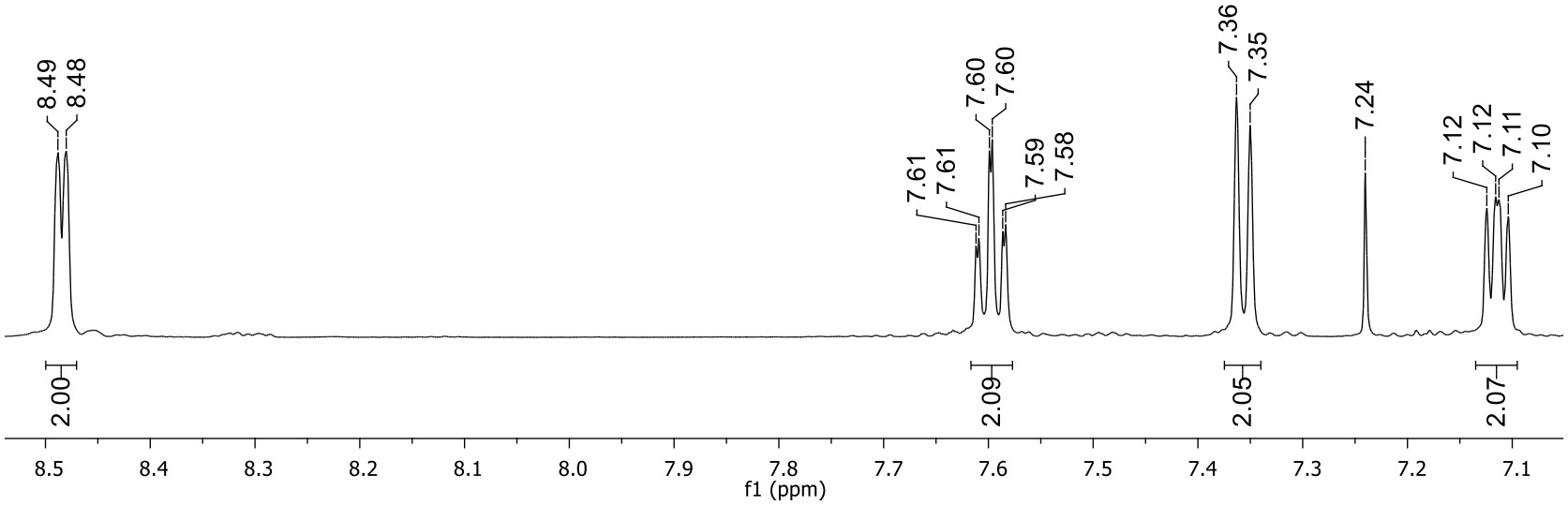

Figure 3.7: ^{1}H NMR spectrum of the aromatic region of **(*R*,*R*)-L3.6**.

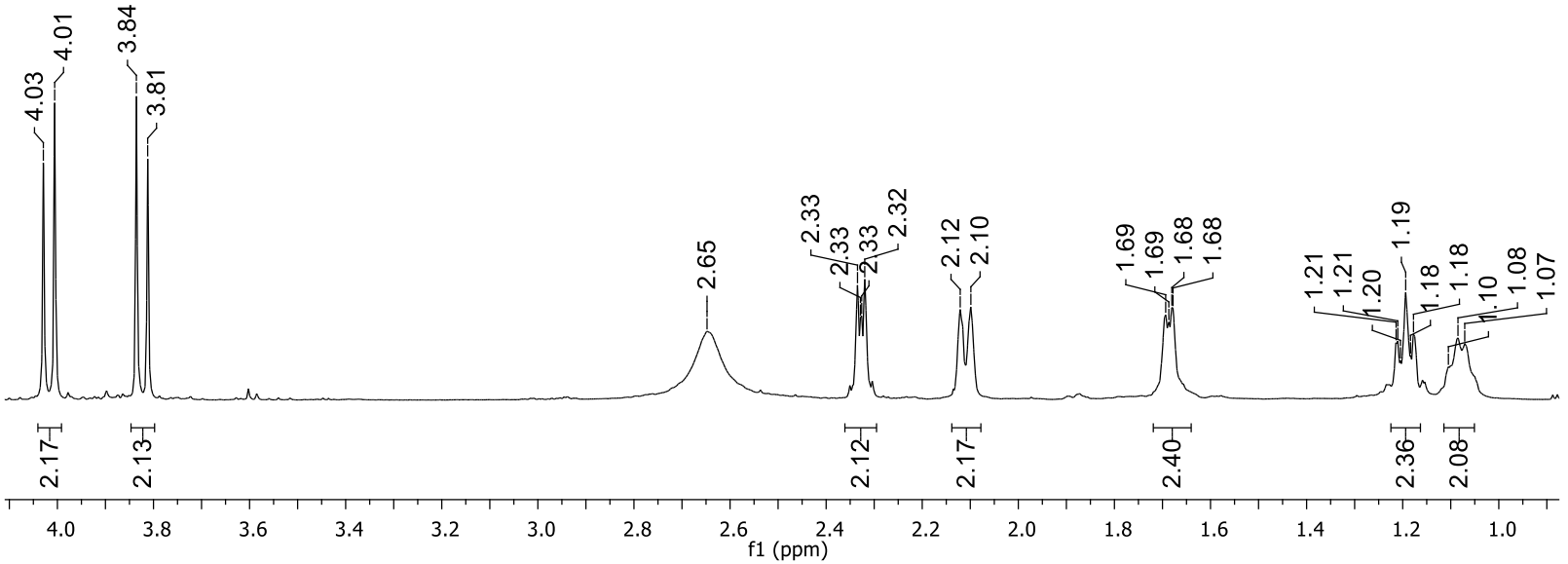

Figure 3.8: ^{1}H NMR spectrum of the aliphatic region of **(*R*,*R*)-L3.6**.

3.2.6 Complex synthesis with (*R,R*) secondary diamine ligands: Reaction of the diamine ligands L3.6 to L3.10 with $Fe(OTf)_2$

The corresponding (*R,R*) bis-heterocyclic secondary diamine ligands were reacted with $Fe(OTf)_2$ in dry acetonitrile (Scheme 3.4 and Figure 3.9). The solvent was removed under vacuum, and the addition of diethyl ether resulted in the product precipitating. This method was used for the preparation of all the complexes.

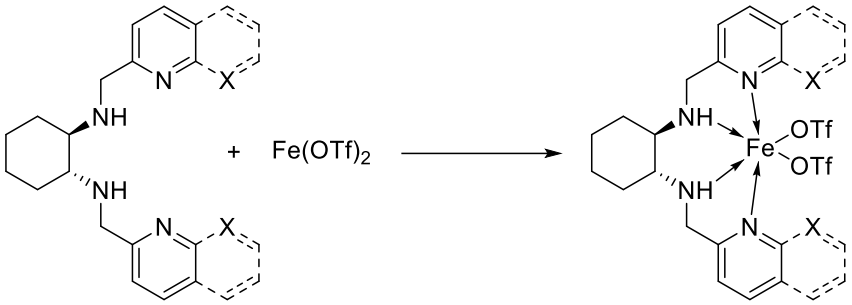

Scheme 3.4: Synthesis of the iron(II) complexes.

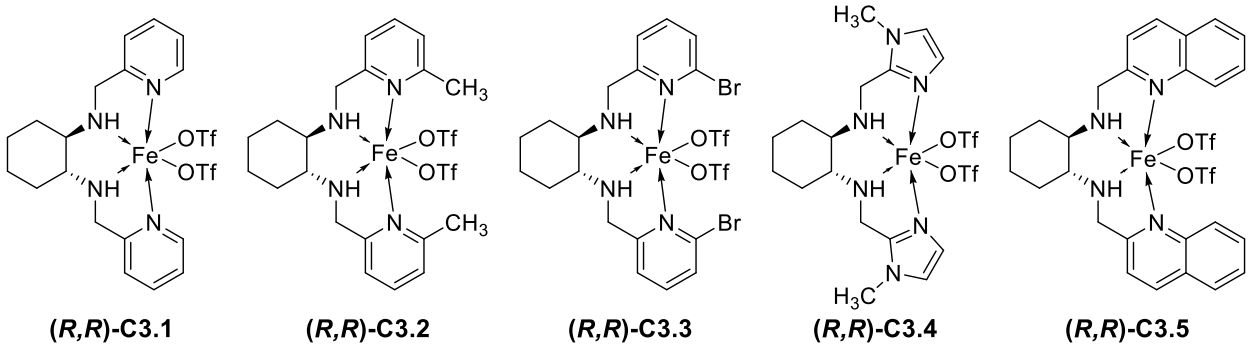

Figure 3.9: Iron(II) complexes synthesised employing **(*R,R*)-L3.6** to **(*R,R*)-L3.10**.

The complexes were synthesised in low to moderate yields (24 to 55%) and isolated as solids. **(*R,R*)-C3.1** was isolated as a red powder, **(*R,R*)-C3.2** and **(*R,R*)-C3.3** as yellow powders, **(*R,R*)-C3.4** as an orange powder and **(*R,R*)-C3.5** as a green powder. These complexes displayed air- and moisture-sensitivity and were stored under an argon atmosphere in a glove box. All the complexes were characterised by ESI mass spectrometry, elemental analysis and UV-Vis spectroscopy. The ESI-MS spectra of the complexes displayed a characteristic fragment that correspond with the complex minus one triflate group as has been seen for other triflate complexes.[12] For **(*R,R*)-C3.3**, the molar mass is 808.18 g/mol and $[M\text{-}OTf]^+$ is 659.12 g/mol, which is the fragment seen in the ESI-MS spectrum and confirms that the correct complex has been formed (Figure 3.10). There is also good correlation between the simulated and experimental isotope pattern. The same fragmentation pattern is seen for the other synthesised complexes.

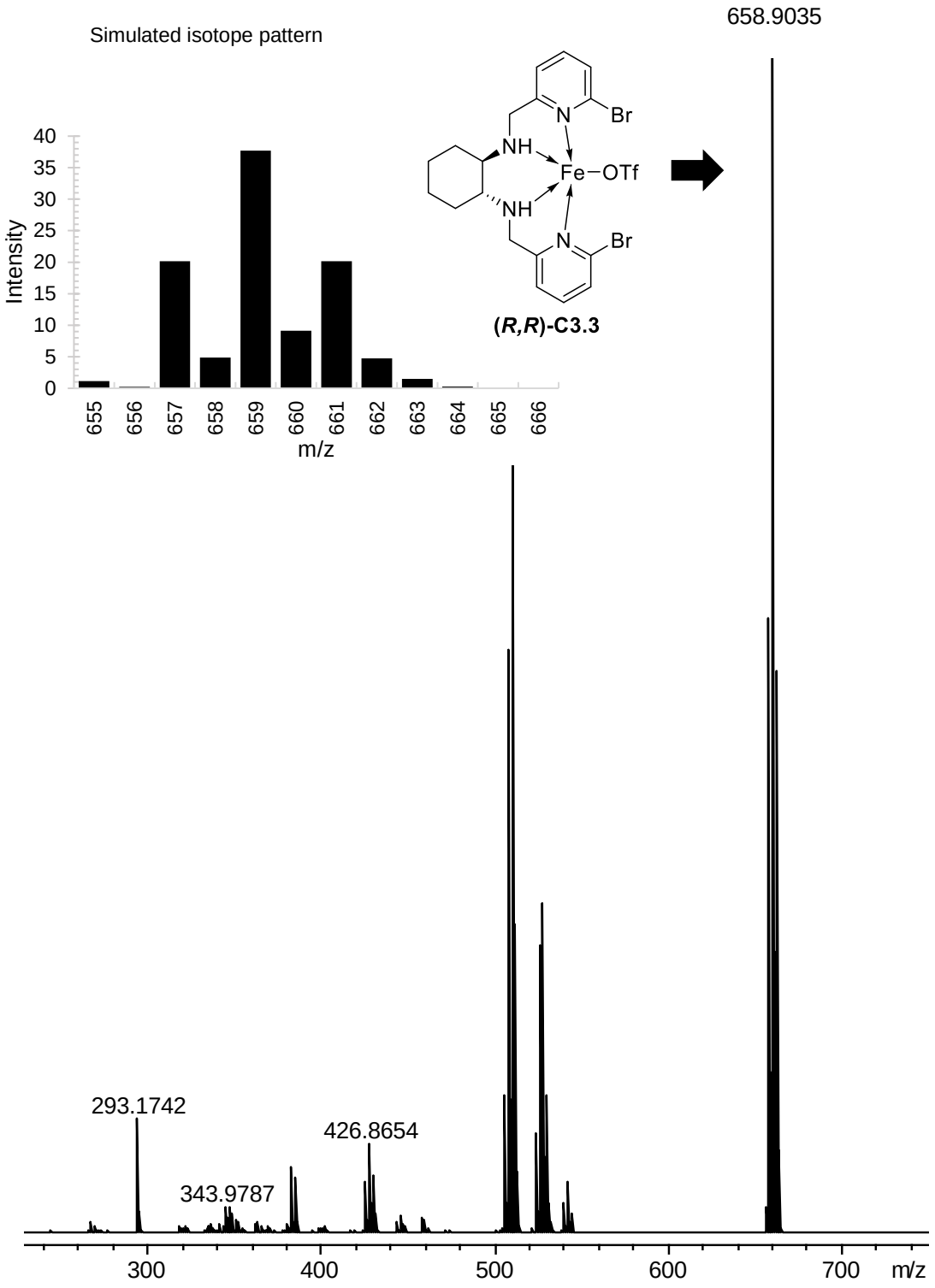

Figure 3.10: MS spectrum and simulated isotope pattern of **(*R,R*)-C3.3**.

Elemental analysis was used to determine the composition of the synthesised complexes, but accurate elemental analysis could not be obtained because of the instability of these complexes. The difference between the calculated and experimental data also indicated that there was still residual solvent present in the complexes (Table 3.2).

Table 3.2: Comparison between the **experimental** and (calculated) elemental analysis data for the secondary diamine iron(II) complexes

Entry	Catalyst	C	H	N
1	**(*R,R*)-C3.1**	**34.42** (36.93)	**4.59** (3.72)	**7.87** (7.96)
2	**(*R,R*)-C3.2**	**28.50** (38.95)	**3.67** (4.16)	**5.74** (8.26)
3	**(*R,R*)-C3.3**	**25.28** (29.72)	**3.51** (2.74)	**5.49** (6.93)
4	**(*R,R*)-C3.4**	**26.55** (32.94)	**3.74** (3.99)	**9.82** (12.80)
5	**(*R,R*)-C3.5**	**43.73** (44.81)	**3.66** (3.76)	**7.28** (7.74)

The UV-Vis spectra for the secondary diamine iron(II) complexes are shown in Figure 3.11. In the range of 200 to 300 nm, an intense band dominates the spectrum. This absorption can be attributed to ligand-centred π-π* transitions.[13, 14] In other iron(II) complexes, the UV-Vis spectrum shows a strong absorption at ~400 nm, which is a result of metal-to-ligand charge transfer between the ligand π* orbitals and the t_{2g} orbitals of iron(II).[15, 16] For this specific iron(II) complexes, **(*R,R*)-C3.1** shows a weak absorption in this specific region, while for **(*R,R*)-C3.2** to **(*R,R*)-C3.5**, a band is not visible in this region. A decrease in the intensity of the metal-to-ligand charge transfer absorption means a decrease in the concentration of complexes in which the metal is in the low-spin configuration. This is a result of the complexes possessing a weak ligand field.

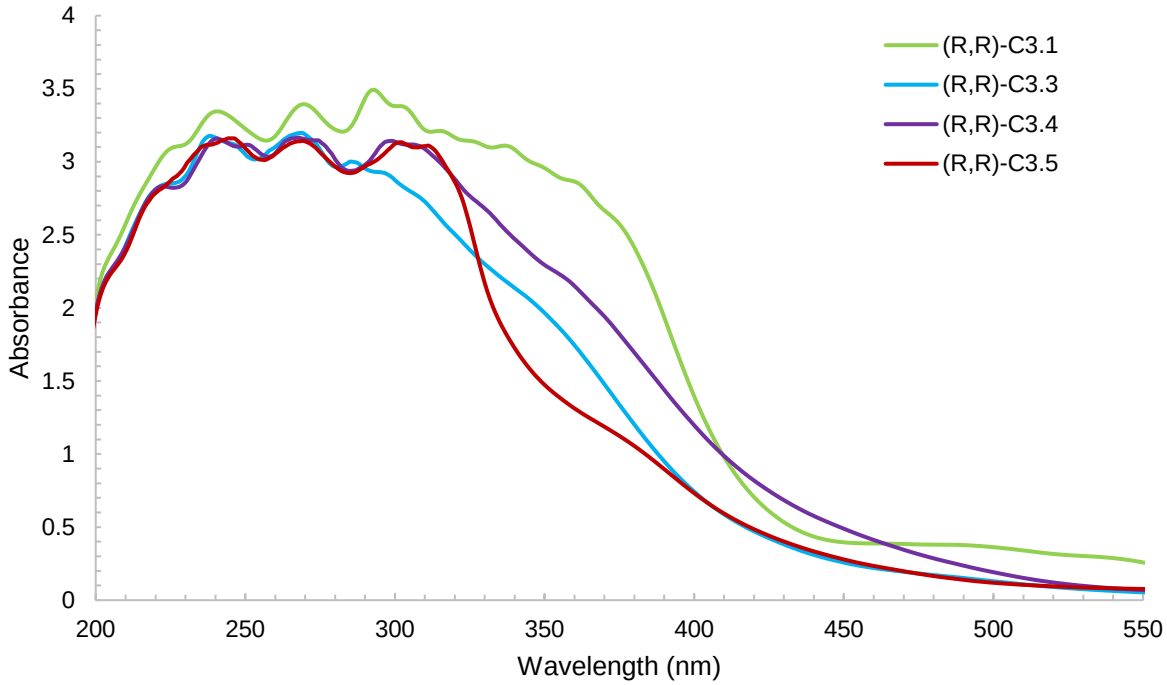

Figure 3.11: UV-Vis spectra of the (*R,R*) secondary diamine complex set, **(*R,R*)-C3.1** to **(*R,R*)-C3.5**.

3.3 Catalytic oxidation of *cis*-cyclooctene

Cis-cyclooctene was oxidised in the presence H_2O_2 to evaluate the catalytic properties of iron(II) complexes containing **(*R,R*)-L3.6** to **(*R,R*)-L3.10** (Scheme 3.5).

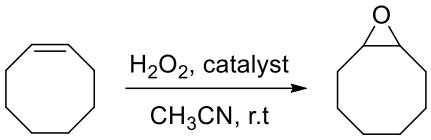

Scheme 3.5: Catalytic epoxidation of *cis*-cyclooctene.

The oxidation reactions were carried out at room temperature in air with acetonitrile as the solvent. Hydrogen peroxide was added with a syringe pump over a period of 25 minutes. A problem with the use of H_2O_2 as oxidant is that it easily decomposes to hydroxyl radicals, which leads to unselective oxidation. However, addition with a syringe pump eliminates this problem. This reaction was done under substrate-limiting conditions. Table 3.3 provides the conversion (%), turnover number as well as oxidation efficiency for the five complexes.

Table 3.3: Oxidation of *cis*-cyclooctene with **(*R,R*)-C3.1** to **(*R,R*)-C3.5**[a]

Entry	Catalyst	% Conversion[b]	Turnover number[c]	Oxidation efficiency[d]
1	**(*R,R*)-C3.1**	31.68	12.67	17.60
2	**(*R,R*)-C3.2**	30.39	12.20	17.00
3	**(*R,R*)-C3.3**	29.89	11.96	16.61
4	**(*R,R*)-C3.4**	29.97	12.00	16.65
5	**(*R,R*)-C3.5**	24.03	9.60	13.50

[a] Reaction conditions: See experimental section. [b] (moles of substrate converted/moles of substrate added) x 100. [c] (moles of product/moles of catalyst) [d] (moles of product/moles of oxidant) x 100. The data reported is the average of two runs.

The most active catalyst, **(*R,R*)-C3.1**, displayed a conversion of approximately 32% to cyclooctene oxide as sole product and an oxidation efficiency of only 17%. When comparing the conversion, turnover number and oxidation efficiency of all the complexes, it is evident that there is barely any difference between them. One would have expected to see a difference due to the variation in the steric and electronic properties of these complexes. [7, 17, 18, 19] However, because the activity is more or less the same for all the complexes, it may be reasonable to assume that the different steric and electronic properties do not have an influence on the observed catalytic activity of the secondary diamine iron(II) complexes. The observed catalytic activity may be attributed to the inherent instability of the complexes, as evident from elemental analysis.

Different additives can also be used to improve the efficiency of the oxidation reaction. The most common additive used is acetic acid. There are various examples that show the use of these additives increased the conversion, turnover number and yield. It is believed that the addition of acetic acid promotes heterolytic cleavage of the Fe^{III}-OOH species and this results in the formation of Fe^{V}-oxo species, which leads to better catalytic activity as well as selectivity.[3, 20, 21] In certain instances, H_2O is also added, which provides an O-atom that is incorporated into the product.[22]

(*R,R*)-C3.1, which showed the best activity, was also investigated as catalyst in the presence of H_2O and acetic acid additives. The data is reported in Table 3.4. The addition of these additives had a negligible effect on the activity seen for **(*R,R*)-C3.1**. It seems likely that the stability of the ligand dominates the catalytic activity and because these complexes are unstable, not even the additives cause an increase in catalytic activity. A strong ligand field is needed to stabilise the high-valent iron-oxo species that are formed during the oxidation reaction. It appears that the

secondary diamine iron(II) complexes have a weak ligand field, as evidenced by UV-Vis spectroscopy, and resulted in poor catalytic activity.

Table 3.4: Oxidation of *cis*-cyclooctene with **(*R,R*)-C3.1** in the presence of different additives[a]

Catalyst	% Conversion[b]	Turnover number[c]	Oxidation efficiency[d]
(*R,R*)-C3.1	31.68	12.67	17.60
Added H_2O	21.15	8.5	11.75
Added AcOH	32.05	12.8	17.80

[a] Reaction conditions: See experimental section. [b] (moles of substrate converted/moles of substrate added) x 100. [c] (moles of product/moles of catalyst) [d] (moles of product/moles of oxidant) x 100. The data reported is the average of two runs.

3.4 Investigation of the stability of the ligand and complex

Because all the catalysts exhibited similar catalytic activity, we decided to investigate the stability of the secondary diamine ligands and their Fe(II) complexes. This was done by reacting the ligand with H_2O_2 in the absence of the substrate and $Fe(OTf)_2$. If the ligand is oxidised, FT-IR spectroscopy would show the formation of the imine absorption band. The ligand, **(*R,R*)-L3.6**, was dissolved in acetonitrile and H_2O_2 was added with a syringe pump over a period of 25 minutes. After the addition, the solution was stirred for 72 hours. The solvent was removed and an IR spectrum of the resulting product was recorded. The formation of a low intensity peak was visible at 1640 cm^{-1} (Figure 3.12) and provided experimental evidence that the ligand may be oxidised during the reaction, leading to imine formation. This causes the catalyst to be prone to degradation and inhibits the catalytic activity. Earlier on, we showed that reacting the diimine ligand with an iron precursor resulted in the hydrolysis of one of the bonds. The imine bonds was not stable against degradation and this results in the low catalytic activity seen for all the (*R,R*) bis-heterocyclic secondary diamine iron(II) complexes.

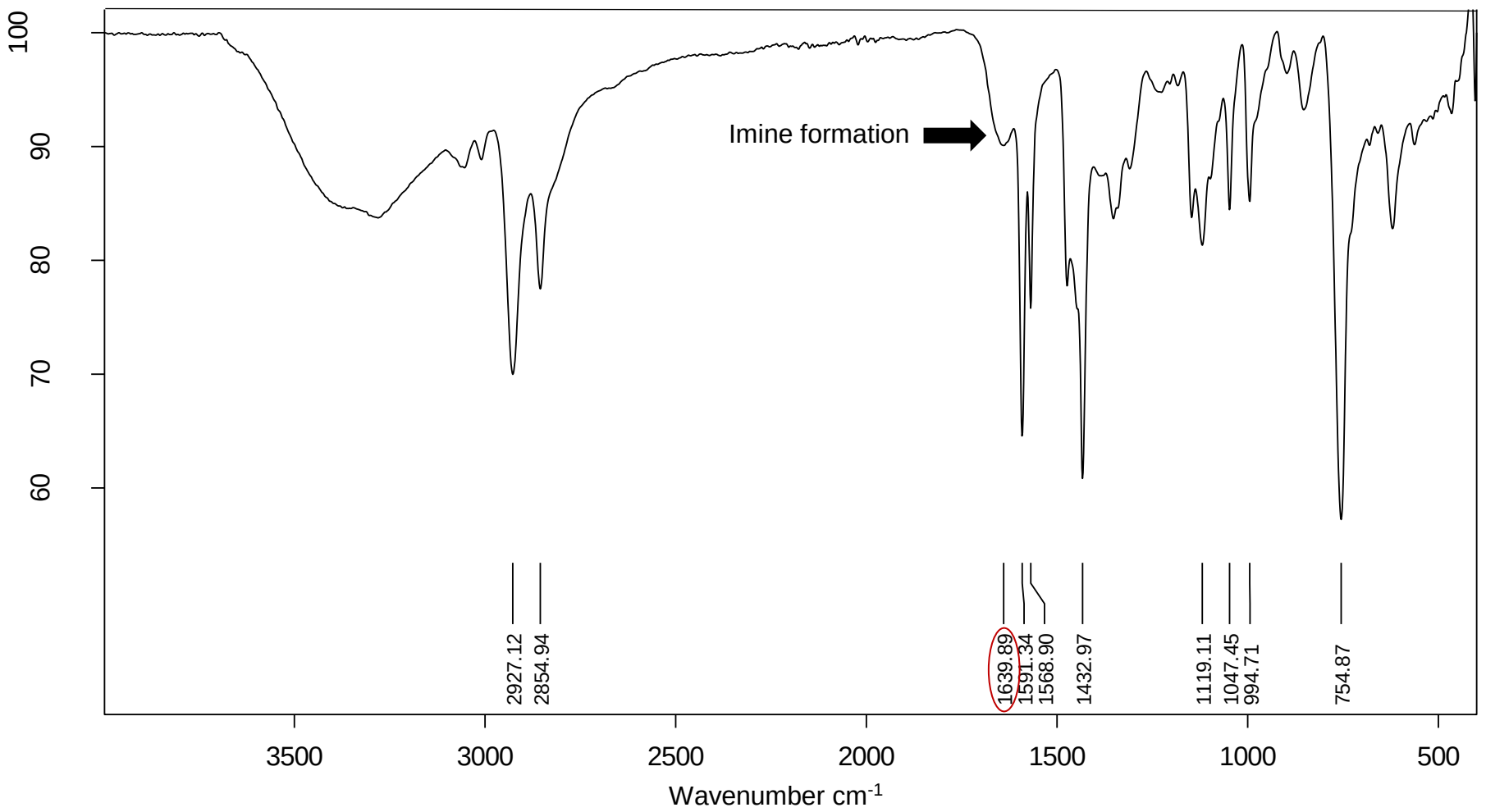

Figure 3.12: FT-IR spectrum of the ligand after reacting with H_2O_2.

An ESI-MS experiment was also conducted to investigate the different active species that may form during the oxidation reaction. An oxidation reaction can proceed via a metal-based or free radical oxidation mechanism. This depends on the reaction conditions, the nature of the oxidant and catalyst structure. A standard epoxidation reaction was conducted with **(*R,R*)-C3.1** as catalyst and *cis*-cyclooctene as substrate in acetonitrile with H_2O_2 addition over a period of 25 minutes. A sample was taken at 0, 5, 15 and 25 minutes and analysed with ESI-MS. The spectrum recorded at t = 25 minutes is shown in Figure 3.13.

After 25 minutes, two high intensity peaks are visible at *m/z* 501.08 and *m/z* 555.21. These peaks do not correspond to the calculated mass fragment values for a Fe^{V} (*m/z* 386.26), Fe^{IV} (*m/z* 386.26) or Fe^{III}-OOH (*m/z* 385.27) species. The cluster present at *m/z* 501.08 corresponds to the $[M\text{-}OTf]^+$ ion. The cluster present at *m/z* 555.21 is attributed to products that are a result of the oxidation of the ligand and iron. During the addition of H_2O_2, the ligand is oxidised and a formal bond is formed between one N-atom and Fe. This is accompanied by an oxidation state change from Fe(II) to Fe(III). This has been previously reported for imine-based oxidation systems.[23] The oxidation of the ligand results in lower stability and therefore lower catalytic activity. The ESI-MS results indicate that the ligand is oxidised during the reaction and the catalyst is deactivated via oxidative degradation, which contributes to the low catalytic activity exhibited by these complexes.

The oxidative degradation of these types of catalysts has been seen before. It is the most common pathway that leads to catalyst deactivation and it is a concern when developing non-heme iron catalysts.[24] Oxidation can take place at the CH_2NH and other parts of the ligand and this leads to deterioration of the ligand.[25] Catalyst degradation has been investigated for a variety of oxidation systems, which include porphyrin ligands. The degradation of the porphyrin ligands was attributed to the decomposition of H_2O_2, which results in a large amount of hydroxyl radicals that attack the porphyrin ring.[26, 27] Britovsek and co-workers also concluded that the main pathway for catalyst deactivation is oxidative degradation.[14, 28] They suggested that the aliphatic C-H bonds in the ligand are oxidised and that further rearrangement of the ligand is possible. This then results in no coordination between the ligand and the metal centre. For our bis-heterocyclic secondary diamine iron(II) complexes, we also see the effect of oxidative degradation, which results in all the complexes exhibiting similar catalytic activity.

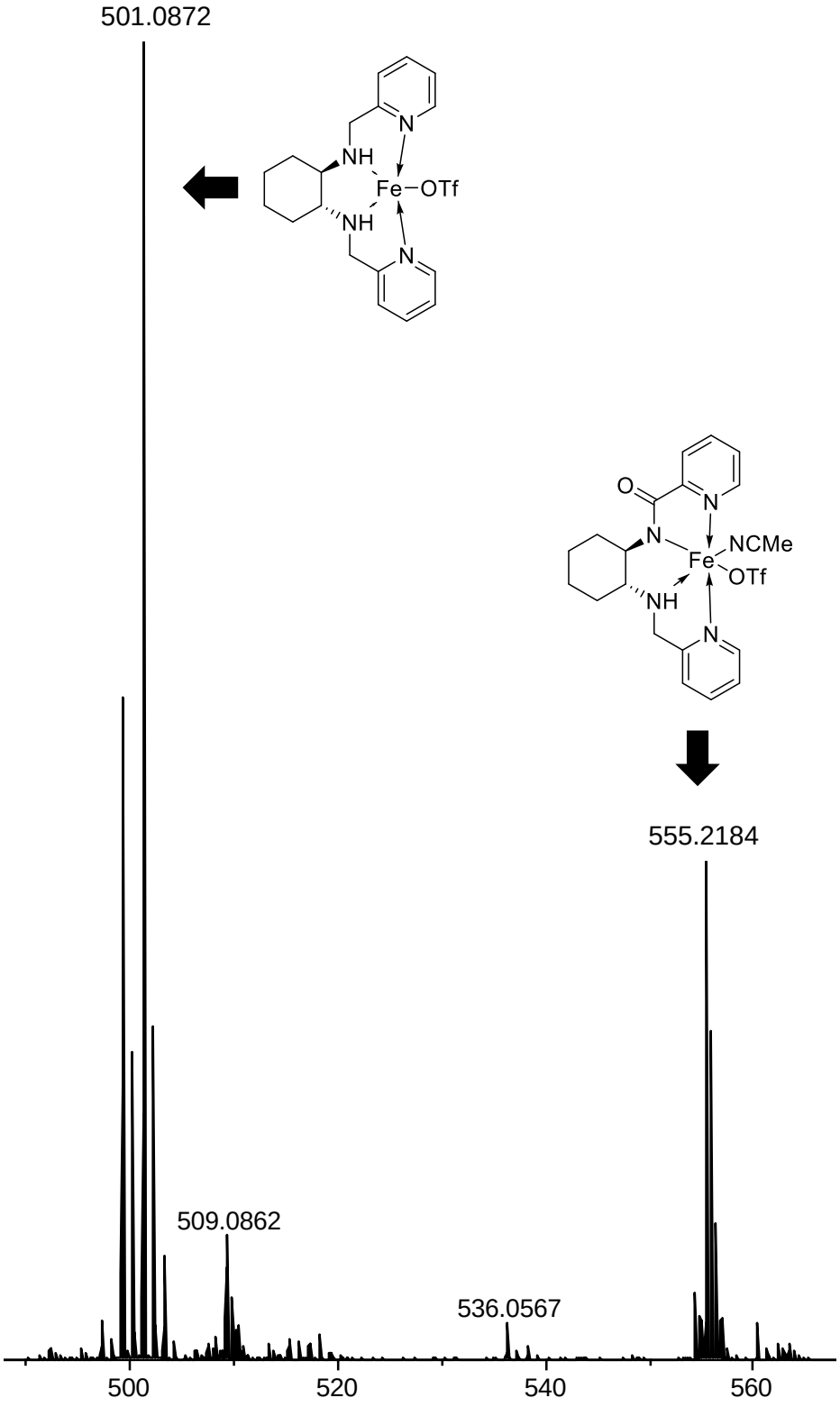

Figure 3.13: MS-spectrum of a catalysis reaction with **(*R,R*)-C3.1**, recorded at *t* = 25 minutes, indicating the oxidative degradation of the catalyst.

3.5 Conclusions

Five different (*R,R*) bis-heterocyclic secondary diamine ligands, **(*R,R*)-L3.6** to **(*R,R*)-L3.10**, and their corresponding Fe(II)-triflate complexes, **(*R,R*)-C3.1** to **(*R,R*)-C3.5**, were synthesised and characterised. ^{1}H NMR, UV-Vis spectroscopy and ESI-MS confirmed that the desired ligands and complexes were formed. The UV-Vis results indicated that these complexes possess a weak ligand field. These complexes were used as catalysts in the oxidation of *cis*-cyclooctene with H_2O_2 as oxidant, yielding cyclooctene oxide as the sole product. From the % conversion, turnover number and oxidation efficiency, it was evident that there was no significant difference in the catalytic activity for these complexes. This observation led us to believe that the complexes had low stability. This was confirmed by reacting the secondary diamine ligand with H_2O_2. Analysis by FT-IR showed that this resulted in the oxidation of the amine bond to form the imine bond. ESI-MS data also indicated that the ligand and iron is oxidised during the reaction and this causes lower stability and lifetime of the catalyst. Our experimental results showed that the secondary diamine ligands are not stable against degradation and are not a good option for the harsh oxidising environment needed for the oxidation of unfunctionalised substrates.

3.6 Experimental procedures

3.6.1 General considerations

Reagents were purchased for Sigma-Aldrich and/or Merck and used as received. Reagents and solvents used were commercially available reagent quality unless otherwise stated. Solvents were dried and purified by conventional distillation techniques. Diethyl ether was dried by prolonged reflux over sodium metal with benzophenone indicator under a nitrogen atmosphere. Dichloromethane was dried in a similar manner, but with calcium hydride as the drying agent. The solvents were freshly distilled prior to use.

Standard Schlenk techniques were used to prepare all oxygen- and moisture-sensitive compounds. Further storage and handling of these compounds were done in a standard glove box (MBraun) with H_2O and O_2 concentrations smaller than 0.1 ppm. ^{1}H NMR and ^{13}C NMR spectra were recorded on a Bruker 600 MHz Ultrashield Plus spectrometer and chemical shifts are reported in ppm relative to the residual deuterated solvent peak. Peak splitting patterns are indicated as s, singlet; d, doublet; t, triplet; m, multiplet. FT-IR spectra were recorded on a Bruker Alpha-P range infrared instrument equipped with an ATR (attenuated total reflectance) accessory as neat samples. Gas chromatographic analyses were performed on an Agilent 6890 Series GC System equipped with a HP 5 column: 30 m in length, 0.320 mm internal diameter and 0.25 mm film thickness. N_2 served as the carrier gas, acetonitrile (CH_3CN) and dichloromethane (DCM) were used as the rinsing solutions and biphenyl as the internal

standard. Elemental analysis was performed by the University of KwaZulu-Natal Mass Spectrometry Laboratory. Electrospray ionisation mass spectrometric analysis (ESI-MS, positive ion mode) was performed on a Bruker microTOF-Q II mass spectrometer.

3.6.2 Synthesis of ligands and complexes

Isolation of (*R,R*)-1,2-diaminecyclohexane

Tartaric acid (0.5 mol) was dissolved in 25 mL distilled water (dH_2O). The mixture was stirred and 0.10 mol of 1,2-diaminecyclohexane (mixture of *cis* and *trans*) was added. Following complete dissolution, 5 mL of glacial acetic acid was added. The reaction mixture was placed in an ice bath for a minimum of 30 minutes. Suction filtration was used to filter the solid product, which was washed with 5 mL ice cold water and 3 × 5 mL room temperature methanol. The product was purified by recrystallisation from water.

(*R,R*)-N,N′-bis(pyridyl-2-methylene)-1,2-cyclohexanediimine (L3.1)

In a round bottom flask, (*R,R*)-1,2-diaminecyclohexane mono-(+)-tartrate salt (0.005 mol), potassium carbonate (0.010 mol) and dH_2O (3 mL) was added and stirred until dissolved. Ethanol (EtOH, 5 mL) was added and the mixture was heated till reflux temperature. A solution of 2-pyridinecarboxaldehyde (0.010 mol) in EtOH (3 mL) was added to the reaction mixture. The reaction mixture was refluxed for 4 hours after which 3 mL of H_2O was added and the reaction mixture cooled in an ice bath for 30 minutes. The aqueous phase was extracted with 3 × 10 mL DCM. The organic phase was washed with 2 × 5 mL H_2O and 5 mL saturated sodium chloride (NaCl) mixture. The organic phase was dried with anhydrous magnesium sulphate ($MgSO_4$) and the solvent removed to yield a brown product. The product was dissolved in a minimum amount of diethyl ether (Et_2O) and placed in the freezer, which resulted in the formation of light yellow crystals. (390.2 mg, 26.33% yield).

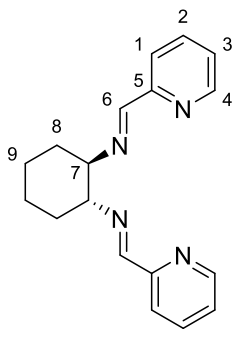

^{1}H NMR (600MHz, $CDCl_3$) δ 8.54 – 8.53 (d, 2H, J_{H-H}=4.53, H^4), 8.30 (s, 2H, H^6, CH=N), 7.88 – 7.86 (d, 2H, J_{H-H}=7.88, H^1), 7.64 – 7.62 (t, 2H, J_{H-H}=7.69, H^3), 7.22 – 7.20 (t, 2H, J_{H-H}=6.11, H^2), 3.53 – 3.52 (m, 2H, H^7), 1.88 – 1.80 (m, 6H, H^8, H^9), 1.52 – 1.49 (m, 2H, H^9); ^{13}C NMR (150 MHz, $CDCl_3$) δ 159.99 (C^6), 155.68 (C^5), 141.20 (C^4), 138.74 (C^2), 128.88 (C^3), 119.67 (C^1), 73.42 (C^7), 32.46 (C^8), 24.15 (C^9). FT-IR ν (cm^{-1}) 2927 (s), 2862 (s), 1643 (s), 1586 (s), 1567 (s), 1365 (s), 1137 (s), 992 (s), 868 (s), 744 (s), 618 (s), 512 (s), 407 (s).

(*R,R*)-N,N′-bis(6-methyl-2-pyridyl-2-methylene)-1,2-cyclohexanediimine (L3.2)

(*R,R*)-L3.2 was synthesised following the same procedure as for **(*R,R*)-L3.1**, employing 6-methyl-2-pyridinecarboxaldehyde (2.48 mmol). Yellow oil (328.0 mg, 82.55% yield).

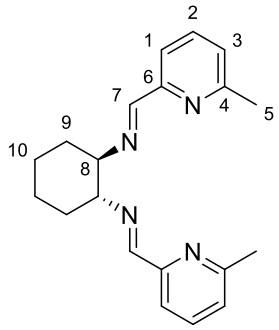

^{1}H NMR (600MHz, $CDCl_3$) δ 8.27 (s, 2H, H^7, CH=N), 7.69 – 7.68 (d, 2H, J_{H-H}=7.88, H^3), 7.51 – 7.48 (t, 2H, J_{H-H}=7.90, H^2), 7.06 – 7.05 (d, 2H, J_{H-H}=7.62, H^1), 3.49 – 3.47 (m, 2H, H^8), 2.49 (s, 6H, H^5), 1.84 – 1.75 (m, 6H, H^9,H^{10}), 1.48 – 1.45 (m, 2H, H^{10}); ^{13}C NMR (150MHz, $CDCl_3$) δ 161.68 (C^7), 157.74 (C^2), 154.18 (C^3), 136.60 (C^1), 124.05 (C^6), 118.24 (C^4), 73.58 (C^5), 32.68 (C^8), 24.34 (C^9), 24.25 (C^{10}). FT-IR ν (cm^{-1}) 2927, 2857, 1646, 1590, 1572, 1455, 1374, 1251, 1136, 1084, 987, 935, 861, 791, 735, 652, 447.

(*R,R*)-N,N′-bis(6-bromo-2-pyridyl-2-methylene)-1,2-cyclohexanediimine (L3.3)

(*R,R*)-L3.3 was synthesised following the same procedure as for **(*R,R*)-L3.1**, employing 6-bromo-2-pyridinecarboxaldehyde (2.96 mmol). After the reaction mixture was cooled in an ice bath, the product precipitated. The product was filtered and washed with EtOH. White solid (376.0 mg, 56.44% yield).

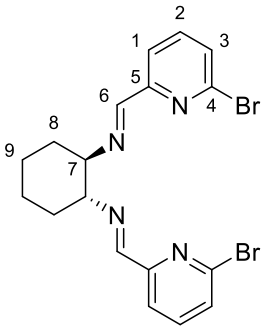

^{1}H NMR (600MHz, $CDCl_3$) δ 8.19 (s, 2H, H^6, CH=N), 7.88 – 7.86 (d, 2H, J_{H-H}=7.65, H^3), 7.52 – 7.49 (t, 2H, J_{H-H}=7.74, H^2), 7.41 – 7.40 (d, 2H, J_{H-H}=7.91, H^1), 3.46 – 3.44 (m, 2H, H^8), 1.85 – 1.84 (m, 4H, H^9), 1.79 – 1.73 (m, 2H, H^{10}), 1.48 – 1.45 (m, 2H, H^{10}); ^{13}C NMR (150MHz, $CDCl_3$) δ 160.05 (C^6), 155.74 (C^2), 141.26 (C^3), 138.80 (C^1), 128.93 (C^4), 119.73 (C^5), 73.48 (C^7), 32.50 (C^8), 24.20 (C^9). FT-IR ν (cm^{-1}) 2930, 2855, 1649, 1576, 1546, 1439, 1158, 1119, 1032, 983, 936, 860, 791, 730, 706, 642, 476, 446.

(*R,R*)-N,N′-bis(1-methyl-2-imidazole-2-methylene)-1,2-cyclohexanediimine (L3.4)

(*R,R*)-L3.4 was synthesised following the same procedure as for **(*R,R*)-L3.1**, employing 1-methyl-2-imidazolecarboxaldehyde (4.58 mmol). The solvent was removed to afford the product. Yellow oil (515.5 mg, 75.38% yield).

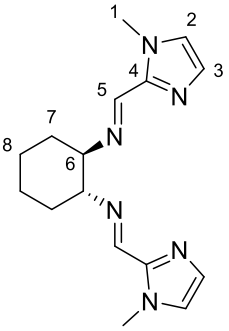

^{1}H NMR (600MHz, $CDCl_3$) δ 8.19 (s, 2H, H^5, CH=N), 7.00 (s, 2H, H^3), 6.83 (s, 2H, H^2), 3.85 (s, 6H, H^1), 3.25 – 3.24 (m, 2H, H^6), 1.83 – 1.75 (m, 4H, H^7), 1.67 – 1.65 (m, 2H, H^8), 1.46 – 1.42 (m, 2H, H^8); ^{13}C NMR (150MHz, $CDCl_3$) δ 152.11 (C^5), 143.11 (C^4), 128.82 (C^3), 124.68 (C^2), 74.74 (C^1), 35.45 (C^6), 32.85 (C^7), 24.27 (C^8). FT-IR ν (cm^{-1}) 2928, 2858, 1646, 1475, 1437, 1369, 1284, 935, 862, 812, 752, 706.

(*R,R*)-N,N′-bis(quinolyl-2-methylene)-1,2-cyclohexanediimine (L3.5)

(*R,R*)-L3.5 was synthesised following the same procedure as for **(*R,R*)-L3.1**, employing 2-quinolinecarboxaldehyde (2.50 mmol). After the reaction mixture was cooled in an ice bath, the product precipitated. The product was filtered and washed with EtOH. White solid (305.0 mg, 61.19% yield).

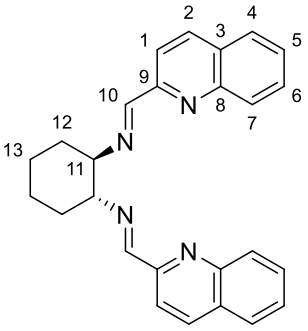

^{1}H NMR (600MHz, $CDCl_3$) δ 8.51 (s, 2H, H^{10}, CH=N), 8.08 – 8.01 (m, 6H, H^1, H^2,H^4) 7.74 – 7.72 (d, 2H, J_{H-H}=8.28, H^7), 7.66 – 7.63 (t, 2H, J_{H-H}=7.56, H^6), 7.49 – 7.47 (t, 2H, J_{H-H}=7.56, H^5), 3.66 – 3.64 (m, 2H, H^{11}), 1.92 – 1.85 (m, 6H, H^{12}, H^{13}), 1.57 – 1.54 (m, 2H, H^{13}); ^{13}C NMR (150MHz, $CDCl_3$) δ 161.83, 154.89, 147.61, 136.35 (C^2), 129.53 (C^6), 129.40 (C^4), 128.66 (C^5), 127.59 (C^3), 127.11 (C^8), 118.52 (C^9), 73.82 (C^{11}), 32.68 (C^{12}), 24.34 (C^{13}). FT-IR ν (cm^{-1}) 2969, 2858, 1640, 1596, 1500, 1427, 1113, 939, 867, 850, 802, 791, 753, 619, 468, 450.

(*R,R*)-N,N′-bis(pyridyl-2-methyl)-1,2-cyclohexanediamine (L3.6)

(*R,R*)-L3.1 (0.612 mmol) was dissolved in 3 mL methanol (MeOH) at 0°C and sodium borohydride ($NaBH_4$, 2.448 mmol) was added portion wise. The mixture was stirred for 1 hour at room temperature and refluxed for 1 hour. The reaction mixture was cooled to room temperature, extracted with 3 × 10 mL DCM and the organic phase washed with 2 × 10 mL dH_2O and 10 mL saturated NaCl mixture and dried with anhydrous $MgSO_4$. The solvent was removed to afford the product. Yellow oil (127.2 mg, 70.12% yield).

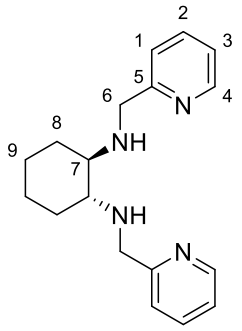

^{1}H NMR (600MHz, $CDCl_3$) δ 8.49 – 8.48 (d, 2H, J_{H-H}=4.81, H^4), 7.61 – 7.58 (t, 2H, J_{H-H}=7.71, H^3), 7.36 – 7.35 (d, 2H, J_{H-H}=7.75, H^1), 7.11 – 7.09 (t, 2H, J_{H-H}=5.03, H^2), 4.03 – 4.01 (d, 2H, J_{H-H}=14.05, H^6, CH_2-N), 3.84 – 3.81 (d, 2H, J_{H-H}=14.13, H^6, CH_2-N), 2.33 – 2.32 (m, 2H, H^7), 2.12 – 2.10 (m, 2H, H^8), 1.69 – 1.68 (m, 2H, H^8), 1.21 – 1.07 (m, 4H, H^9); ^{13}C NMR (150MHz, $CDCl_3$) δ 160.02 (C^4), 149.00 (C^3), 136.48 (C^1), 122.40 (C^5), 121.87 (C^2), 61.19 (C^6), 52.15 (C^7), 31.34 (C^8), 24.88 (C^9). FT-IR ν (cm^{-1}) 2925, 2853, 1590, 1569, 1432, 1119, 1047, 993, 753.

(*R,R*)-N,N′-bis(6-methyl-2-pyridyl-2-methyl)-1,2-cyclohexanediamine (L3.7)

(*R,R*)-L3.7 was synthesised following the same procedure as for **(*R,R*)-L3.6**, employing **(*R,R*)-L3.2** (0.397 mmol). Yellow oil (114.8 mg, 89.13% yield).

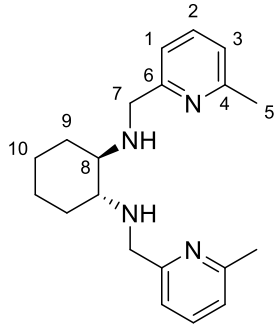

^{1}H NMR (600MHz, $CDCl_3$) δ 7.50 – 7.47 (t, 2H, J_{H-H}=7.67, H^2), 7.18 – 7.17 (d, 2H, J_{H-H}=7.67, H^3), 6.98 – 6.96 (d, 2H, J_{H-H}=7.64, H^1), 4.01 – 3.99 (d, 2H, J_{H-H}=14.21, H^7), 3.79 – 3.77 (d, 2H, J_{H-H}=14.05, H^7), 2.47 (s, 6H, H^5), 2.35 – 2.33 (m, 2H. H^8), 2.13 – 2.11 (m, 2H, H^9), 1.70 – 1.68 (m, 2H, H^9), 1.22 – 1.18 (m, 2H, H^{10}), 1.10 – 1.08 (m, 2H, H^{10}) ; ^{13}C NMR (150MHz, $CDCl_3$) δ 159.26 (C^2), 157.64 (C^3), 136.69 (C^1), 121.38 (C^6), 119.20 (C^4), 61.22 (C^7), 52.12 (C^5), 31.35 (C^8), 24.90 (C^9), 24.34 (C^{10}). FT-IR ν (cm^{-1}) 2925, 2854, 1593, 1577, 1450, 1119, 780.

(*R,R*)-N,N′-bis(6-bromo-2-pyridyl-2-methyl)-1,2-cyclohexanediamine (L3.8)

Synthesised following the same procedure as for **(*R,R*)-L3.6**, employing **(*R,R*)-L3.3** (0.373 mmol). White/light yellow solid (139.7 mg, 82.46% yield).

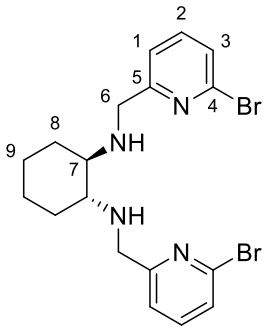

^{1}H NMR (600MHz, $CDCl_3$) δ 7.51 – 7.50 (t, 2H, J_{H-H}=7.64, 1, H^2), 7.43 – 7.41 (d, 2H, J_{H-H}=7.53, H^3), 7.32 – 7.31 (d, 2H, J_{H-H}=7.82, H^1), 4.03 – 4.01 (d, 2H, J_{H-H}=14.66, H^6), 3.81 – 3.79 (d, 2H, J_{H-H}=14.68, H^6), 2.30 – 2.28 (m, 2H, H^7), 2.12 – 2.10 (m, 2H, H^8), 1.71 – 1.70 (m, 2H, H^8), 1.22 – 1.18 (m, 2H, H^9), 1.06 – 1.05 (m, 2H, H^9); ^{13}C NMR (150MHz, $CDCl_3$) δ 162.00 (C^2), 141.37 (C^3), 138.98 (C^1), 126.16 (C^4), 121.20 (C^5), 61.27 (C^6), 51.61 (C^7), 31.42 (C^8), 24.85 (C^9). FT-IR ν (cm^{-1}) 2925, 2853, 1580, 1552, 1434, 1405, 1232, 1153, 1117, 983, 859, 787, 675.

(*R,R*)-N,N′-bis(1-methyl-2-imidazole-2-methyl)-1,2-cyclohexanediamine (L3.9)

(*R,R*)-L3.9 was synthesised following the same procedure as for **(*R,R*)-L3.6**, employing **(*R,R*)-L3.4** (1.06 mmol) Yellow oil (210.6 mg, 65.69% yield).

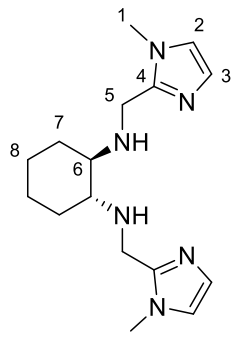

^{1}H NMR (600MHz, $CDCl_3$) δ 6.86 (s, 2H, H^3), 6.75 (s, 2H, H^2), 3.91 – 3.89 (d, 2H, J_{H-H}=13.54, H^5), 3.67 – 3.65 (d, 2H, J_{H-H}=13.54, H^5), 3.59 (s, 6H, H^1), 2.22 – 2.21 (m, 2H, H^6), 2.12 – 2.10 (m, 2H, H^7), 1.70 – 1.69 (m, 2H, H^7) 1.23 – 1.19 (m, 2H, H^8), 1.04 – 0.98 (m, 2H, H^8); ^{13}C NMR (150MHz, $CDCl_3$) δ 146.75 (C^4), 126.90 (C^3), 121.07 (C^2), 61.09 (C^1), 42.92 (C^5), 32.73 (C^6), 31.18 (C^7), 24.82 (C^8). FT-IR ν (cm^{-1}) 2926, 2854, 1499, 1449, 1282, 1108, 977, 733.

(*R,R*)-N,N′-bis(quinolyl-2-methyl)-1,2-cyclohexanediamine (L3.10)

Synthesised following the same procedure as for **(*R,R*)-L3.6**, employing **(*R,R*)-L3.5** (0.357 mmol). Yellow oil (115.9 mg, 81.87% yield).

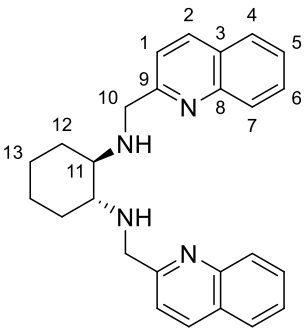

^{1}H NMR (600MHz, $CDCl_3$) δ 8.06 – 8.04 (d, 2H, J_{H-H}=8.44, H^7), 7.94 – 7.93 (d, 2H, J_{H-H}=8.33, H^1), 7.75 – 7.74 (d, 2H, J_{H-H}=8.20, H^2), 7.61 – 7.58 (t, 2H, J_{H-H}=7.59, H^6), 7.54 – 7.52 (d, 2H, J_{H-H}=8.44, H^4), 7.47 – 7.45 (t, 2H, J_{H-H}=7.59, H^5), 4.28 – 4.26 (d, 2H, J_{H-H}=14.64, H^{10}), 4.06 – 4.04 (d, 2H, J_{H-H}=14.64, H^{10}), 2.49 – 2.48 (m, 2H, H^{11}), 2.20 – 2.18 (m, 2H, H^{12}), 1.72 – 1.70 (m, 2H, H^{12}), 1.22 – 1.16 (m, 4H, H^{13}); ^{13}C NMR (150MHz, $CDCl_3$) δ 147.47 (C^7), 136.46 (C^1), 129.39 (C^2), 128.83 (C^6), 127.53 (C^4), 127.29 (C^5), 126.02 (C^3), 120.67 (C^8), 61.43 (C^9), 52.49 (C^{10}), 31.26 (C^{11}), 30.87 (C^{12}), 24.85 (C^{13}). FT-IR ν (cm^{-1}) 2923, 2854, 1599, 1564, 1504, 1448, 1425, 1309, 1113, 823, 748, 619, 476.

[Fe(CF_3SO_3)$_2$-(*R,R*)-N,N′-bis(pyridyl-2-methyl)-1,2-cyclohexanediamine] (C3.1)

$Fe(OTf)_2$ (0.399 mmol) was dissolved in dry CH_3CN in a Schlenk flask. **(*R,R*)-L3.6**, dissolved in dry CH_3CN, was added dropwise to the $Fe(OTf)_2$ mixture under an argon atmosphere and stirred for 24 hours. Afterwards, the solvent was reduced, the addition of dry Et_2O resulted in precipitation of the product. The product was washed two more times with dry Et_2O and thereafter the solvent was removed. Red solid (143.0 mg, 55.0% yield).

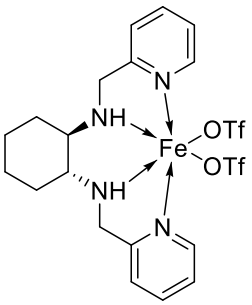

MS (ESI) *m/z* (%): $[M–OTf]^+$: calc. 501.33, found 501.08. Elemental Analysis $C_{20}H_{24}N_4FeF_6O_6S_2$ (MW = 650.39 g/mol) Calc. (%) C 36.93, H 3.72, N 8.61; Found (%) C 34.42, H 4.59, N 7.86.

[Fe(CF_3SO_3)$_2$-(*R,R*)-N,N′-bis(6-methyl-2-pyridyl-2-methyl)-1,2-cyclohexanediamine] (C3.2)

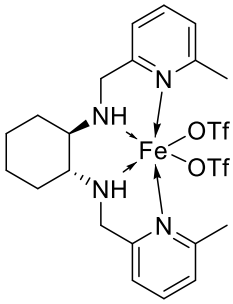

(*R,R*)-C3.2 was synthesised following the same procedure as for **(*R,R*)-C3.1**, employing **(*R,R*)-L3.7** (0.191 mmol) as ligand. Yellow solid (35.1 mg, 27.09% yield).

MS (ESI) *m/z* (%): $[M–OTf]^+$: calcd 529.38, found 529.12 Elemental Analysis $C_{22}H_{28}N_4FeF_6O_6S_2$ (MW = 678.44 g/mol) Calc. (%) C 38.95, H 4.16, N 8.26; Found (%) C 28.50, H 3.67, N 5.74.

[Fe(CF_3SO_3)$_2$-(*R,R*)-N,N′-bis(6-bromo-2-pyridyl-2-methyl)-1,2-cyclohexanediamine] (C3.3)

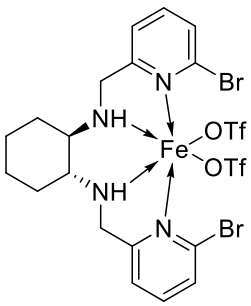

(*R,R*)-C3.3 was synthesised following the same procedure as for **(*R,R*)-C4.1**, employing **(*R,R*)-L3.8** (0.169 mmol) as ligand. Yellow solid (34.0 mg, 24.91% yield).

MS (ESI) *m/z* (%): $[M–OTf]^+$: calcd 659.12, found 658.91 Elemental Analysis $C_{20}H_{22}Br_2N_4FeF_6O_6S_2$ (MW = 808.18 g/mol) Calc. (%) C 29.72, H 2.74, N 6.93; Found (%) C 25.28, H 3.51, N 5.49.

[Fe(CF_3SO_3)$_2$-(*R,R*)-N,N′-bis(1-methyl-2-imidazole-2-methyl)-1,2-cyclohexanediamine] (C3.4)

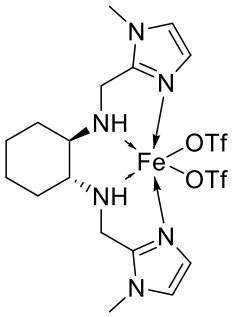

(*R,R*)-C3.4 was synthesised following the same procedure as for **(*R,R*)-C3.1**, employing **(*R,R*)-L3.9** (0.496 mmol) as ligand. Orange solid (140.1 mg, 43.0% yield).

MS (ESI) *m/z* (%): $[M–OTf]^+$: calcd 507.33, found 507.10 Elemental Analysis $C_{18}H_{26}N_4FeF_6O_6S_2$ (MW = 656.40 g/mol) Calc. (%) C 32.94, H 3.99, N 12.80; Found (%) C 26.55, H 3.74, N 9.82.

[Fe(CF_3SO_3)$_2$-(*R,R*)-N,N′-bis(quinolyl-2-methyl)-1,2-cyclohexanediamine] (C3.5)

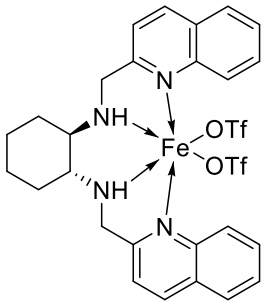

(*R,R*)-C3.5 was synthesised following the same procedure as for **(*R,R*)-C3.1**, employing **(*R,R*)-L3.10** as ligand (0.536 mmol). Green solid (135.8 mg, 33.78% yield).

MS (ESI) *m/z* (%): $[M–OTf]^+$: calc. 601.45, found 601.33. Elemental Analysis $C_{28}H_{28}N_4FeF_6O_6S_2$ (MW = 750.51 g/mol) Calc. (%) C 44.81, H 3.76, N 7.47; Found (%) C 43.73, H 3.65, N 7.27.

Procedure for the epoxidation reaction

The catalyst (25 µmol) and the substrate (1.0 mmol) was dissolved in 2 mL of acetonitrile. 32% aqueous hydrogen peroxide (191 µL, 1.8 mmol) was added with a syringe pump over a period of 25 minutes at room temperature. After H_2O_2 addition, the reaction mixture was stirred for a further 15 minutes. The reaction mixture was filtered through a column packed with silica gel and celite as well as a syringe filter. To the resulting mixture a measured amount of biphenyl was added as internal standard for GC analysis. GC analysis was used to determine the conversion of the substrate and the yield of cyclooctene epoxide. Products were identified by comparison to the GC retention time of authentic samples.

Procedure for epoxidation with additives

The substrate (2500 µmol) was added to the catalyst (2.5 µmol) dissolved in 2 mL of acetonitrile. 2500 µmol of the additive (H_2O or AcOH) was mixed with 25 µmol of H_2O_2 (70 mM stock solution) and added over a period of 25 minutes with a syringe pump. After addition, the reaction mixture was stirred for a further 15 minutes and filtered through a column packed with silica gel and celite as well as a syringe filter. Biphenyl was used as internal standard and the reaction mixture analysed on a GC.

3.7 References

1. Correa, A.; Mancheño, O. G.; Bolm, C., *Chem. Soc. Rev.*, **2008,** *37* (6), 1108-1117.
2. Zhang, S.; Miao, C.; Xu, D.; Sun, W.; Xia, C., *Chin. J. Cat.*, **2014,** *35* (11), 1864-1870.
3. Chen, M. S.; White, M. C., *Science*, **2007,** *318* (5851), 783-787.
4. Oloo, W. N.; Que Jr, L., *Acc. Chem. Res.*, **2015,** *48* (9), 2612-2621.
5. Olivo, G.; Cussó, O.; Borrell, M.; Costas, M., *J. Biol. Inorg. Chem.*, **2017,** *22* (2-3), 425-452.
6. Britovsek, G. J.; England, J.; White, A. J., *Inorg. Chem.*, **2005,** *44* (22), 8125-8134.
7. Costas, M.; Tipton, A. K.; Chen, K.; Jo, D. H.; Que, L., *J. Am. Chem. Soc.*, **2001,** *123* (27), 6722-6723.
8. Olivo, G.; Lanzalunga, O.; Di Stefano, S., *Adv. Synth. Catal.*, **2016**.
9. Amendola, V.; Fabbrizzi, L.; Gianelli, L.; Maggi, C.; Mangano, C.; Pallavicini, P.; Zema, M., *Inorg. Chem.*, **2001,** *40* (14), 3579-3587.
10. Cristau, H. J.; Cellier, P. P.; Hamada, S.; Spindler, J. F.; Taillefer, M., *Org. Lett.*, **2004,** *6* (6), 913-916.
11. Florián, J.; McLauchlan, C. C.; Kissel, D. S.; Eichman, C. C.; Herlinger, A. W., *Inorg. Chem.*, **2015,** *54* (21), 10361-10370.
12. Wu, M.; Miao, C. X.; Wang, S.; Hu, X.; Xia, C.; Kühn, F. E.; Sun, W., *Adv. Synth. Catal.*, **2011,** *353* (16), 3014-3022.
13. Balland, V.; Banse, F.; Anxolabéhère-Mallart, E.; Nierlich, M.; Girerd, J. J., *Eur. J. Inorg. Chem.*, **2003,** (13), 2529-2535.
14. England, J.; Davies, C. R.; Banaru, M.; White, A. J.; Britovsek, G. J., *Adv. Synth. Catal.*, **2008,** *350* (6), 883-897.
15. Mialane, P.; Nivorojkine, A.; Pratviel, G.; Azema, L.; Slany, M.; Godde, F.; Simaan, A.; Banse, F.; Kargar-Grisel, T.; Bouchoux, G., *Inorg. Chem.*, **1999,** *38* (6), 1085-1092.
16. Borovik, A.; Papaefthymiou, V.; Taylor, L. F.; Anderson, O. P.; Que Jr, L., *J. Am. Chem. Soc.*, **1989,** *111* (16), 6183-6195.
17. Chen, K.; Que, L., *J. Am. Chem. Soc.*, **2001,** *123* (26), 6327-6337.
18. White, M. C.; Doyle, A. G.; Jacobsen, E. N., *J. Am. Chem. Soc.*, **2001,** *123* (29), 7194-7195.
19. Prat, I.; Company, A.; Corona, T.; Parella, T.; Ribas, X.; Costas, M., *Inorg. Chem.*, **2013,** *52* (16), 9229-9244.
20. Cussó, O.; Garcia-Bosch, I.; Ribas, X.; Lloret-Fillol, J.; Costas, M., *J. Am. Chem. Soc.*, **2013,** *135* (39), 14871-14878.
21. Lyakin, O. Y.; Ottenbacher, R. V.; Bryliakov, K. P.; Talsi, E. P., *ACS Catal.*, **2012,** *2* (6), 1196-1202.

22. Garcia-Bosch, I.; Codolá, Z.; Prat, I.; Ribas, X.; Lloret, F.; Costas, M., *Chem. Eur. J.*, **2012,** *18*, 13268-13273.
23. Olivo, G.; Nardi, M.; Vìdal, D.; Barbieri, A.; Lapi, A.; Gómez, L.; Lanzalunga, O.; Costas, M.; Di Stefano, S., *Inorg. Chem.*, **2015,** *54* (21), 10141-10152.
24. Collins, T. J., *Acc. Chem. Res.*, **1994,** *27* (9), 279-285.
25. Shejwalkar, P.; Rath, N. P.; Bauer, E. B., *Dalton Trans.*, **2011,** *40* (29), 7617-7631.
26. Cunningham, I. D.; Danks, T. N.; Hay, J. N.; Hamerton, I.; Gunathilagan, S., *Tetrahedron*, **2001,** *57* (31), 6847-6853.
27. Stephenson, N. A.; Bell, A. T., *J. Am. Chem. Soc.*, **2005,** *127* (24), 8635-8643.
28. England, J.; Gondhia, R.; Bigorra-Lopez, L.; Petersen, A. R.; White, A. J.; Britovsek, G. J., *Dalton Trans.*, **2009,** (27), 5319-5334.

Chapter 4

Evaluating (*R*,*R*) and (*S*,*S*) bis-heterocyclic tertiary diamine Fe(II) complexes in the oxidation of alkene and alcohol substrates

4.1 Introduction

Over the years, a large number of iron catalysts have been developed for the oxidation of a variety of substrates. This includes heme-based iron complexes that incorporate porphyrin ligands and more recently the development of non-heme iron complexes. Of the non-heme complexes, the ligands with tetradentate N-donor groups have received a great deal of attention and these types of complexes show good activity towards the oxidation of substrates.[1, 2,3] The steric and electronic properties of the ligand are an important consideration and have been the subject of numerous studies.[4, 5, 6] These studies have shown that there are a few key properties of the ligand that will influence the catalytic activity of the complex. These include the two labile coordination sites that are available for substitution reactions with the solvent or the oxidant; ligands that are capable of sustaining the high oxidation states of iron as well as the ligand topology. An important discovery is that different topologies are possible when the tetradentate N4 ligands coordinate to an iron centre. These topologies are *cis*-α, *cis*-β and *trans* and have an effect on the catalytic activity seen for the iron complex.[7] H_2O_2 activation takes place at these coordination sites and also influences the formation of metal-based oxidants.[8]

For alcohol oxidation, a wide range of catalysts have been investigated that employ metals such as Pd, Ru, Co and Cu. Copper complexes have received a great deal of attention because they mimic enzymes responsible for oxidation in living organisms, for example galactose oxidase.[9] Many reported systems for catalytic alcohol oxidation suffer from drawbacks such as high catalyst load, unfavourable reaction conditions and expensive metals.[10] Iron catalysis has become a very promising research field because of the advantages associated with the metal. These include low cost, ease of availability and its non-toxic nature.[11] A few systems for alcohol oxidation use iron and H_2O_2 as oxidant,[12, 13] but extensive research on the catalytic application of N4 tetradentate non-heme Fe(II) complexes for the oxidation of alcohols has not been conducted.[14]

This chapter will describe the synthesis and characterisation of (*R,R*) and (*S,S*) bis-heterocyclic tertiary diamine ligands and the corresponding iron(II) complexes. The catalytic activity of the complexes as catalysts in the epoxidation of *cis*-cyclooctene will be evaluated. It will also describe the effect of the ligand topology and steric and electronic effects of the ligands on the catalytic activity of the different complexes. The oxidation of benzyl alcohol will be evaluated and different parameters with respect to the alcohol oxidation reaction will be optimised. Finally, the alcohol substrate scope will be extended to include benzylic, allylic and aliphatic primary and secondary alcohols.

4.2 Synthesis of ligands and complexes

4.2.1 (*R,R*) ligand set

Because the (*R,R*) secondary diamine ligands exhibited poor stability, we decided to methylate the ligands to form tertiary diamine ligands. In literature, various examples of tertiary diamine ligands used in the oxidation of alkanes and alkenes are described.[3, 15] (*S,S*)-1,2-diaminecyclohexane will also be employed to synthesise another set of ligands and the corresponding iron(II) complexes. The configuration of the internal diamine donor influences the ligand topology and subsequently the catalytic activity.[16] The catalytic activity of the (*R,R*) and (*S,S*) complexes can be compared and this will describe the effect of the ligand topology on the oxidation of different substrates.

The tertiary diamine ligands, **L4.1** to **L4.4**, with (*R,R*) configuration, were synthesised by reacting **(*R,R*)-L3.6** to **(*R,R*)-L3.9** with formaldehyde, sodium borohydride and acetic acid (Scheme 4.1 and Figure 4.1). These ligands were synthesised in moderate to excellent yields (60 to 90%) and were isolated as yellow oils.

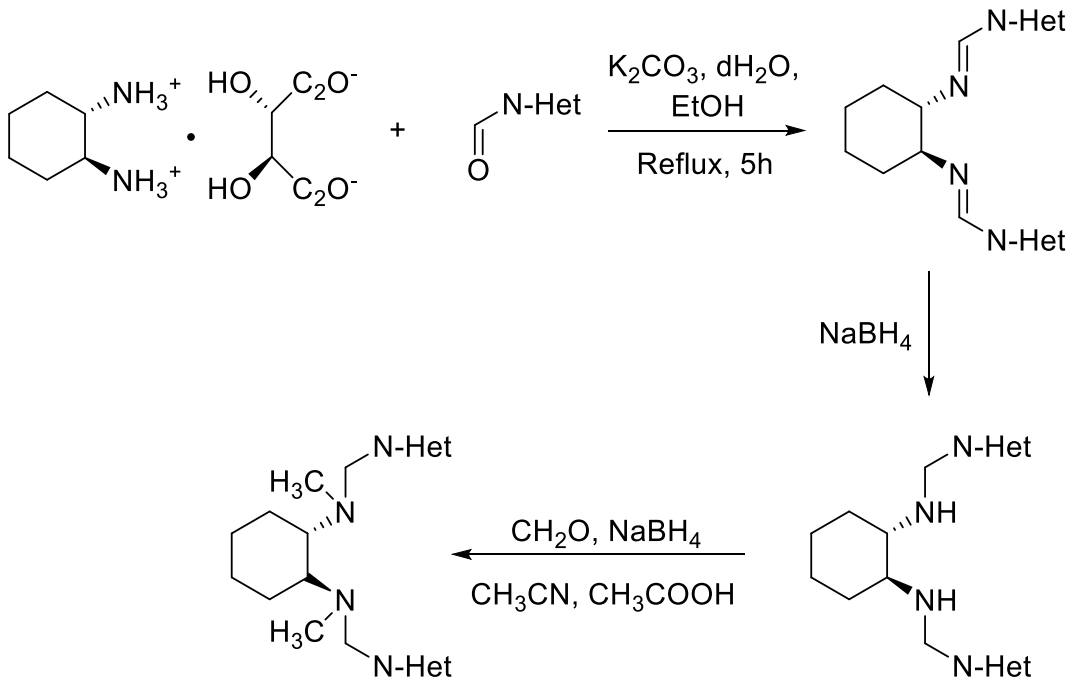

Scheme 4.1: Synthesis of tertiary diamine ligands starting with (*R,R*) or (*S,S*)-1,2-diaminecyclohexane mono-(+)-tartrate salt and the specific carboxaldehyde.

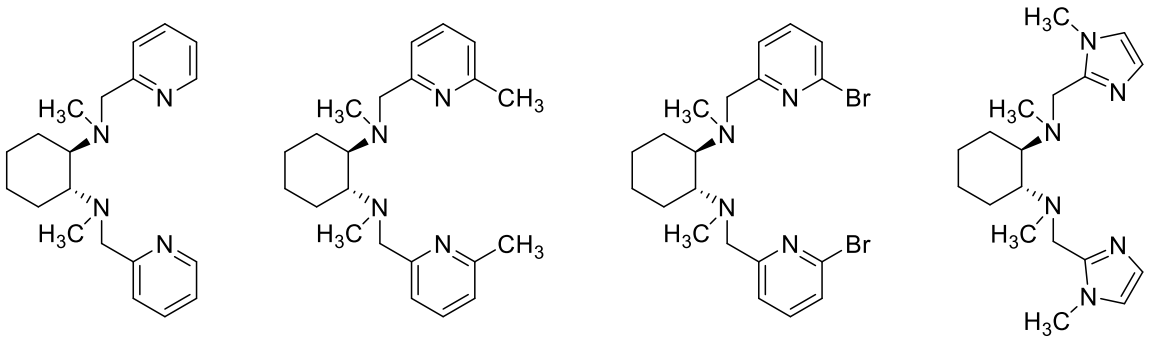

(*R,R*)-L4.1 **(*R,R*)-L4.2** **(*R,R*)-L4.3** **(*R,R*)-L4.4**

Figure 4.1: Tertiary diamine ligand set formed when **(*R,R*)-L3.6** to **(*R,R*)-L3.9** is methylated.

4.2.1.1 FT-IR spectroscopic data of (*R,R*) tertiary diamine ligands, L4.1 to L4.4

In the FT-IR spectra of these ligands, the small, broad peak at ~3200 cm^{-1}, which represents the secondary amine, is not visible. The C-H stretching vibrations of the aliphatic region of the ligands are represented by two peaks in the range of 2850 to 2930 cm^{-1}. The C-H bending vibrations of cyclohexane are represented by the strong peak at ~1432 cm^{-1}. In the region of 1250 to 1020 cm^{-1}, the medium to weak absorption bands are a result of the C-N stretching vibrations for the aliphatic tertiary amine, and the C-N stretching vibration for the aromatic tertiary amine is seen at ~1354 cm^{-1}. The absorption band at ~1589 cm^{-1} is due to the cyclic imine stretch (Figure 4.2).

4.2.1.2 ^{1}H NMR spectroscopic data of (*R,R*) tertiary diamine ligands, L4.1 to L4.4

For all the ligands, the methyl proton resonance was seen as a singlet in the range of δ 2.00 to 2.50 ppm and integrated for six protons. The N-CH_2 resonances were still observed as two doublets in the range of δ 3.80 to 4.10 ppm. The cyclohexyl proton resonances were still poorly resolved and seen as broad multiplets. The integration values in the aromatic and aliphatic region correspond with the total expected for the protons present in the ligand. As an example the ^{1}H NMR spectrum of **(*R,R*)-L4.1** is shown in Figure 4.3. The ^{1}H NMR data for the ligands **L4.1** to **L4.4** correlate well with literature values.[17]

4.2.2 (*S,S*) ligand set

(*S,S*)-1,2-diaminecyclohexane was dissolved in diethyl ether and the specific carboxaldehyde was added. **(*S,S*)-L3.1** and **(*S,S*)-L3.3** precipitated after approximately 1 hour of stirring. The other two ligands, **(*S,S*)-L3.2** and **(*S,S*)-L3.4**, did not precipitate and were extracted with dichloromethane and were isolated as yellow oils. The ligands were synthesised in a moderate to good yield (47 to 72%) and characterised with FT-IR and NMR spectroscopy.

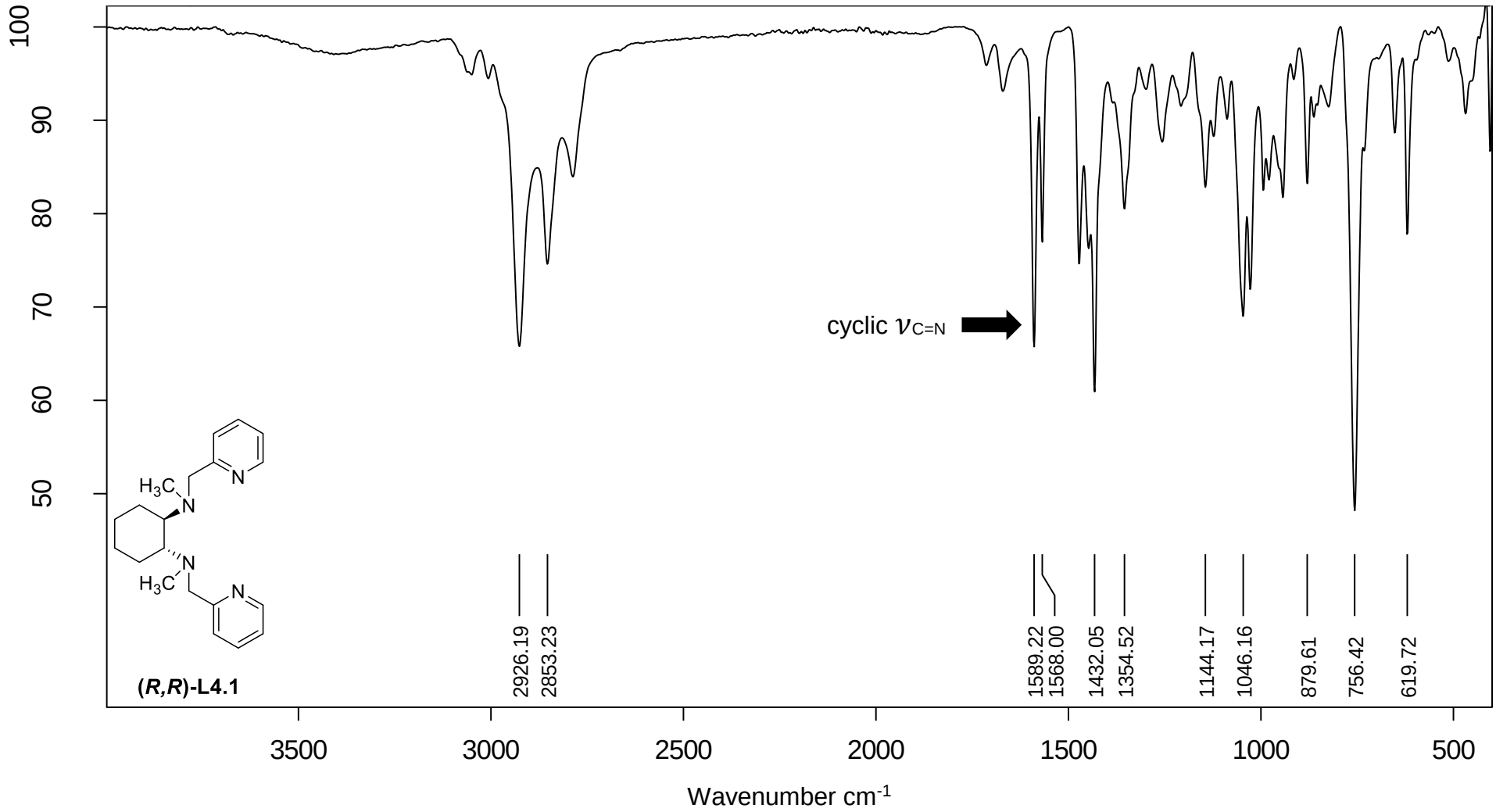

Figure 4.2: FT-IR spectrum of **(*R,R*)-L4.1**.

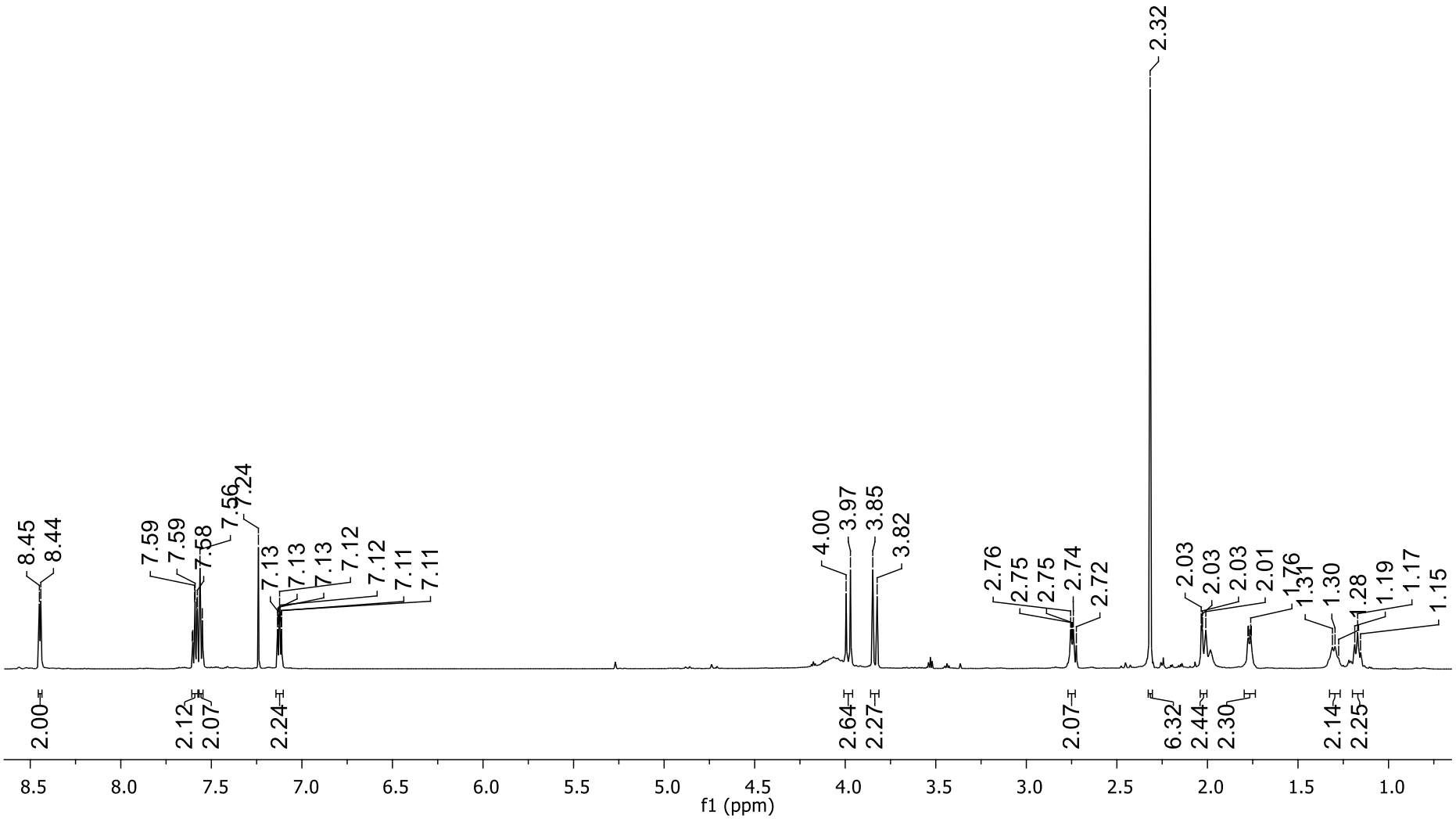

Figure 4.3: ^{1}H NMR spectrum of **(*R,R*)-L4.1**.

4.2.2.1 FT-IR spectroscopic data of (*S,S*) diimine ligands, L3.1 to L3.4

The FT-IR spectra of the (*S,S*) diimine ligand set contain the same spectral features as that of the (*R,R*) diimine ligand set. FT-IR spectroscopy does not reveal the difference in the topology. These ligands also displayed the characteristic $\nu_{C=N}$ absorption band in the range of 1640 to 1650 cm^{-1}. Similar to the other ligands, the peaks in the range of 2850 to 2930 cm^{-1} can be attributed to C-H stretching vibrations of cyclohexane. The cyclic imine absorption band is represented by the medium intensity peak at ~1585 cm^{-1} and the C-N stretching vibration of the aromatic tertiary amine is seen at ~1365 cm^{-1} (Figure 4.4).

4.2.2.2 ^{1}H NMR spectroscopic data of (*S,S*) diimine ligands, L3.1 to L3.4

There is no difference between the ^{1}H NMR spectra of the (*R,R*) and (*S,S*) diimine ligand set. The imine proton resonance is seen as a singlet in the range of δ 8.10 to 8.40 ppm. In the aliphatic region, the broad multiplets are assigned to poorly resolved cyclohexyl proton resonances. The splitting patterns and integration values of the remaining peaks correspond with expected values for the ligands (Figure 4.5).

4.2.2.3 FT-IR spectroscopic data of (*S,S*) secondary diamine ligands, L3.6 to L3.9

(*S,S*)-L3.1 to **(*S,S*)-L3.4** was reduced following the same procedure as for **(*R,R*)-L3.1** to **(*R,R*)-L3.4**. The products, **(*S,S*)-L3.1** to **(*S,S*)-L3.4** were isolated as yellow oils with excellent yields of 84 to 98%. For the reduced ligands, the presence of the secondary amine is confirmed by a weak, broad peak at ~3200 cm^{-1}. The absence of the characteristic $\nu_{C=N}$ absorption band in the range of 1640 to 1650 cm^{-1} confirms that the CH=N bond has been reduced. The cyclohexane C-H stretching vibrations are in the range of 2850 to 2930 cm^{-1} and the C-N stretching vibrations of the secondary amine are seen as a medium intensity absorption band at ~1120 cm^{-1} (Figure 4.6).

4.2.2.4 ^{1}H NMR spectroscopic data of (*S,S*) secondary diamine ligands, L3.6 to L3.9

The presence of two doublets in the range of δ 3.80 to 4.10 ppm is attributed to the N-CH_2 groups now present after the reduction of the imine bonds. The absence of a singlet in the aromatic region also confirms that the imine bonds has been reduced. The presence of the NH bond is confirmed by a small, broad peak in the range of δ 2.30 to 2.40 ppm. The signals in the aliphatic region are seen as broad, poorly resolved multiplets and the integration values correspond with the expected proton values for the ligand (Figure 4.7).

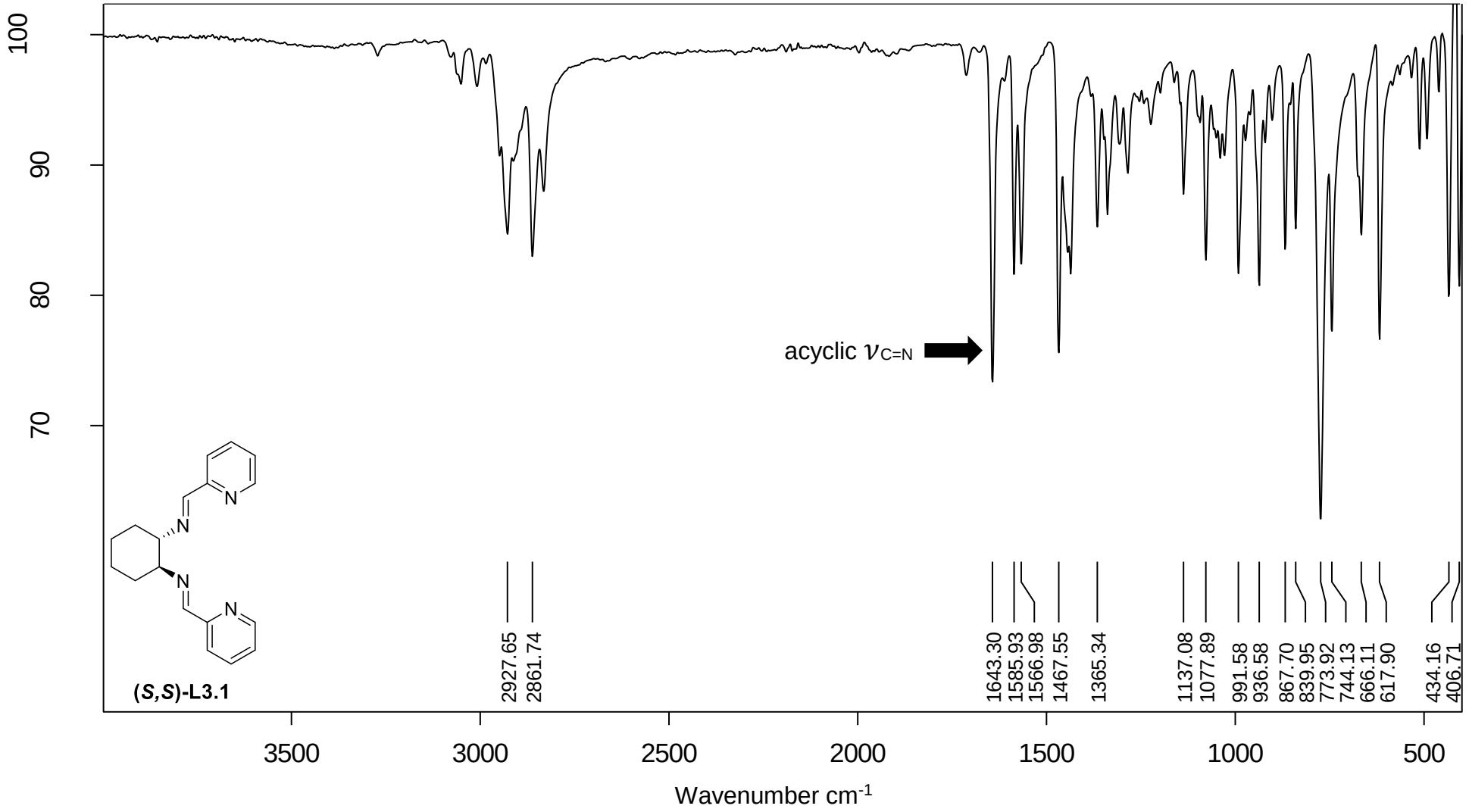

Figure 4.4: FT-IR spectrum of **(*S,S*)-L3.1**.

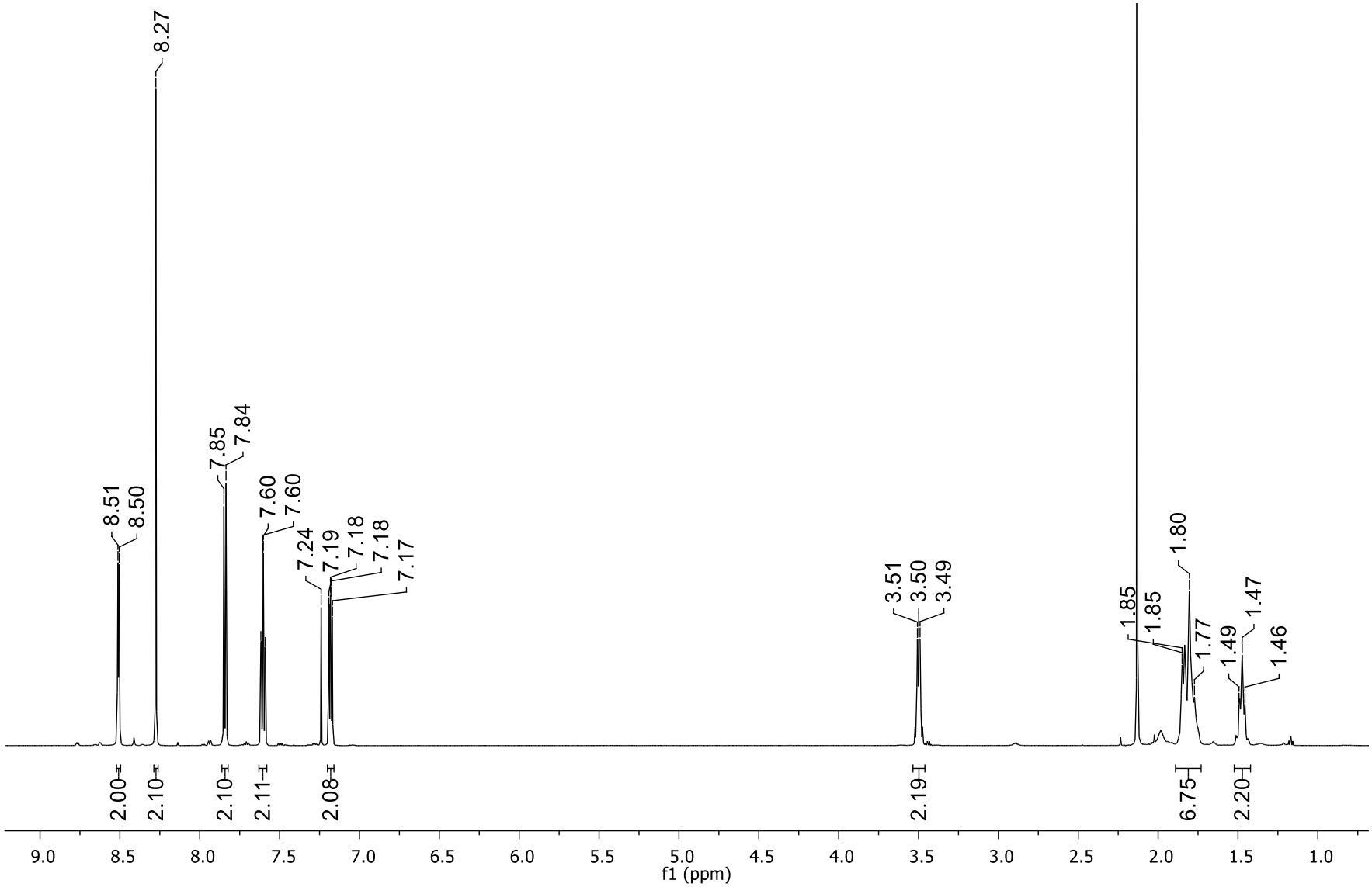

Figure 4.5: ^{1}H NMR spectrum of **(*S,S*)-L3.1**.

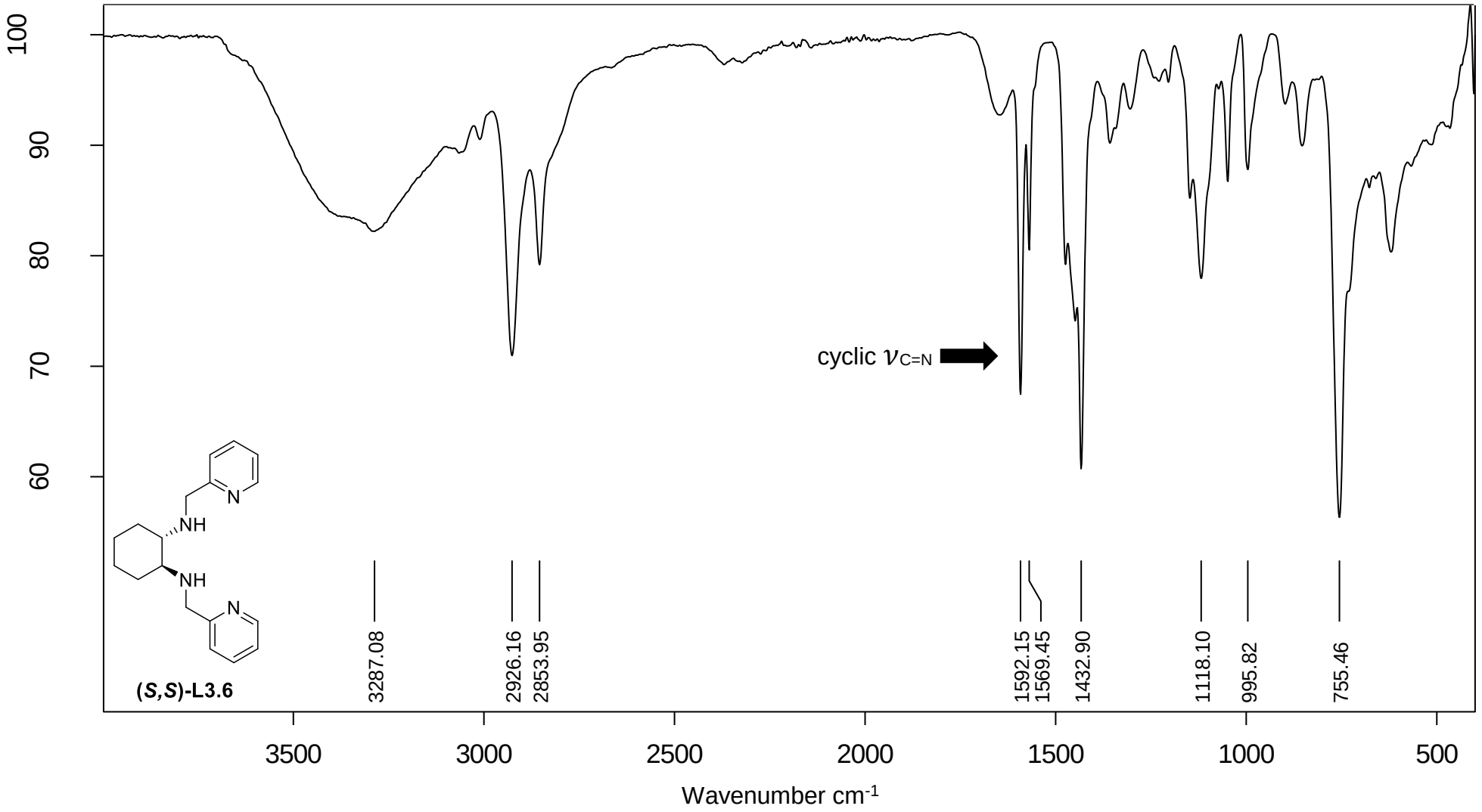

Figure 4.6: FT-IR spectrum of **(*S*,*S*)-L3.6**.

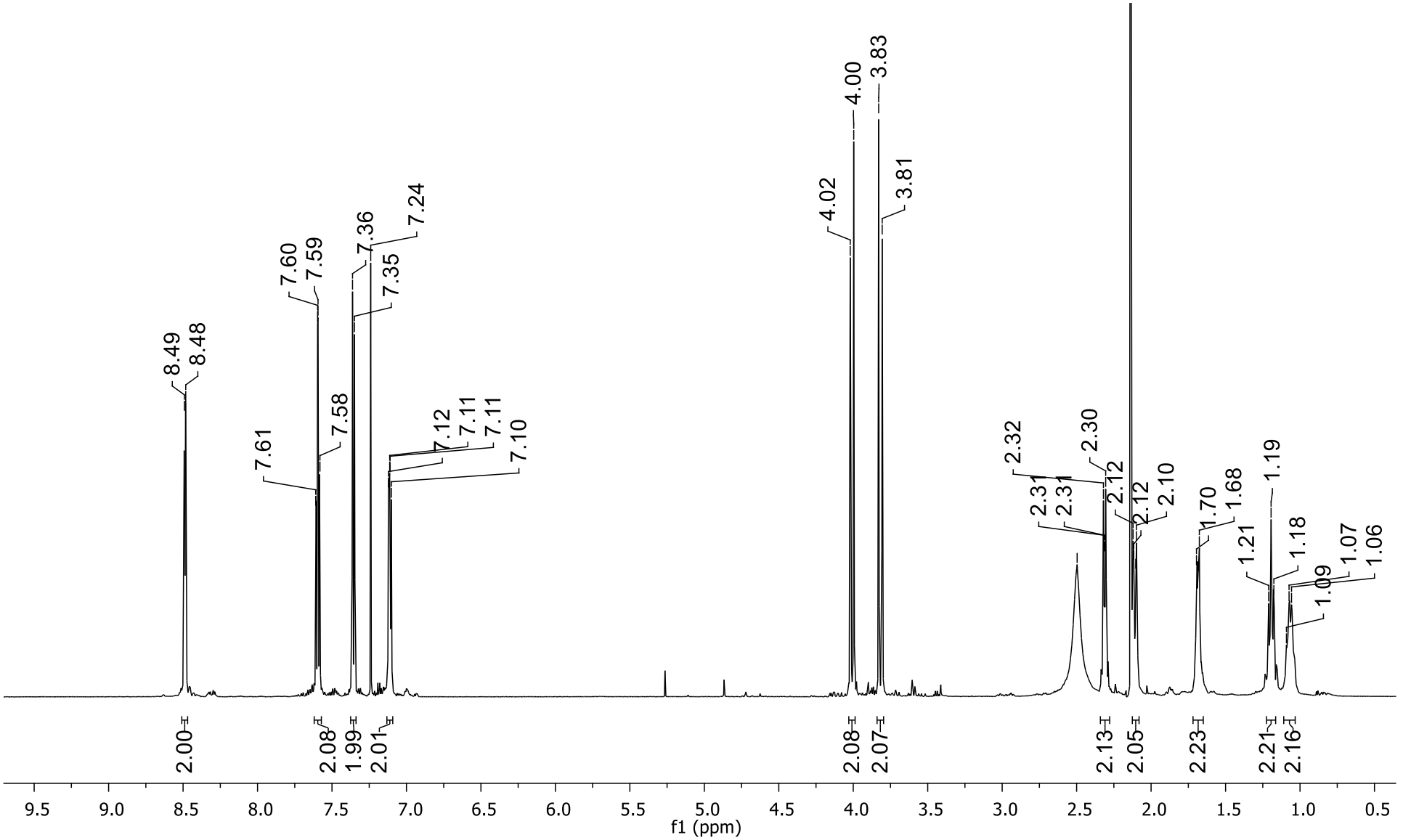

Figure 4.7: ^{1}H NMR spectrum of **(*S*,*S*)-L3.6**.

The same procedure followed for the synthesis of **(*R,R*)-L4.1** to **(*R,R*)-L4.4** was used to synthesise **(*S,S*)-L4.1** to **(*S,S*)-L4.4** (Figure 4.8). The ligands were isolated as oils in good to excellent yields (74 to 89%), with the colour varying from light to dark yellow.

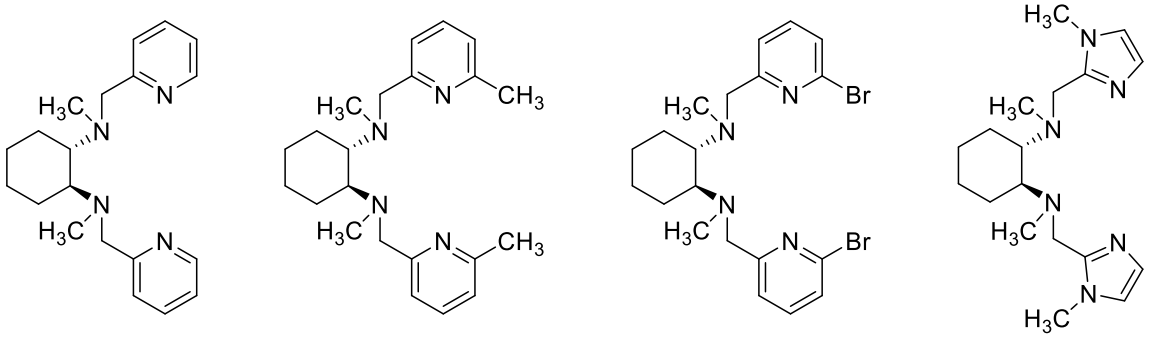

Figure 4.8: Tertiary diamine ligand set that is formed when **(*S,S*)-L3.6** to **(*S,S*)-L3.9** is methylated.

4.2.2.5 FT-IR spectroscopic data of (*S,S*) tertiary diamine ligands, L4.1 to L4.4

In the FT-IR spectra of the methylated ligands, the tertiary amine vibration is visible as a medium intensity peak at ~1200 cm^{-1}. No peak is visible at ~3200 cm^{-1}, which confirms that the secondary amine is not present in the ligands. The absorption bands in the range of 2850 to 2930 cm^{-1} are attributed to the C-H stretching vibrations of cyclohexane (Figure 4.9).

4.2.2.6 ^{1}H NMR spectroscopic data of (*S,S*) tertiary diamine ligands, L4.1 to L4.4

The aliphatic region of the methylated ligands is characterised by a singlet in the range of δ 2.01 to 2.28 ppm. This resonance is assigned to the N-CH_3 groups present in the ligand. The N-CH_2 groups are still observed as two doublets in the range of δ 3.70 to 4.10 ppm. The cyclohexyl proton resonances are poorly resolved and observed as broad multiplets (Figure 4.10). The integration values correspond with the expected proton values for these ligands.

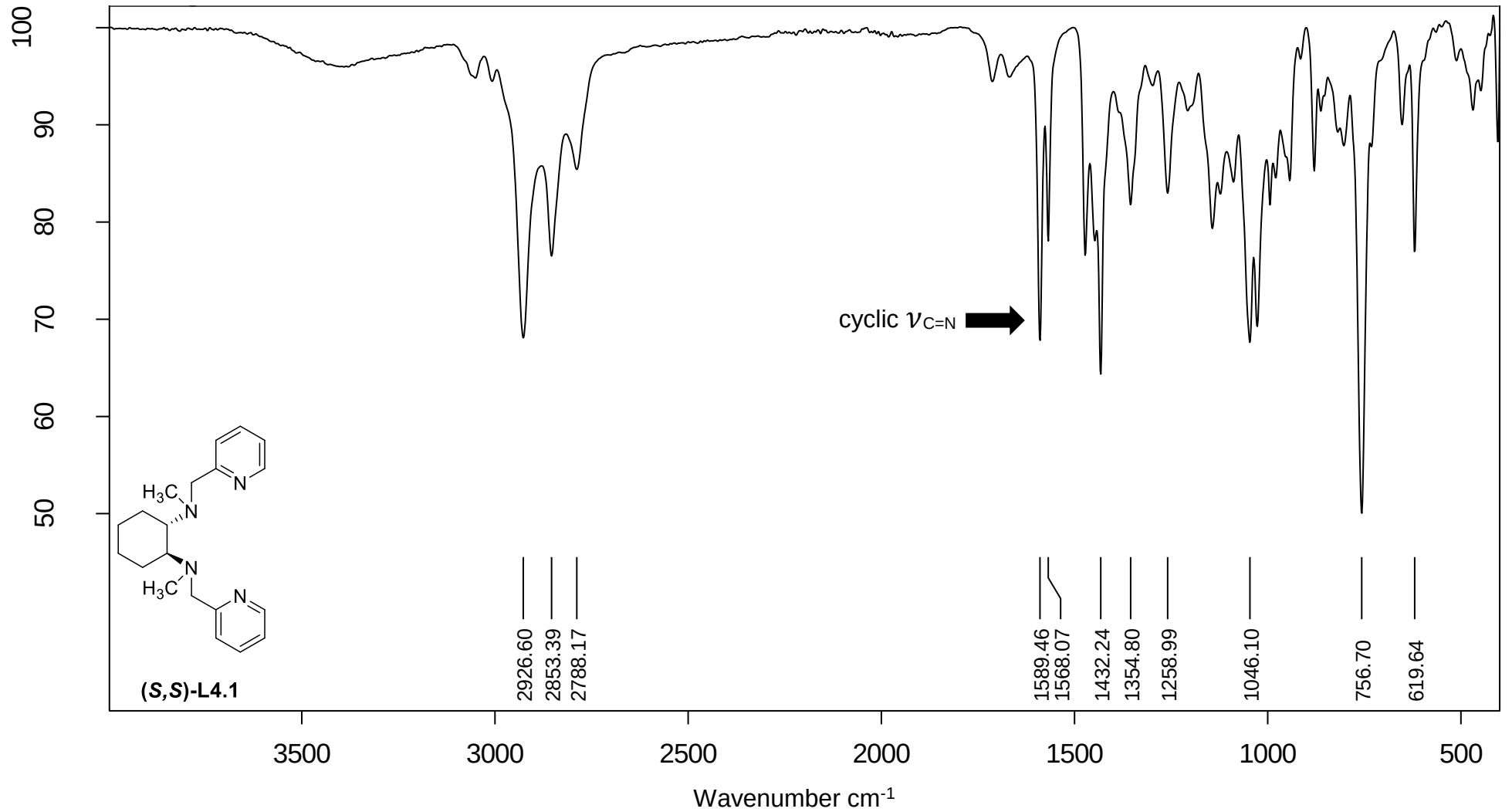

Figure 4.9: FT-IR spectrum of **(*S*,*S*)-L4.1**.

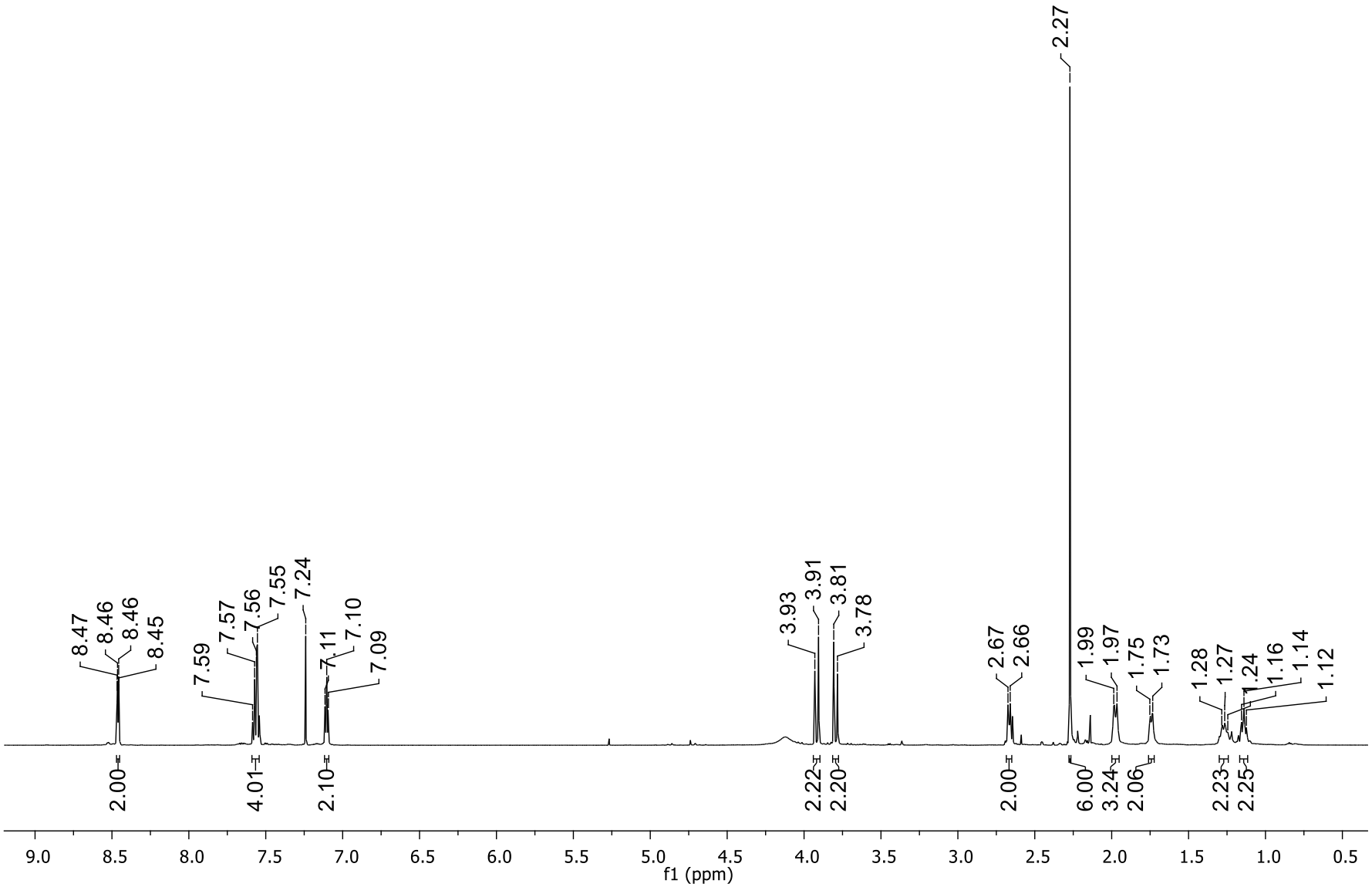

Figure 4.10: ^{1}H NMR spectrum of **(*S,S*)-L4.1**.

4.2.3 (*R,R*) and (*S,S*) complex set

Currently, it is believed that ligands with pyridine donors are the most effective catalysts for oxidation reactions.[18] By investigating this combination of ligands, we will be able to determine the influence of an electron-donating and electron-withdrawing substituent on the pyridine ring. In **(*R,R*)** and **(*S,S*)-L4.4**, the pyridine donor is replaced with an imidazole donor and this will determine whether the pyridine donor is necessary for good catalytic activity or whether the pyridine can be replaced with another N-donor.

The synthesis of the complexes was done under an inert atmosphere and the same procedure was used for both the (*R,R*) and (*S,S*) ligand set (Scheme 4.2 and Figure 4.11). The tertiary diamine ligands were reacted with $Fe(OTf)_2$ in dry dichloromethane. The addition of dry diethyl ether to the reaction mixture resulted in the precipitation of the product. The complexes were isolated as powders and the colours ranged from light yellow to orange/brown. This synthesis route gave low to good yields (36 to 87%). MALDI-MS, elemental analysis, UV-Vis spectroscopy and magnetic susceptibility were used to characterise the complexes.

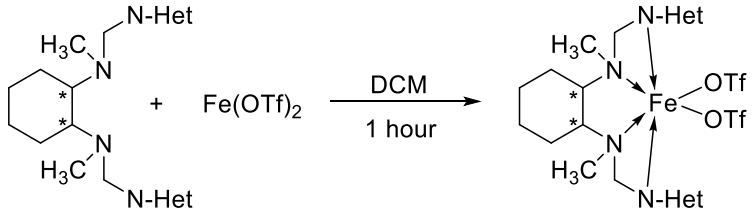

Scheme 4.2: Synthesis of the complexes by reacting the ligands with $Fe(OTf)_2$. N-Het represents the different heterocycles of the ligands.

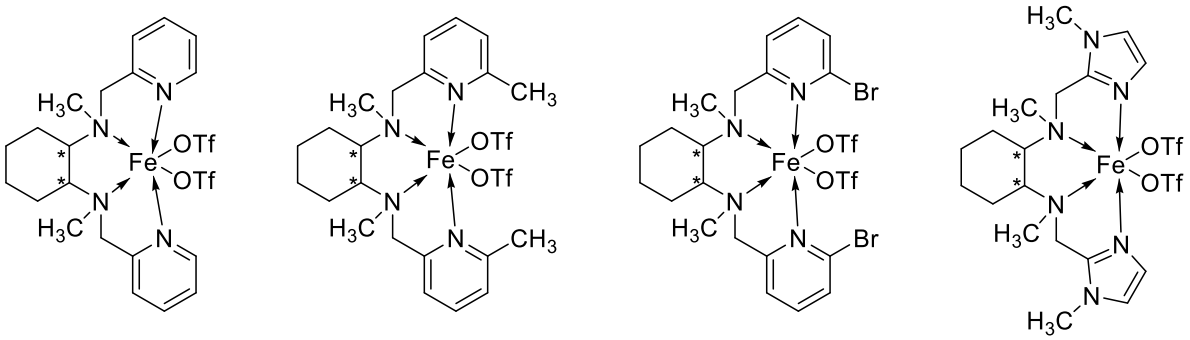

(*R,R*)-C4.1 **(*S,S*)-C4.1** **(*R,R*)-C4.2** **(*S,S*)-C4.2** **(*R,R*)-C4.3** **(*S,S*)-C4.3** **(*R,R*)-C4.4** **(*S,S*)-C4.4**

Figure 4.11: Iron(II) complexes bearing **(*R,R*)** and **(*S,S*)**-**L4.1** to **L4.4**.

4.2.3.1 MALDI-MS data of (*R,R*) and (*S,S*) C4.1 to C4.4

Matrix-assisted laser desorption ionisation mass spectrometry (MALDI-MS) was used to determine the molecular mass of the isolated iron(II) complexes. Characterisation of these complexes with MALDI showed the loss of one of the triflate groups. The *m/z* value corresponds with $[M\text{-}OTf]^+$ and has been observed for similar iron(II) complexes.[19] As an example, for **(*R,R*)-C4.1**, the calculated *m/z* value for this complex is 529.38, which corresponds with the experimental value obtained. The isotope pattern seen for this fragment is the same as the isotope pattern for the simulated mass spectrum, which confirms the structure of the complex (Figure 4.12). For all the iron(II) complexes, the same fragmentation pattern is seen and the experimental values match the calculated values. The mass spectral data for the other complexes is provided in the experimental section.

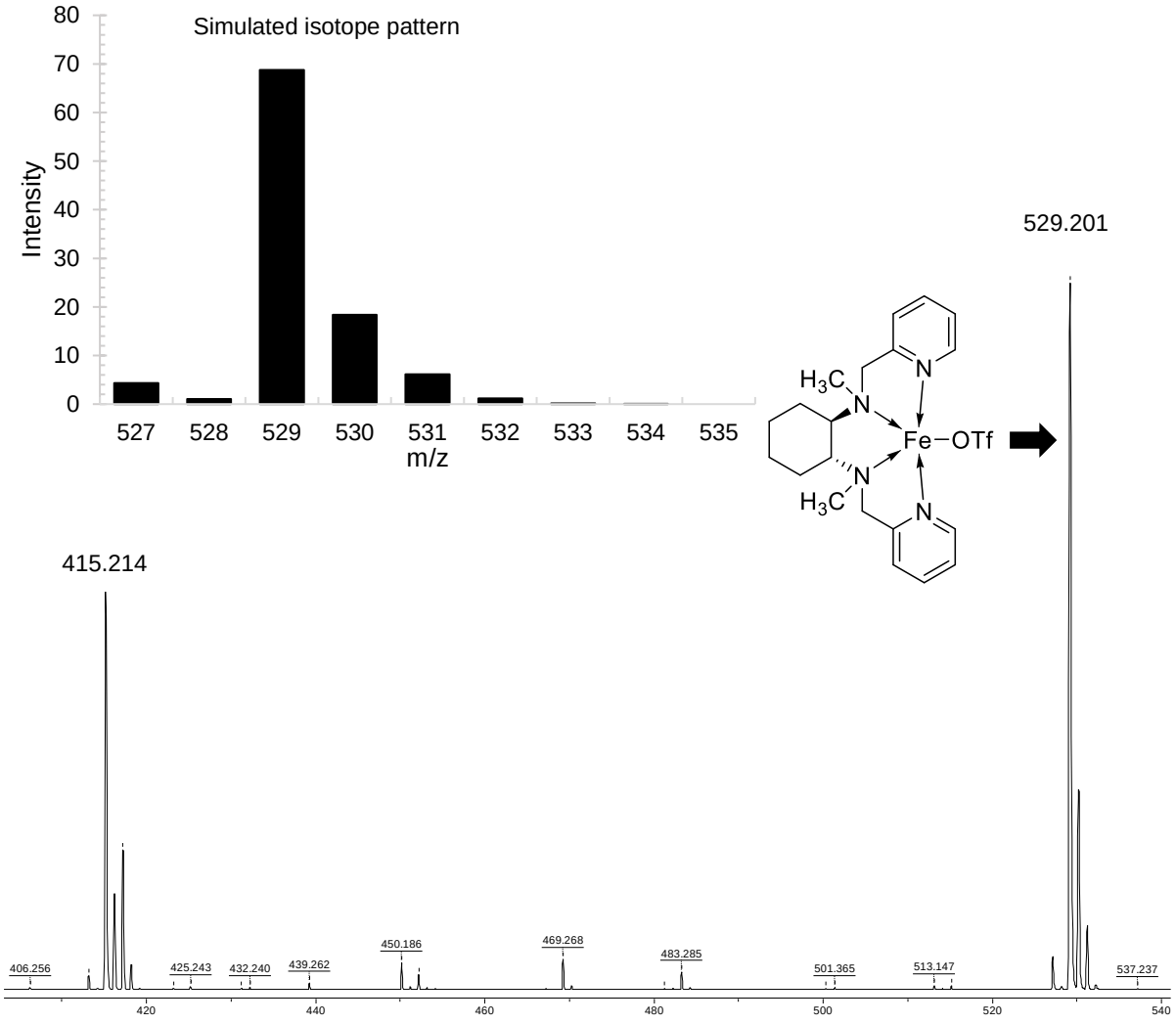

Figure 4.12: MALDI-MS spectrum and simulated isotope pattern of **(*R,R*)-C4.1**.

4.2.3.2 Elemental analysis of (*R,R*) and (*S,S*) C4.1 to C4.4

The elemental analysis results for the complexes are provided in Table 4.1. There is a good correlation between the calculated and the experimental values. In some instances, the experimental data correlates with the inclusion of trace amounts of dichloromethane and diethyl ether solvent.

Table 4.1: Comparison between the **experimental** and (calculated) elemental analysis for the (*R,R*) and (*S,S*) iron(II) complex sets

Entry	Catalyst	C	H	N	S
1	**(*R,R*)-C4.1**	**38.99** (38.95)	**4.07** (4.16)	**7.89** (8.26)	**9.11** (9.45)
2	**(*R,R*)-C4.2**	**40.67** (40.80)	**4.22** (4.57)	**7.81** (7.93)	**8.99** (9.05)
3	**(*R,R*)-C4.3**	**31.30** (31.60)	**3.00** (3.13)	**6.55** (6.70)	**7.43** (7.67)
4	**(*R,R*)-C4.4**	**34.90** (35.10)	**4.23** (4.42)	**11.99** (12.28)	**9.01** (9.37)
5	**(*S,S*)-C4.1**	**38.77** (38.95)	**3.99** (4.16)	**8.20** (8.26)	**9.39** (9.45)
6	**(*S,S*)-C4.2**	**40.70** (40.80)	**4.41** (4.57)	**7.80** (7.93)	**9.00** (9.05)
7	**(*S,S*)-C4.3**	**29.76** (31.60)	**3.92** (3.13)	**6.60** (6.70)	**7.15** (7.67)
8	**(*S,S*)-C4.4**	**34.47** (35.10)	**4.36** (4.42)	**11.91** (12.28)	**9.10** (9.37)

4.2.3.3 UV-Vis spectroscopic data of (*R,R*) and (*S,S*) C4.1 to C4.4

The UV-Vis spectra of the (*R,R*) and (*S,S*) tertiary iron(II) complexes in acetonitrile displayed a dominant band at ~400 nm (see Figures 4.13 and 4.14). This high energy transition is attributed to the charge transfer transitions between the iron(II) and pyridine/imidazole donors and is seen for various iron(II) complexes.[20, 21, 22] The band between 200 to 280 nm is a result of the π – π* transitions of the ligand. The UV-Vis cut-off point of acetonitrile is also in this range and that is the reason for the noise observed in this region.

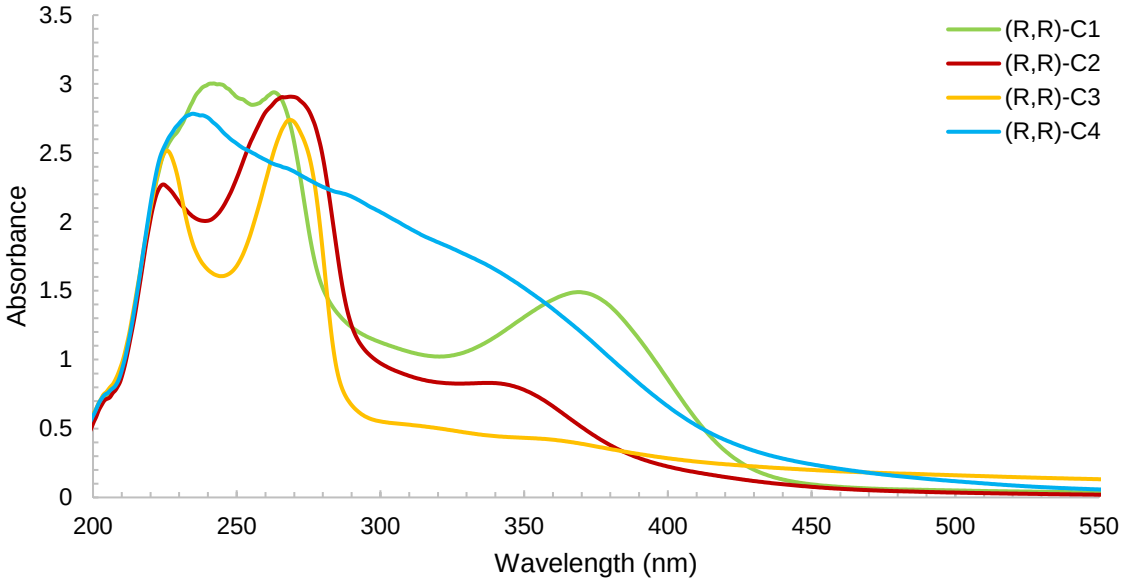

Figure 4.13: UV-Vis spectra of (*R,R*)-iron(II) bistriflate complexes in acetonitrile. (*c* = 0.5 mM)

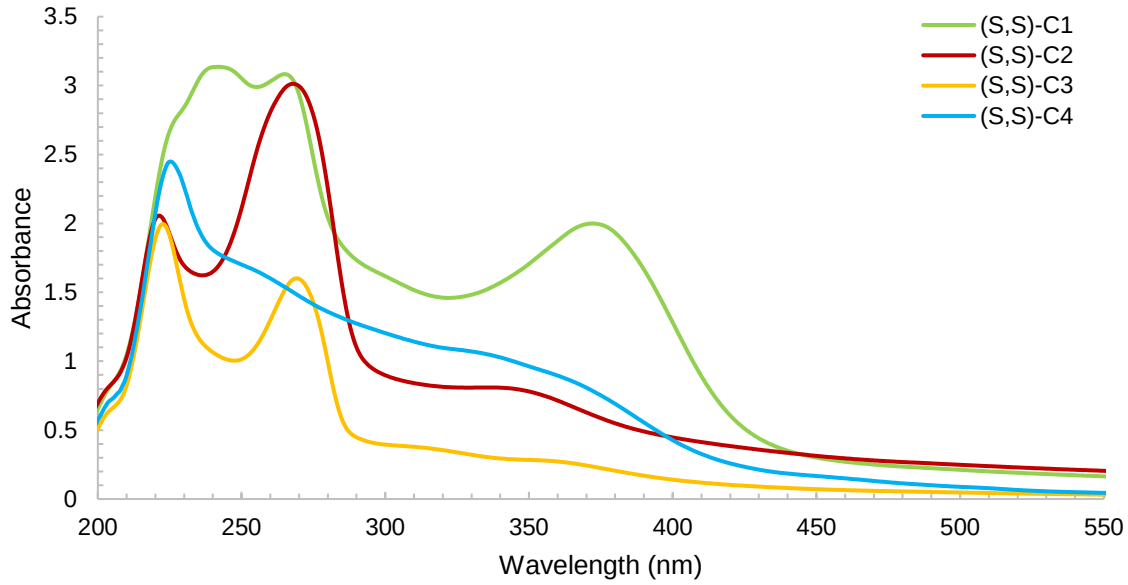

Figure 4.14: UV-Vis spectra of (*S,S*)-iron(II) bistriflate complexes in acetonitrile. (*c* = 0.5 mM)

In **(*R,R*)** and **(*S,S*)-C4.1**, the peak has higher intensity than for the other complexes, which results in a higher absorption coefficient (Table 4.2) for these complexes, with **(*S,S*)-C4.1** having the highest absorption coefficient value (ε_{max}= 5008.44 $M^{-1}.cm^{-1}$). For low-spin complexes, a high ε_{max} value is seen (~8000 $M^{-1}.cm^{-1}$) and for high-spin complexes the ε_{max} values are much lower (~1600 $M^{-1}.cm^{-1}$). Based on the absorption coefficient for **(*R,R*)** and **(*S,S*)-C4.1**, it can be assumed that these complexes interchange between the high- and low-spin configuration. This has been previously observed for analogous iron(II) complexes.[18]

The addition of substituents in the 6-position on the ligands causes a decrease in the intensity of the peak with a reduction in the ε_{max} value. This is indicative of high-spin complexes. For **(*R,R*)** and **(*S,S*)-C4.4**, no band is visible at ~400 nm, because no pyridine donors are present in the ligand.[18]

Table 4.2: Maximum wavelength, absorption coefficient and magnetic moment for the (*R,R*) and (*S,S*) complex sets

Entry	Catalyst	λ_{max}(nm)[a]	ε_{max}($M^{-1}.cm^{-1}$)[a]	μ_{eff}(BM)
1	**(*R,R*)-C4.1**	370.5	4119.48	4.52
2	**(*R,R*)-C4.2**	340	2411.56	5.25
3	**(*R,R*)-C4.3**	360	1612.00	5.20
4	**(*R,R*)-C4.4**	-	-	4.67
5	**(*S,S*)-C4.1**	388	5008.44	4.60
6	**(*S,S*)-C4.2**	346	2775.20	5.49
7	**(*S,S*)-C4.3**	354	1647.25	5.59
8	**(*S,S*)-C4.4**	-	-	5.03

[a] *c* = 0.5 mM in CH_3CN

4.2.3.4 Magnetic susceptibility

The strength of the ligand field exhibited by these non-heme iron(II) complexes can be determined by employing magnetic susceptibility measurements. The magnetic moments of the iron(II) complexes were measured in CH_3CN at 296K (Table 4.2). For the Fe^{2+} oxidation state, values between 5.0 and 5.6 BM are expected. The μ_{eff} values for **(*R,R*)** and **(*S,S*)-C4.2**, **(*R,R*)** and **(*S,S*)-C4.3** and **(*S,S*)-C4.4** indicate that these complexes are high-spin at room temperature. The high-spin configuration is expected because the triflate anions have a weak ligand field and are easily replaced with acetonitrile ligands when the complex is dissolved. Lower μ_{eff} values are seen for **(*R,R*)** and **(*S,S*)-C4.1** and **(*R,R*)-C4.4**. It is believed that this is because the complexes interchange between the high- and low-spin configuration.[23] The same trend as observed here has been seen for a variety of iron(II) complexes.[5, 15, 20]

4.3 Catalytic oxidation of alkene and alcohol substrates

4.3.1 Epoxidation of *cis*-cyclooctene

The oxidation of *cis*-cyclooctene was investigated with the (*R,R*) and (*S,S*) iron(II) bistriflate complex sets with H_2O_2 as oxidant (Scheme 4.3). The catalytic oxidation reactions were performed in the same manner as described in Chapter 3. The oxidation reactions were conducted under both substrate- and oxidant-limiting conditions.

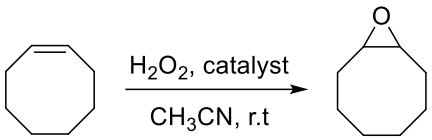

Scheme 4.3: Epoxidation of *cis*-cyclooctene with H_2O_2 as oxidant.

For these specific complex sets, the only product of this reaction, as determined by GC analysis, is *cis*-cyclooctene epoxide. The formation of the 1,2-diol is not observed as is the case in other oxidation reactions.[8, 24] The data for both the (*R,R*) and (*S,S*) complex set is shown in Table 4.3. Under substrate-limiting conditions, **(*R,R*)-C4.1** converts 96% of the substrate into the epoxide. The addition of either the 6-methyl or 6-bromo substituent on the pyridine ring results in a large decrease in the conversion. For **(*R,R*)** and **(*S,S*)-C4.4**, the conversion is only 47% and 51%, respectively, which shows that replacing the pyridine donor with an imidazole donor results in much lower catalytic activity. This strengthens the idea that the pyridine donor is necessary for high catalytic activity and that no substituents should be present on the pyridine ring.

In Figure 4.15, the catalytic activity for the (*R,R*) and (*S,S*) complex set is compared. This graph indicates that the catalytic activity is more or less the same independent of the configuration of the internal diamine donor.

Table 4.3: Oxidation of *cis*-cyclooctene with (*R,R*) and (*S,S*) complex set under substrate-limiting conditions[a]

Entry	Catalyst	% Conversion[b]	Turnover number[c]	Oxidation efficiency[d]
1	**(*R,R*)-C4.1**	96.20	38.48	53.45
2	**(*R,R*)-C4.2**	35.80	14.32	19.89
3	**(*R,R*)-C4.3**	44.85	17.94	24.92
4	**(*R,R*)-C4.4**	47.09	18.84	26.16
5	**(*S,S*)-C4.1**	87.53	35.01	48.63
6	**(*S,S*)-C4.2**	30.24	12.09	16.80
7	**(*S,S*)-C4.3**	43.80	17.52	24.33
8	**(*S,S*)-C4.4**	51.87	20.75	28.82

[a] Reaction conditions: See experimental section. [b] (moles of substrate converted/moles of substrate added) x 100. [c] (moles of product/moles of catalyst) [d] (moles of product/moles of oxidant) x 100. The data reported is the average of two runs.

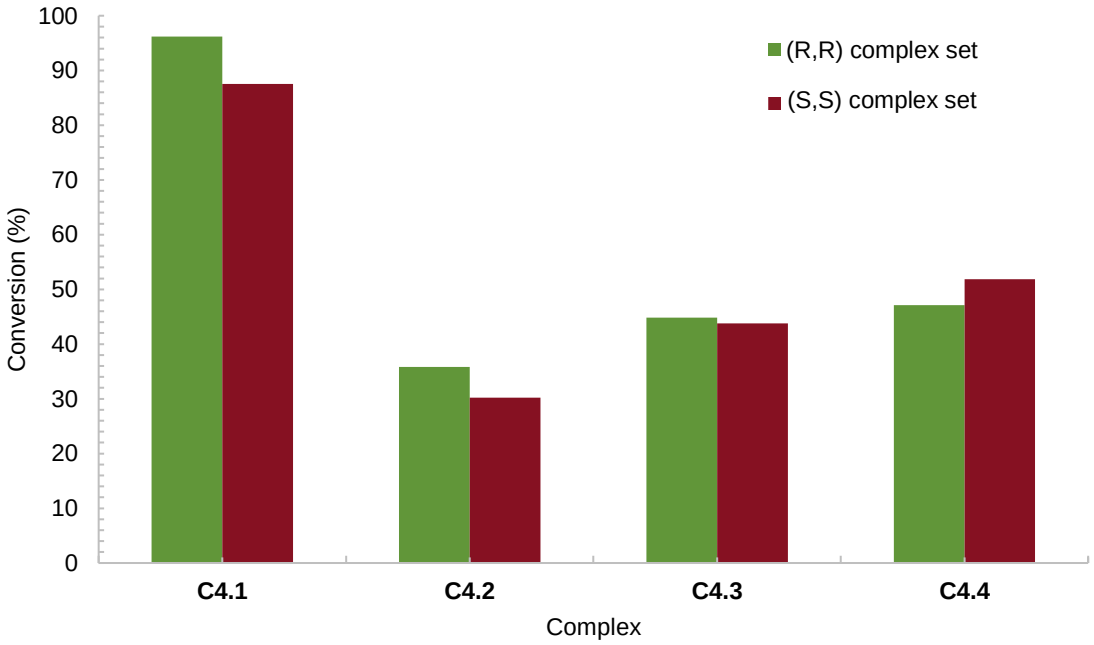

Figure 4.15: Comparison of the conversion (%) of *cis*-cyclooctene for the (*R,R*) and (*S,S*) complex set under substrate-limiting conditions.

Usually the oxidation reactions are performed with the substrate in excess, i.e. oxidant-limiting conditions. This is done in an attempt to minimise over-oxidation of the substrate. For the oxidation of *cis*-cyclooctene under oxidant-limiting conditions, the ratio of catalyst: oxidant: substrate is 1:10:1000. The data for the (*R,R*) and (*S,S*) complex set is provided in Table 4.4.

Table 4.4: Oxidation of *cis*-cyclooctene with (*R,R*) and (*S,S*) complex set under oxidant-limiting conditions[a]

Entry	Catalyst	% Conversion[b]	Turnover number[c]	Oxidation efficiency[d]
1	**(*R,R*)-C4.1**	10.96	109.64	1096.39
2	**(*R,R*)-C4.2**	9.02	90.16	901.60
3	**(*R,R*)-C4.3**	4.48	44.78	447.76
4	**(*R,R*)-C4.4**	9.26	92.64	926.43
5	**(*S,S*)-C4.1**	9.36	93.59	935.89
6	**(*S,S*)-C4.2**	3.98	39.80	398.22
7	**(*S,S*)-C4.3**	5.90	58.95	589.51
8	**(*S,S*)-C4.4**	6.79	67.58	675.77

[a] Reaction conditions: See experimental section. [b] (moles of substrate converted/moles of substrate added) x 100. [c] (moles of product/moles of catalyst) [d] (moles of product/moles of oxidant) x 100. The data reported is the average of two runs.

For the oxidation reactions done under oxidant-limiting conditions, the conversion of *cis*-cyclooctene is very low. The highest conversion seen is 11% with **(*R,R*)-C4.1**. The turnover numbers and oxidation efficiency are much higher than for the complexes when done under substrate-limiting conditions. In Figure 4.16, the conversion for the (*R,R*) and (*S,S*) complex set is compared. Although the conversions are much lower under oxidant-limiting conditions than substrate-limiting conditions, the same trend is observed. The (*R,R*) and (*S,S*) configurations display more or less the same catalytic activity. Again, the best conversion is seen for the pyridine donors, with the added 6-methyl and 6-bromo substituents causing a decrease in the catalytic activity as well as when the pyridine is replaced with an imidazole donor.

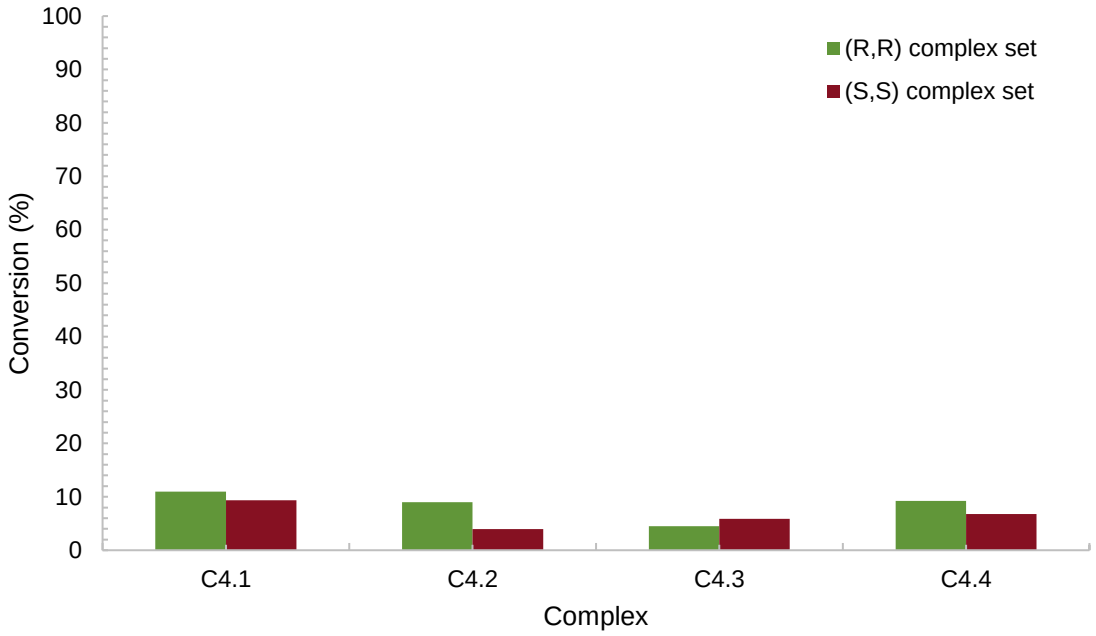

Figure 4.16: Comparison of the conversion (%) of *cis*-cyclooctene for the (*R,R*) and (*S,S*) complex set under oxidant-limiting conditions.

In literature, there are a few studies that have performed *cis*-cyclooctene oxidation with BPMCN ligands, their derivatives and iron(II). Que and co-workers found a turnover number of 5.8 for the epoxide and 0.7 for the diol when using 10 equiv of H_2O_2 with (*R,R*)-[Fe(BPMCN)(OTf)$_2$] as catalyst. When using (*S,S*)-[Fe(6Me-BPMCN)(OTf)$_2$] and 10 equiv of H_2O_2, they observed turnover numbers of 3.5 and 5.8 for the epoxide and diol, respectively. When increasing the amount of H_2O_2 to 20 equiv, the turnover numbers for the epoxide and the diol increased to 5.4 and 11.2.[24] Contrary to these reported results, we found no formation of the diol and only the epoxide product was observed. Furthermore, these reactions were done only under oxidant-limiting conditions. We investigated the effect of oxidant- as well as substrate-limiting conditions. Under substrate-limiting conditions, almost 100% conversion of the substrate was seen, but the conversion decreased dramatically under oxidant-limiting conditions. Comparing the turnover numbers, we see that under substrate-limiting conditions, the turnover numbers and oxidation efficiency are much lower than under oxidant-limiting conditions. The reason for this is that under oxidant-limiting conditions the amount of catalyst and oxidant used is much less as compared to the reaction conditions under substrate-limiting conditions.

Costas and co-workers investigated the oxidation of *cis*-cyclooctene with the *cis*-α and *cis*-β topology of [Fe(BPMCN)(OTf)$_2$]. For α-[Fe(BPMCN)(OTf)$_2$], the oxidation reaction gave a TON of 6.5 (diol + epoxide) when using 7 mM H_2O_2 and a reaction time of 30 minutes. The TON increased to 7.7 when β-[Fe(BPMCN)(OTf)$_2$] was used as catalyst. They observed a

significant difference in the catalytic activity of the *cis*-α and *cis*-β topology.[25] It is believed that the (*S,S*) configuration results in the ligand being in the *cis*-α topology and the ligand will be in the *cis*-β topology if the internal diamine donor is in the (*R,R*)-configuration. When comparing the catalytic activity of our (*R,R*) and (*S,S*) complexes, there is no remarkable difference. This suggests that, in this case, the ligand topologies of the complexes are not different and when the complex is in solution, an equilibrium exists between the two configurations.

4.3.2 Effect of steric and electronic properties on catalytic activity

An increase in the metal-to-ligand charge transfer was observed by UV-Vis for ligands containing only pyridine donors. This causes a stronger ligand field that is then able to stabilise the high-valent iron-oxo intermediates. When the pyridine donors are replaced with imidazole donors, there is a dramatic decrease in catalytic activity due to the weaker ligand field.[18] Replacing the pyridine donors results in the weakening of the Fe-N(Me-Im) bond and the iron complexes are in a high-spin configuration.[3] There is also a steric effect because of the geometry of the five-membered ring that will cause additional strain in the chelate ring.[23]

It is expected that the introduction of the methyl group on the pyridine ring will enhance the catalysis and the bromine substituent will result in lower catalytic activity for the complexes. The catalysis data shows that the substituents on the pyridyl ring have a significant steric effect on the metal centre, which prevents the pyridyl groups from getting too close to the iron centre. This results in the substituted ligands favouring metal centres that have larger ionic radii; for example, high-spin over low-spin.[23, 26] The contribution of this steric effect on the observed catalytic activity is larger than the electronic effects that the electron-donating or electron-withdrawing substituents can have and causes the complex to be less stable.[27]

4.3.3 Effect of ligand topology on catalytic activity

Studies have shown that there can be a significant difference in the catalytic activity of (*R,R*) and (*S,S*) iron(II) complexes.[24] The reason for this difference in catalytic activity is because the configuration causes a difference in the topology of the ligand. The complex can be in either the *cis*-α or *cis*-β topology. Que and co-workers were able to isolate the two topologies of [Fe(BPMCN)$(OTf)_2$] and characterised it with NMR spectroscopy. The two topologies displayed distinctly different spectral features. In the case of the *cis*-α topology, the ^{1}H NMR spectrum was characterised by well-defined resonances within a narrow spectral window. In contrast, the *cis*-β topology displayed broad, poorly resolved resonances over a wide spectral

window. Their results demonstrated that these topologically different complexes retain their specific configuration in solution and that the topological differences result in a significant difference in the catalytic activity of these complexes.[25] For the oxidation of cyclohexane, the complex in the *cis*-α topology was much more active than the *cis*-β topology and showed a turnover number that was three times higher. They also found that the reactions with the *cis*-α topology were highly stereoselective. When *cis*- and *trans*-2-heptene was oxidised, the corresponding *cis*-diols and epoxides were formed with no loss of stereochemistry.

Considering that both **(*R,R*)** and **(*S,S*)-C4.1** to **C4.4** displayed similar catalytic activity in the epoxidation of *cis*-cyclooctene, the solution structures of the two derivates were investigated by ^{1}H NMR spectroscopy. The ^{1}H NMR spectra for these complexes are shown in Figure 4.17. It is evident that there is no difference between the spectra for the two complexes. The reason for this may be that, in solution, both complexes have the same configuration. When the complexes are dissolved in CD_3CN, the triflate groups undergo fast substitution to give $[Fe(L)(CD_3CN)](OTf)_2$ complexes, which are in a spin crossover regime.[5] The broad ^{1}H NMR signals are because the triflate and acetonitrile ligands are constantly being exchanged, along with the interconversion between low- and high-spin configurations and the paramagnetic nature of iron(II). This makes it very difficult to characterise these complexes with NMR spectroscopy. The idea that these complexes interchange between the two configurations is supported by UV-Vis spectroscopy as well as magnetic susceptibility measurements. The UV-Vis spectra showed weak metal-to-ligand charge transfer interactions that are indicative of complexes in the *cis*-β configuration. From the magnetic susceptibility measurements, it is evident that most complexes are in a high-spin configuration and the complexes with lower than expected μ_{eff} values interchange between the high- and low-spin configuration. The ^{1}H NMR spectra of these complexes are also consistent with complexes that interchange between the *cis*-α and *cis*-β configurations. Even though the ligands are synthesised with either (*R,R*)- or (*S,S*)-1,2-diaminecyclohexane, in solution, the configurations interchange. This also provides a reason for the similar catalytic activity exhibited by the (*R,R*) and (*S,S*) complex sets.

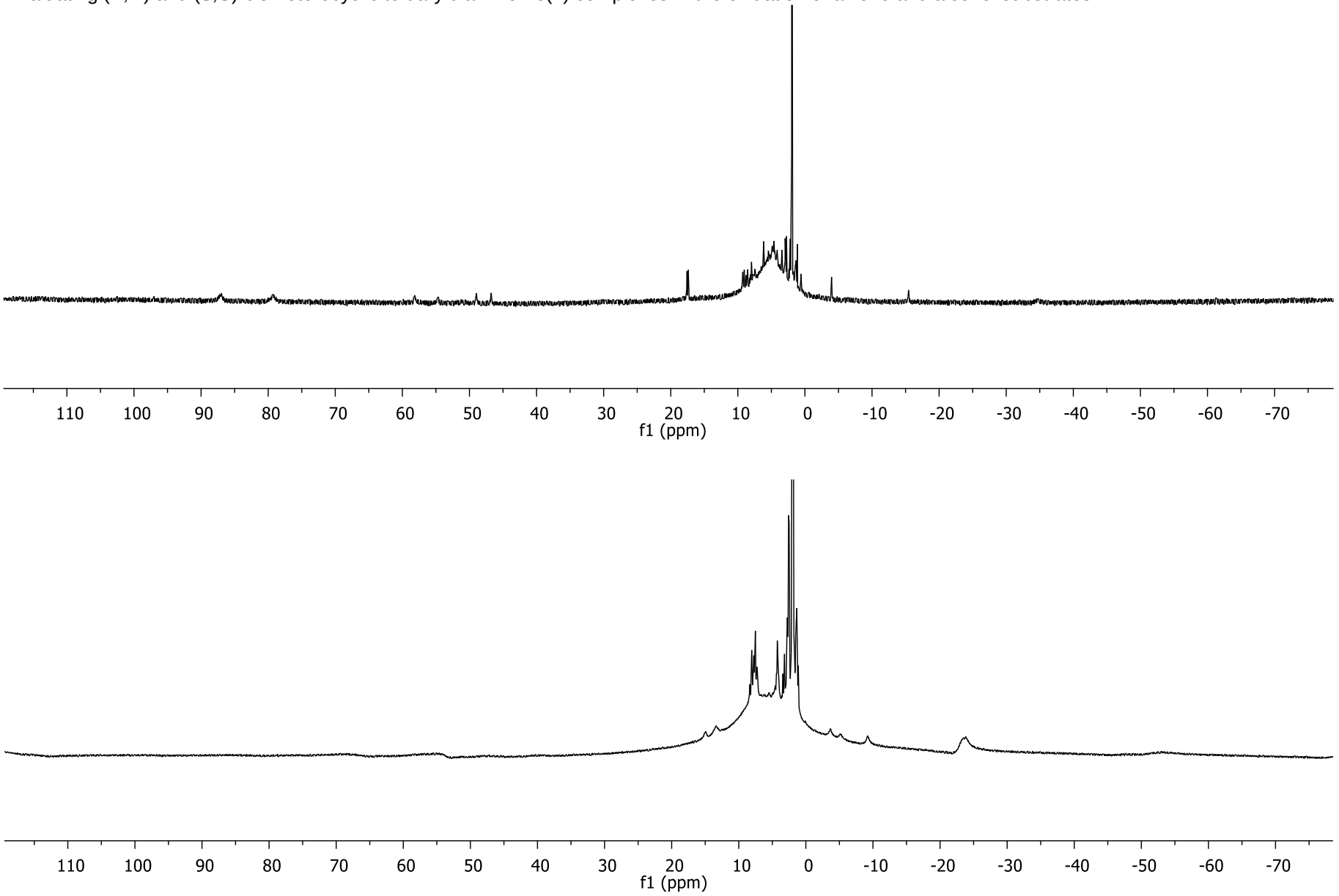

Figure 4.17: ^{1}H NMR spectra of **(*R*,*R*)-C4.3** (top) and **(*S*,*S*)-C4.3** (bottom), which suggests that both catalysts have the same configuration when in solution.

4.3.4 Effect of additives on catalytic activity

Various examples show that added acetic acid leads to an increase in the catalytic activity of iron(II) complexes.[6, 28, 29] Jacobsen and co-workers first observed this effect with two different complexes, $[Fe(BPMCN)(CH_3CN)_2]^{2+}$ and $[Fe(TPA)(CH_3CN)_2]^{2+}$ with 1-decene as substrate.[30] For olefin oxidation, it was found that acetic acid inhibits the *cis*-dihydroxylation pathway and favours epoxidation and therefore leads to an increase in the selectivity for the epoxidised product. The effect of the AcOH was investigated with **(*S,S*)-C4.1** and **(*S,S*)-C4.4** and can be seen in Figure 4.18.

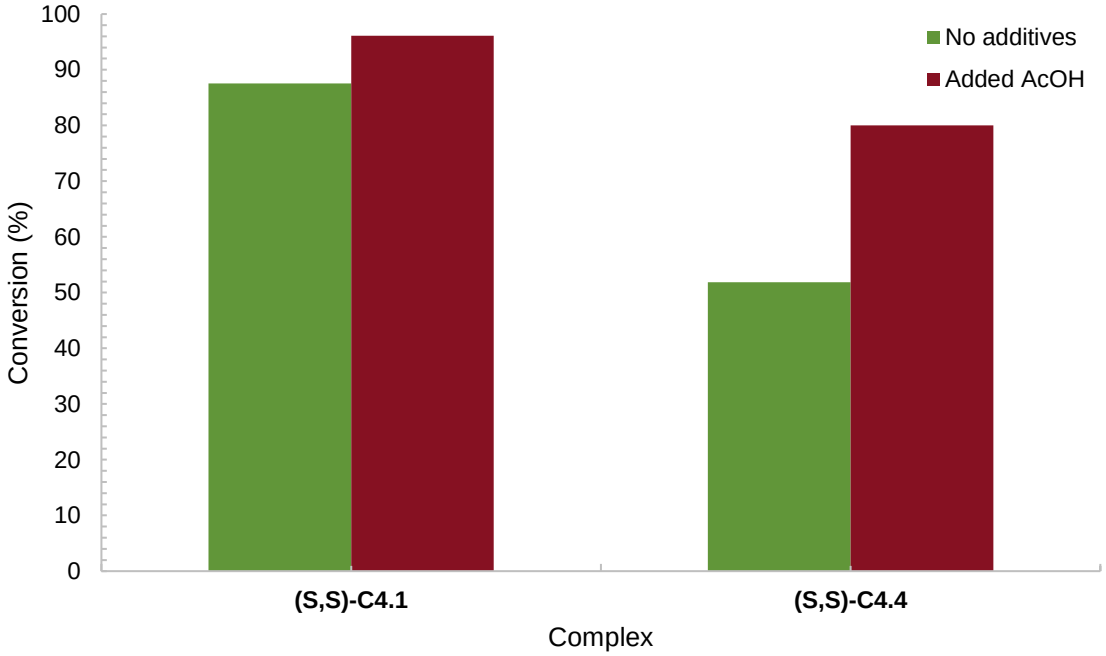

Figure 4.18: Effect of added AcOH on the conversion (%) of *cis*-cyclooctene for **(*S,S*)-C4.1** and **(*S,S*)-C4.4** under substrate-limiting conditions.

The addition of AcOH resulted in an increase in the conversion seen for these complexes. **(*S,S*)-C4.4** shows an approximately 30% increase in the conversion. Because this reaction is 100% selective for the epoxide product, we could not show if *cis*-dihydroxylation is inhibited upon addition of AcOH. It is believed that acetic acid assists with the formation of the metal-based active species, $Fe^{V}(O)(OAc)$, since it aids the heterolytic cleavage of the O-O bond in the Fe^{III}-OOH species.[31]

4.3.5 Oxidation of benzyl alcohol

Next we evaluated the catalytic application of **(*R,R*)** and **(*S,S*)-C4.1** to **C4.4** in alcohol oxidation.

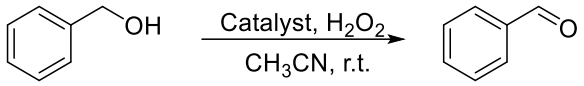

Scheme 4.4: Benzyl alcohol oxidation with H_2O_2 as oxidant.

Benzyl alcohol was used as a model substrate to investigate the influence of the amount and type of catalyst as well as the amount of hydrogen peroxide (Scheme 4.4). Firstly, the oxidation of benzyl alcohol was performed with all the (*R,R*) and (*S,S*) complexes under substrate-limiting conditions (Table 4.5).

Table 4.5: Oxidation of benzyl alcohol with (*R,R*) and (*S,S*) complex set under substrate-limiting conditions[a]

Entry	Catalyst	% Conversion[b]	Turnover number[c]	Oxidation efficiency[d]
1	**(*R,R*)-C4.1**	43.49	34.79	24.16
2	**(*R,R*)-C4.2**	22.15	17.72	12.31
3	**(*R,R*)-C4.3**	17.20	13.76	9.56
4	**(*R,R*)-C4.4**	24.98	19.99	13.88
5	**(*S,S*)-C4.1**	57.37	45.90	31.87
6	**(*S,S*)-C4.2**	22.34	17.87	12.41
7	**(*S,S*)-C4.3**	20.91	16.73	11.62
8	**(*S,S*)-C4.4**	32.56	26.05	18.09

[a] Reaction conditions: See experimental section. [b] (moles of substrate converted/moles of substrate added) x 100. [c] (moles of product/moles of catalyst) [d] (moles of product/moles of oxidant) x 100. The data reported is the average of two runs.

In general, lower conversion to benzaldehyde was observed in comparison to *cis*-cyclooctene. The highest conversion is 57% when using **(*S,S*)-C4.1** as catalyst. In Figure 4.19, the conversions of the (*R,R*) and (*S,S*) complex sets are compared. The (*S,S*) complexes show higher conversion, but it is not a considerable difference between the two complex sets. The same trend as for *cis*-cyclooctene epoxidation is also observed for benzyl alcohol oxidation. The complexes with the pyridine donors have the best catalytic activity. Again, the added

methyl and bromine substituents result in a dramatic decrease in catalytic activity. The complex with the imidazole donor also shows low catalytic activity.

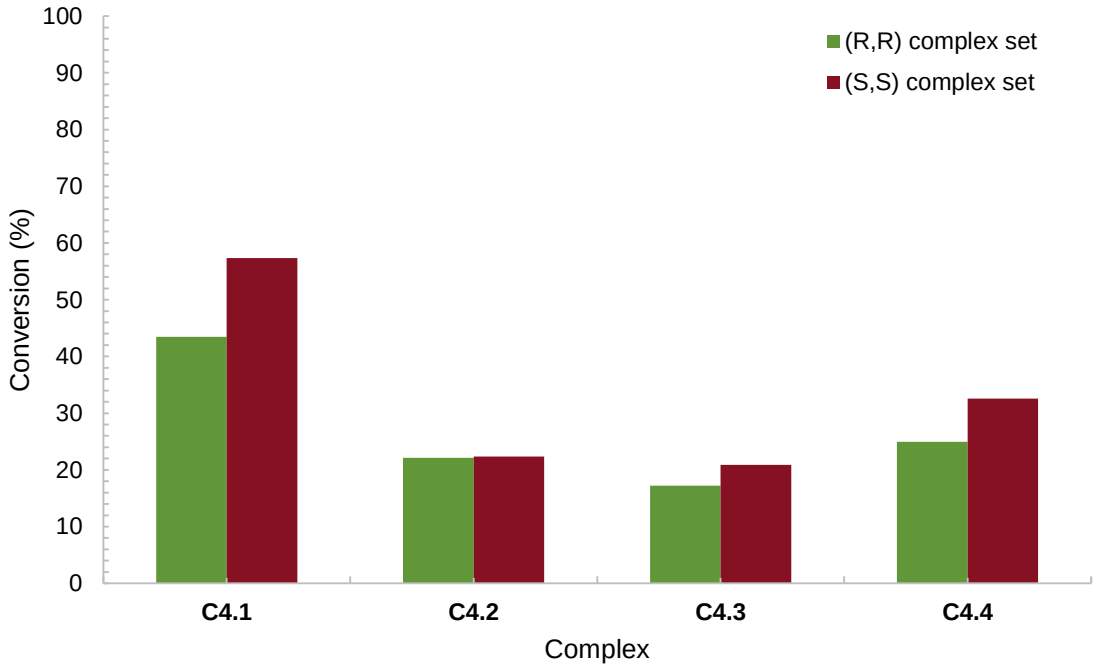

Figure 4.19: Comparison of the conversion (%) of benzyl alcohol for the (*R,R*) and (*S,S*) complex set under substrate-limiting conditions.

Catalysts **(*R,R*)** and **(*S,S*)-C4.1** were employed to investigate the influence of the change in amount of oxidant and amount of catalyst. For the standard reaction, 1.8 mmol of H_2O_2 was added. The effect of oxidant variation is shown in Figure 4.20. For **(*R,R*)-C4.1**, as the oxidant amount increased, the conversion of benzyl alcohol increased. It reaches a maximum at 2.5 mmol and increasing the amount of H_2O_2 to 3.5 mmol does not cause a significant increase in the conversion. Increasing the amount of oxidant also resulted in the formation of trace amounts of benzoic acid for both **(*R,R*)** and **(*S,S*)-C4.1**. For **(*S,S*)-C4.1**, the conversion stayed more or less constant with varying oxidant concentration. When increasing the amount of oxidant, the possibility for over-oxidation increases and this does not result in an increase in the amount of oxygenated product formed.[20] The reaction of the Fe(II) complex with H_2O_2 results in the formation of Fe^{III}-OOH hydroperoxo or Fe^{IV}/Fe^{V}-oxo active species. The amount of active species formed is limited by the amount of catalyst present, and increasing the amount of oxidant does not result in higher catalytic activity.

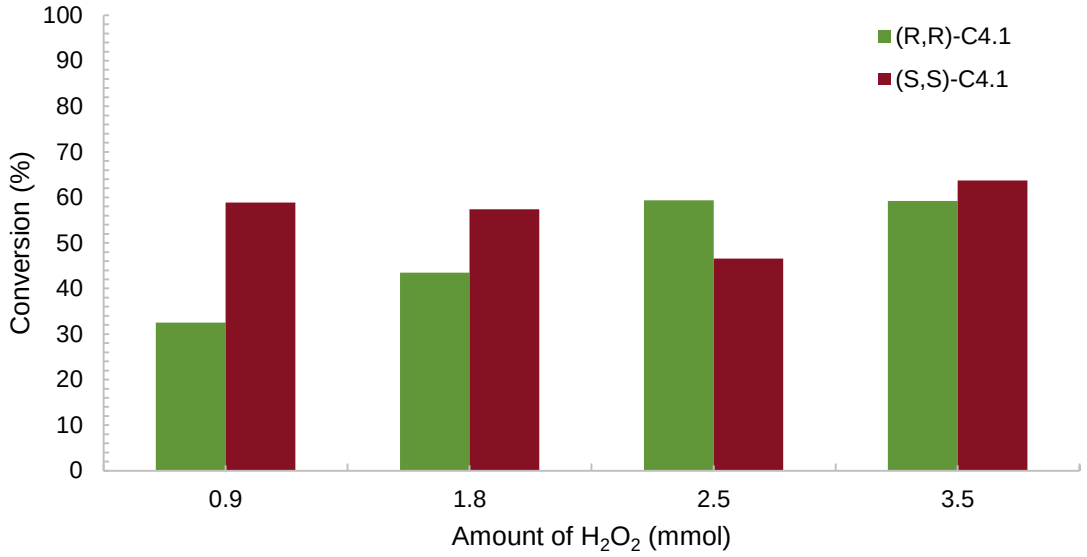

Figure 4.20: Effect of the change in amount of H_2O_2 (mmol) on the conversion (%) of benzyl alcohol catalysed by **(*R,R*)** and **(*S,S*)-C4.1**.

(*R,R*) and **(*S,S*)-C4.1** were also used to investigate the effect of the catalyst loading on the catalytic activity. This data is shown in Figure 4.21. When 2.5 µmol of catalyst is used, no oxidation of the substrate takes place. Increasing the amount five-fold to 12.5 µmol, results in a significant increase for both the catalysts. With 25 µmol of the catalyst, the conversion for **(*S,S*)-C4.1** reaches 73% and **(*R,R*)-4.1** is 56%. Studies have shown that an increase in the catalyst loading results in an increase in the conversion of the substrate.[19, 28] More catalyst means that more active sites are available for the activation of H_2O_2 to form the active species that are responsible for the oxidation of the substrate.

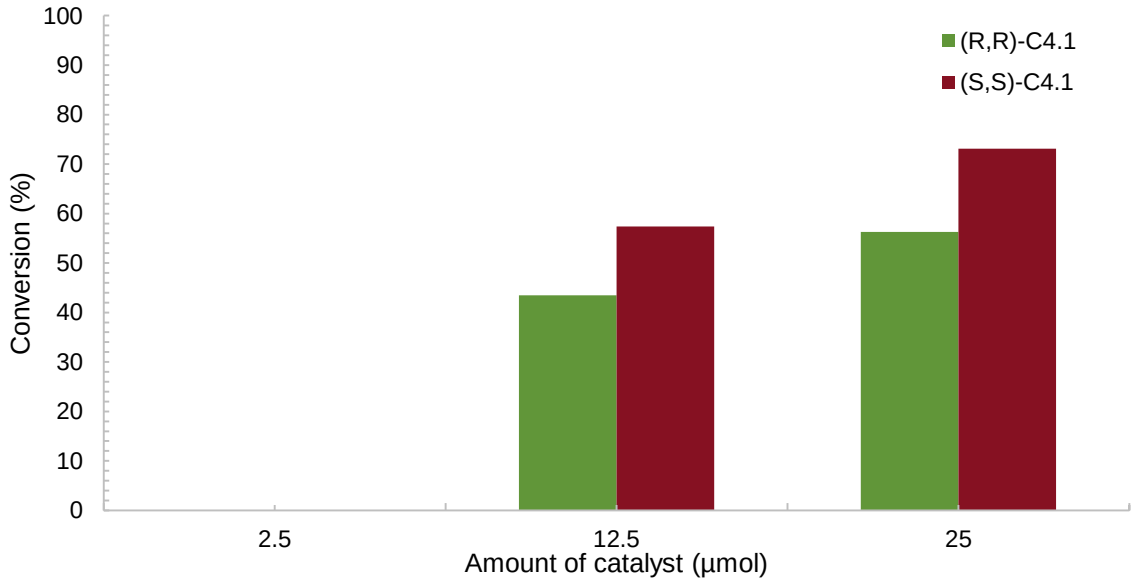

Figure 4.21: Effect of the amount of catalyst on the conversion (%) of benzyl alcohol for **(*R,R*)** and **(*S,S*)-C4.1**.

Next, the effect of acetic acid as additive was investigated. The % conversion for **(*R,R*)** and **(*S,S*)-C4.1** without AcOH and with added AcOH is compared in Figure 4.22. From the graph, it is clear that AcOH has no effect on the catalytic activity. The reason for this is that in alcohol oxidation there is no need for oxygen atom transfer from the high-valent iron-oxo species to the substrate. Instead, hydrogen-atom abstraction is the driving force for product formation.

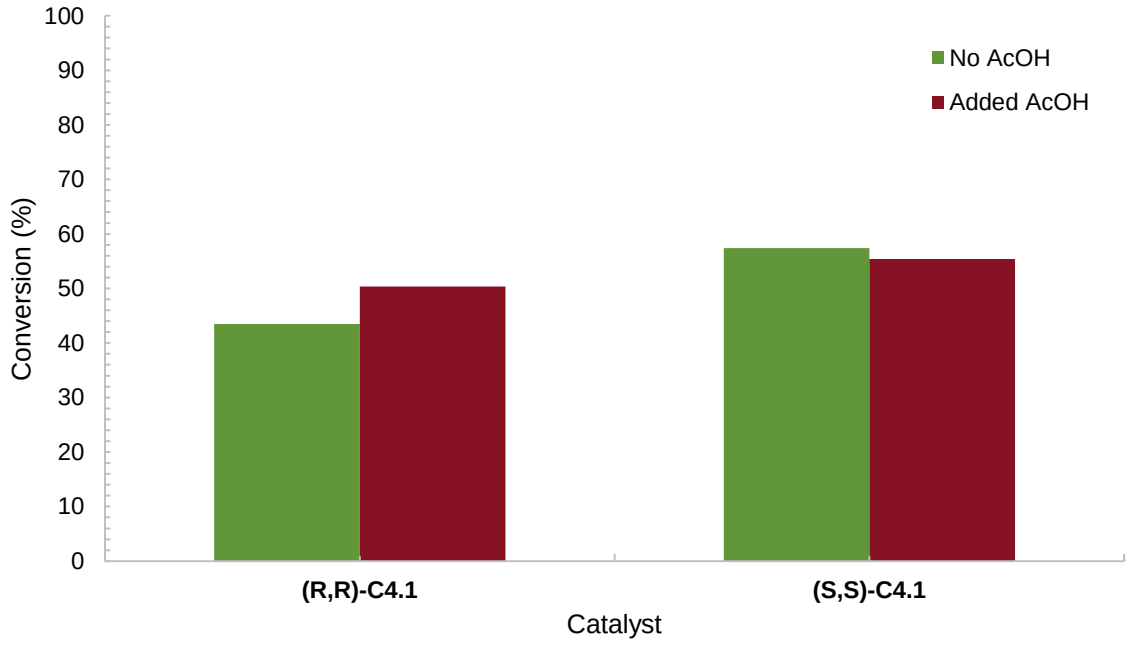

Figure 4.22: Effect of added AcOH on the conversion (%) seen for **(*R,R*)** and **(*S,S*)-C4.1** in the oxidation of benzyl alcohol.

Different iron systems have been investigated for alcohol oxidation, but there are no examples of BPMCN ligands in combination with iron(II). Xia and co-workers performed benzyl alcohol oxidation with CuBr, BPMCN and TEMPO. After a reaction time of 30 minutes, they obtained a conversion of 37% and yield of 33%. Increasing the reaction time to 50 minutes, resulted in an increase in the conversion and yield to 77% and 75%, respectively.[14] An iron(II) catalyst system was investigated by Sato and co-workers. They combined $Fe(OAc)_2$, picH, Me-picH and H_2O_2 to oxidise benzyl alcohol. This system gave a yield of 50% and selectivity of 91% towards benzaldehyde.[32] Feringa and co-workers also used a µ-oxo diiron(II) complex and H_2O_2 as oxidant for benzyl alcohol oxidation. After 75 minutes reaction time, a TON of 50 is seen, with a trace amount of benzoic acid present.[33]

Under the optimised conditions, the best conversion seen for our system was 73% with only trace amounts of benzoic acid detected. These results are similar and in some cases better than the results for other types of iron systems discussed above. In addition, this oxidation system has the advantage of mild reaction conditions, while still being effective in oxidising the substrates.

4.3.6 Substrate scope

The oxidation of a range of alcohols was investigated to determine the efficiency and limitations of this catalyst system. Table 4.6 provides a summary of the oxidation results.

Table 4.6: Oxidation of various alcohol substrates with non-heme iron(II) complexes

Entry	Substrate	Product	Time	Yield[a] (%)
1	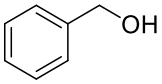	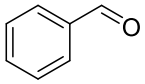	40 min	39
2	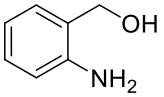	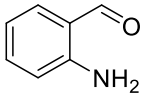	40 min	32
3	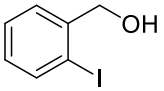	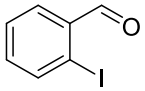	40 min	15
4	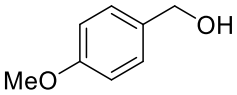	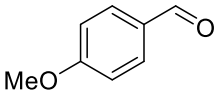	40 min	59
5	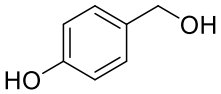	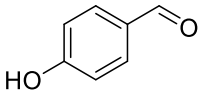	40 min	15
6	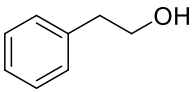	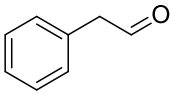	40 min	12
7	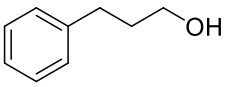	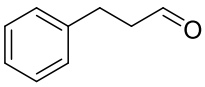	40 min	5
8	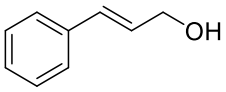	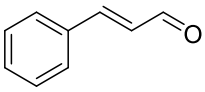	40 min	64
9	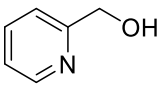	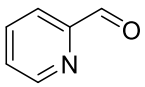	40 min	21
10	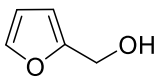	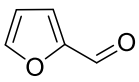	40 min	68
11	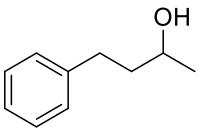	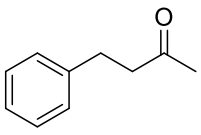	40 min	27
12	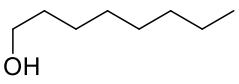	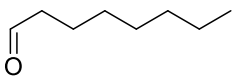	40 min	47
13	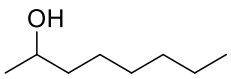	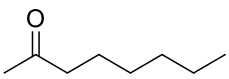	40 min	54

Reaction conditions: Substrate (1 mmol) was dissolved in 2 mL acetonitrile and added to the catalyst (25 µmol). H_2O_2 (1.8 mmol) was added with a syringe pump for 25 min and the reaction mixture stirred for a further 15 min. [a]GC yield. The data reported is the average of two runs.

The optimised reaction conditions were used for the investigation of the different substrates. Introducing substituents on the *ortho*-position of benzyl alcohol resulted in a decrease in the yield of aldehyde (Table 4.6, entries 2 and 3). This may be a result of steric pressure induced by the substituent in the *ortho*-position. When the substituent is introduced on the *para*-position, the steric pressure is reduced and the yield increases (Table 4.6, entry 4). The exception was when employing 4-hydroxybenzyl alcohol as substrates. This substrate was oxidised with a very low yield, which may be due to its poor solubility in acetonitrile (Table 4.6, entry 5). Increasing the aliphatic chain length in comparison to benzyl alcohol, i.e. 2-phenylethanol and 3-phenylpropanol resulted in lower aldehyde yield (Table 4.6, entries 6 and 7). The reason for this observation may be that when the OH group moves further away from the ring, the bond is more difficult to oxidise. In contrast, employing cinnamyl alcohol as substrate resulted in an aldehyde yield of 64% (Table 4.6, entry 8). The reason for this higher yield compared to the other substrates may be the conjugated double bonds that promote oxidation. Two heterocyclic alcohols were also investigated (Table 4.6, entries 9 and 10). Good yields were seen for furfuryl alcohol, but 2-pyridinemethanol gave poor yields. This is likely due to the substrate coordinating with the metal, i.e. competitive inhibition. Experimental evidence for this has been obtained during Cu-catalysed alcohol oxidation.[34] Aliphatic alcohols are usually more difficult to oxidise; however, this system was successful in oxidising 1-octanol and gave a yield of 42% (Table 4.6, entry 12), but a trace amount of octanoic acid is seen. An advantage of this system is that it is able to oxidise benzylic and aliphatic secondary alcohols (Table 4.6, entries 11 and 13). Data for these specific secondary alcohols that we investigated has not been previously reported in literature.

4.4 Conclusions

A range of (*R,R*) and (*S,S*) tertiary bis-heterocyclic diamine ligands and the corresponding iron(II) complexes were synthesised and characterised. The structures of the ligands and complexes were confirmed with a variety of analytical techniques, which include FT-IR, NMR, UV-Vis, MS, elemental analysis and magnetic susceptibility. The UV-Vis and magnetic susceptibility measurements indicate that **(*R,R*)** and **(*S,S*)-C4.1** possess the strongest ligand field and interchanges between the low- and high-spin configuration. MS analysis of all the complexes displayed the characteristic mass fragment, $[M\text{-}OTf]^+$. Elemental analysis also confirmed that complexes with the desired composition have been formed. The small difference in the experimental and calculated values can be attributed to the instability of the complexes as well as trace amounts of solvent trapped in the complexes.

These iron(II) complexes were investigated as catalysts for alkene and alcohol oxidation. For the oxidation of *cis*-cyclooctene, the best activity was observed for **(*R,R*)-C4.1**. This complex, under substrate-limiting conditions, was able to convert 96% of the *cis*-cyclooctene into

cyclooctene epoxide with 100% selectivity. The addition of the 6-methyl and 6-bromo substituents on the pyridine ring resulted in a significant decrease in the observed catalytic activity. Replacing the pyridine donor with an imidazole donor also decreased the observed catalytic activity. The addition of acetic acid to the catalyst system resulted in up to a 30% increase in the conversion of *cis*-cyclooctene. The steric and electronic properties of the ligands as well as the influence of ligand topology were investigated. The steric effect is more notable than the electronic effect. The substituents on the pyridine ring prevent the pyridyl ring from getting close to the metal centre and these complexes favour the more unstable high-spin configuration. Replacing the pyridine donor with an imidazole donor also has a steric effect and leads to the Fe-N(Im-Me) bond being weakened. These effects result in a weaker ligand field and also lower catalytic activity. The catalytic activity of the (*R,R*) and (*S,S*) iron(II) complexes were compared, with no significant difference in the catalytic activity seen for the two different configurations. The reason for this is that in solution, these complexes interchange between the two configurations.

The prepared iron(II) complexes were active catalysts for the oxidation of benzyl alcohol and this substrate was used to optimise different parameters of the oxidation reaction. The highest conversion was observed when using **(*S,S*)-C4.1** (25 µmol) and 1.8 mmol H_2O_2 and gave a conversion of 73%. When increasing the amount of H_2O_2, trace amounts of benzoic acid were observed, which is characteristic of over-oxidation. The substrate scope was extended to determine the functional group tolerance and limitations of the iron(II) system. This system was able to oxidise a range of alcohol substrates, which include allylic, benzylic and aliphatic alcohols. Another advantage of this system is that it is able to oxidise primary as well as secondary alcohols.

4.5 Experimental procedures

4.5.1 General considerations

Reagents were purchased for Sigma-Aldrich and/or Merck. Reagents and solvents used were commercially available reagent quality unless otherwise stated. Solvents were dried and purified by conventional distillation techniques. Diethyl ether was dried by prolonged reflux over sodium metal with benzophenone indicator under a nitrogen atmosphere. Dichloromethane was dried in a similar manner, but with calcium hydride as the drying agent. The solvents were freshly distilled prior to use.

Standard Schlenk techniques were used to prepare all oxygen- and moisture-sensitive compounds. Further storage and handling of these compounds were done in a standard glove box (MBraun) with H_2O and O_2 concentrations smaller than 0.1 ppm. ^{1}H NMR and ^{13}C NMR was recorded on a Bruker 600 MHz Ultrashield Plus spectrometer and chemical shifts reported in ppm relative to the residual deuterated solvent peak. Peak splitting patterns are indicated as s, singlet; d, doublet; t, triplet; m, multiplet. FT-IR spectra were recorded on a Bruker Alpha-P range infrared instrument equipped with an ATR accessory as neat samples. Gas chromatographic analysis were performed on an Agilent 6890 Series GC System with a HP 5 column, 30 m in length, 0.320 mm internal diameter and 0.25 mm film thickness. N_2 served as the carrier gas, acetonitrile (CH_3CN) and dichloromethane (DCM) were used as the rinsing solutions and biphenyl as the internal standard. Elemental analysis was performed by the University of KwaZulu-Natal Mass Spectrometry Laboratory. Electrospray ionisation mass spectrometric analysis (ESI-MS, positive ion mode) was performed on a Bruker microTOF-Q II mass spectrometer. Matrix assisted laser desorption ionisation (MALDI) was performed on Autoflex II spectrometers, by employing trans-2-[3-(4-tert-Butylphenyl)-2-methyl-2-propenylidene]malononitrile (DCTB) as matrix. Magnetic susceptibility measurements of complex solutions were done on a Sherwood Scientific MK1 magnetic susceptibility balance.

4.5.2 Synthesis of (*R,R*) bis-heterocyclic diamine ligands and Fe(II) complexes

(*R,R*)-N,N′-dimethyl-N,N′-bis(pyridyl-2-methyl)-1,2-cyclohexanediamine (*R,R*)-L4.1

(*R,R*)-L3.6 (0.563 mmol) was dissolved in a mixture of CH_3CN and acetic acid (AcOH) (2.75 mL CH_3CN + 0.37 mL AcOH). 32% aqueous formaldehyde was added and the mixture stirred for 20 minutes at room temperature. Sodium borohydride ($NaBH_4$) was added portion wise and the mixture stirred for 72 hours at room temperature. CH_3CN was removed *in vacuo* and 2N potassium hydroxide (KOH) was added till pH > 10. The aqueous phase was extracted with 3 × 10 mL DCM and the organic phase was washed with 2 × 10 mL distilled water (dH_2O)

and 1 × 10 mL saturated sodium chloride (NaCl) mixture and dried with anhydrous magnesium sulphate ($MgSO_4$). The solvent was removed to afford the product. Yellow oil (176.0 mg, 96.35% yield).

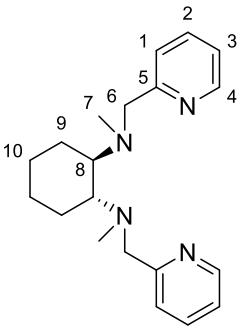

^{1}H NMR (600MHz, $CDCl_3$) δ 8.45 – 8.44 (d, 2H, $J_{H\text{-}H}$=4.77, H^4), 7.61 – 7.58 (t, 2H, $J_{H\text{-}H}$=7.55, H^3), 7.56 – 7.55 (d, 2H, $J_{H\text{-}H}$=7.68, H^2), 7.13 – 7.11 (t, 2H, $J_{H\text{-}H}$=6.01, H^2), 4.00 – 3.97 (d, 2H, $J_{H\text{-}H}$=14.35, H^6), 3.85 – 3.82 (d, 2H, $J_{H\text{-}H}$=14.41, H^6), 2.76 – 2.72 (m, 2H, H^8), 2.32 (s, 6H, H^7), 2.03 – 2.01 (m, 2H, H^9), 1.78 – 1.76 (m, 2H, H^9), 1.31 – 1.28 (m, 2H, H^{10}), 1.19 – 1.15 (m, 2H, H^{10}); ^{13}C NMR (150MHz, $CDCl_3$) δ 159.77, 148.59, 136.60, 123.29, 121.98, 64.25, 59.48, 36.88, 25.47, 25.37. FT-IR ν (cm^{-1}) 2929, 2854, 1590, 1432, 1046, 880, 757, 620.

(*R,R*)-N,N′-dimethyl-N,N′-bis(6-methyl-2-pyridyl-2-methyl)-1,2-cyclohexanediamine (*R,R*)-L4.2

(*R,R*)-L4.2 was synthesised following the same procedure as for **(*R,R*)-L4.1**, employing **(*R,R*)-L3.7** (0.415 mmol). Yellow oil (89.0 mg, 60.9% yield).

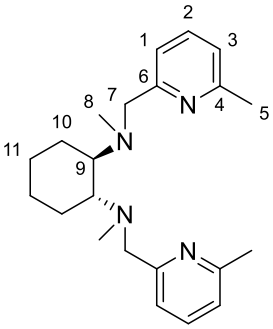

^{1}H NMR (600MHz, $CDCl_3$) δ 7.46 – 7.44 (t, 2H, $J_{H\text{-}H}$=7.60, H^2), 7.37 – 7.36 (d, 2H, $J_{H\text{-}H}$=7.66, H^3), 6.95 – 6.94 (d, 2H, $J_{H\text{-}H}$=7.54, H^1), 3.88 – 3.85 (d, 2H, $J_{H\text{-}H}$=14.79, H^7), 3.75 – 3.72 (d, 2H, $J_{H\text{-}H}$=14.69, H^2), 2.64 – 2.61 (m, 2H, H^9), 2.48 (s, 6H, H^5), 2.26 (s, 6H, H^8), 1.97 – 1.95 (m, 2H, H^{10}), 1.74 – 1.72 (m, 2H, H^{10}), 1.26 – 1.25 (m, 2H, H^{11}), 1.14 – 1.11 (m, 2H, H^{11}); ^{13}C NMR (150MHz, $CDCl_3$) δ 157.10, 136.52, 121.05, 119.67, 67.01, 64.55, 60.25, 36.61, 25.76, 25.53, 24.36. FT-IR ν (cm^{-1}) 2926, 2854, 1591, 1577, 1452, 1053, 876, 779, 651.

(*R,R*)-N,N′-dimethyl-N,N′-bis(6-bromo-2-pyridyl-2-methyl)-1,2-cyclohexanediamine (*R,R*)-L4.3

(*R,R*)-L4.3 was synthesised following the same procedure as for **(*R,R*)-L4.1**, employing **(*R,R*)-L3.8** (0.101 mmol). Yellow oil (45.0 mg, 92.39% yield).

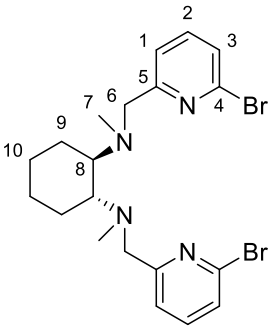

^{1}H NMR (600MHz, $CDCl_3$) δ 7.52 – 7.50 (d, 2H, $J_{H\text{-}H}$=7.52, H^2), 7.46 – 7.43 (t, 2H, $J_{H\text{-}H}$=7.57, H^3), 7.30 – 7.29 (d, 2H, $J_{H\text{-}H}$=7.75, H^1), 3.91 – 3.89 (d, 2H, $J_{H\text{-}H}$=15.10, H^6), 3.79 – 3.76 (d, 2H, $J_{H\text{-}H}$=15.04, H^6), 2.67 – 2.65 (m, 2H, H^8), 2.30 (s, 6H, H^7), 1.99 – 1.96 (m, 2H, H^9), 1.76 – 1.75 (m, 2H, H^9), 1.28 – 1.26 (m, 2H, H^{10}), 1.17 – 1.13 (m, 2H, H^{10}); ^{13}C NMR (150MHz, $CDCl_3$) δ 141.01, 138.77, 126.01, 121.63, 64.68, 59.19, 37.00, 30.91, 25.59, 25.52. FT-IR ν (cm^{-1}) 2927, 2853, 1580, 1553, 1427, 1402, 1151, 1115, 1053, 984, 849, 782, 735, 686, 639.

(*R,R*)-N,N′-dimethyl-N,N′-bis(1-methyl-2-imidazole-2-methyl)-1,2-cyclohexanediamine (*R,R*)-L4.4

(*R,R*)-L4.4 was synthesised following the same procedure as for **(*R,R*)-L4.1**, employing **(*R,R*)-L3.9** (0.377 mmol). Yellow oil (90.0 mg, 72.24% yield).

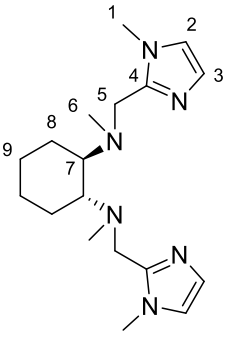

^{1}H NMR (600MHz, $CDCl_3$) δ 6.86 – 6.85 (d, 2H, $J_{H\text{-}H}$=1.16, H^3), 6.77 – 6.76 (d, 2H, $J_{H\text{-}H}$=4.05, H^2), 3.72 – 3.69 (d, 2H, $J_{H\text{-}H}$=18.08, H^5),3.65 (s, 6H, H^6), 3.53 – 3.50 (d, 2H, $J_{H\text{-}H}$=17.61, H^5), 2.57 – 2.56 (m, 2H, H^7), 2.02 (s, 6H, H^6), 1.91 – 1.89 (m, 2H, H^8), 1.72 – 1.71 (m, 2H, H^8), 1.19 – 1.12 (m, 4H, H^9); ^{13}C NMR (150MHz, $CDCl_3$) δ 146.13, 126.79, 121.33, 61.96, 50.65, 35.38, 32.71, 25.53, 24.42. FT-IR ν (cm^{-1}) 2930, 2857, 1500, 1450, 1264, 1116, 1031, 731, 665, 446.

[Fe(CF_3SO_3)$_2$-(*R,R*)-N,N′-dimethyl-N,N′-bis(pyridyl-2-methyl)-1,2-cyclohexanediamine] (*R,R*)-C4.1

Under an Argon atmosphere, $Fe(OTf)_2$ (198 mg, 0.542 mmol) was dissolved in dry DCM (2 mL) and a solution of **(*R,R*)-L4.1** in 2 mL dry DCM was added dropwise. The reaction mixture was stirred for 1 hour at room temperature. After one hour, ~15 mL of dry diethyl ether (Et_2O) was added. Upon addition of Et_2O, a precipitate formed. The reaction mixture was stirred for 15 minutes and then washed twice with 10 mL Et_2O. The precipitate was dried under vacuum to yield the product. Light yellow powder (234.9 mg, 65.23% yield).

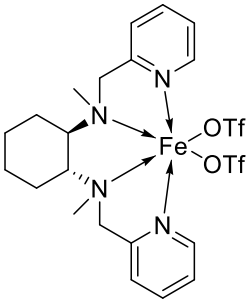

MS (MALDI) *m/z* (%): $[M–OTf]^+$: calcd 529.38, found 529.20 Elemental Analysis $C_{22}H_{28}N_4FeF_6O_6S_2$ (MW = 678.44 g/mol) Calc. (%) C 38.95, H 4.16, N 8.26, S 9.45; Found (%) C 38.99, H 7.07, N 7.89, S 9.10.

[Fe(CF_3SO_3)$_2$-(*R,R*)-N,N′-dimethyl-N,N′-bis(6-methyl-2-pyridyl-2-methyl)-1,2-cyclohexanediamine] (*R,R*)-C4.2

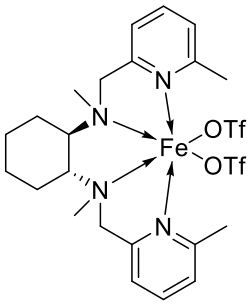

(*R,R*)-C4.2 was synthesised following the same procedure as for **(*R,R*)-C4.1**, employing **(*R,R*)-L4.2** (86.0 mg, 0.244 mmol) as ligand. Yellow powder (83.6 mg, 48.50% yield).

MS (MALDI) *m/z* (%): $[M–OTf]^+$: calcd 557.43, found 557.16 Elemental Analysis $C_{24}H_{32}N_4FeF_6O_6S_2$ (MW = 706.50 g/mol) Calc. (%) C 40.80, H 4.57, N 7.93, S 9.05; Found (%) C 40.67, H 4.22, N 8.72, S 9.00.

[Fe(CF_3SO_3)$_2$-(*R,R*)-N,N′-dimethyl-N,N′-bis(6-bromo-2-pyridyl-2-methyl)-1,2-cyclohexanediamine] (*R,R*)-C4.3

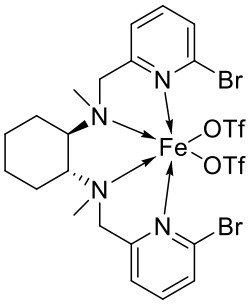

(*R,R*)-C4.3 was synthesised following the same procedure as for **(*R,R*)-C4.1**, employing **(*R,R*)-L4.3** (139.0 mg, 0.288 mmol) as ligand. Brown/orange powder (168.9 mg, 70.13% yield).

MS (MALDI) *m/z* (%): $[M–OTf]^+$: calcd 687.17, found 686.95 Elemental Analysis $C_{22}H_{26}Br_2N_4FeF_6O_6S_2$ (MW = 836.24 g/mol) Calc. (%) C 31.60, H 3.13, N 6.70, S 7.67; Found (%) C 31.30, H 3.00, N 6.55, S 7.43.

[Fe(CF_3SO_3)$_2$-(*R,R*)-N,N′-dimethyl-N,N′-bis(1-methyl-2-imidazole-2-methyl)-1,2-cyclohexanediamine] (*R,R*)-C4.4

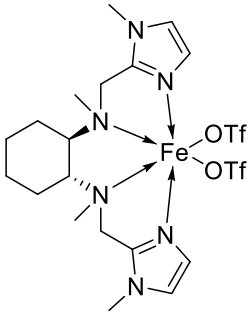

(*R,R*)-C4.4 was synthesised following the same procedure as for **(*R,R*)-C4.1**, employing **(*R,R*)-L4.4** (90.0 mg, 0.270 mmol) as ligand. Orange powder (113.4 mg, 61.36% yield).

MS (MALDI) *m/z* (%): $[M–OTf]^+$: calcd 535.39, found 535.16 Elemental Analysis $C_{20}H_{30}N_6FeF_6O_6S_2$ (MW = 684.45 g/mol) Calc. (%) C 35.10, H 4.42, N 12.28, S 9.37; Found (%) C 34.90, H 4.23, N 12.00, S 9.01.

4.5.3 Synthesis of (*S,S*) bis-heterocyclic diamine ligands and Fe(II) complexes

(*S,S*)-N,N′-bis(pyridyl-2-methylene)-1,2-cyclohexanediimine (*S,S*)-L3.1

In a round bottom flask, (*S,S*)-1,2-diaminecyclohexane (1.38 mmol) was dissolved in 5 mL Et_2O. A mixture of 2-pyridinecarboxaldehyde (2.77 mmol) in 5 mL of Et_2O was added dropwise to (*S,S*)-1,2-diaminecyclohexane. The reaction mixture was stirred for 24 hours at room temperature. The product precipitated, was filtered and washed with cold Et_2O. The filtrate was placed in the freezer, which resulted in the formation of white crystals. (294.0 mg, 72.87% yield).

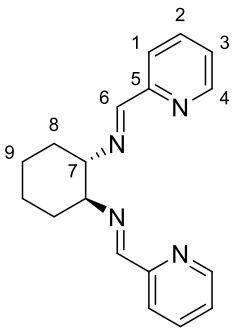

^{1}H NMR (600MHz, $CDCl_3$) δ 8.51 – 8.50 (d, 2H, J_{H-H}=4.59, H^4), 8.27 (s, 2H, H^6, CH=N), 7.85 – 7.84 (d, 2H, J_{H-H}=7.85, H^1), 7.62 – 7.59 (t, 2H, J_{H-H}=7.70, H^3), 7.19 – 7.17 (t, 2H, J_{H-H}=4.90, H^2), 3.52 – 3.49 (m, 2H, H^7), 1.84 – 1.79 (m, 6H, H^8, H^9), 1.49 – 1.46 (m, 2H, H^9); ^{13}C NMR (150MHz, $CDCl_3$) δ 161.49 (C^6), 154.64 (C^4), 149.28 (C^3), 136.49 (C^1), 124.52 (C^5), 121.38 (C^2), 73.60 (C^7), 32.76 (C^8), 24.39 (C^9). FT-IR ν (cm^{-1}) 2927, 2862, 1643, 1586, 1567, 1365, 1137, 992, 868, 744, 618, 512, 407.

(*S,S*)-N,N′-bis(6-methyl-2-pyridyl-2-methylene)-1,2-cyclohexanediimine (*S,S*)-L3.2

(*S,S*)-L3.2 was synthesised following the same procedure as for **(*S,S*)-L3.1**, employing 6-methyl-2-pyridinecarboxaldehyde (2.49 mmol). The product did not precipitate and was extracted with DCM. The solvent was removed to afford the product. Yellow oil (261.0 mg, 65.4% yield).

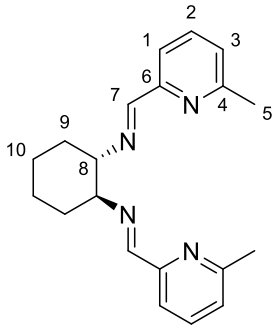

^{1}H NMR (600MHz, $CDCl_3$) δ 8.26 (s, 2H, H^7, CH=N), 7.68 – 7.67 (d, 2H, J_{H-H}=7.80, H^3), 7.50 – 7.47 (t, 2H, J_{H-H}=7.69, H^2), 7.05 – 7.04 (d, 2H, J_{H-H}=7.61, H^1), 3.48 – 3.46 (m, 2H, H^8), 2.48 (s, 6H, H^5), 1.83 – 1.74 (m, 6H, H^9, H^{10}), 1.47 – 1.44 (m, 2H, H^{10}); ^{13}C NMR (150MHz, $CDCl_3$) δ 161.66 (C^7), 157.72 (C^2), 154.15 (C^3), 136.58 (C^1), 124.04 (C^6), 118.23 (C^4), 73.56 (C^5), 32.67 (C^8), 24.33 (C^9), 24.23 (C^{10}). FT-IR ν (cm^{-1}) 2927, 2857, 1646, 1590, 1572, 1455, 1374, 1251, 1136, 1084, 987, 935, 861, 791, 735, 652, 447.

(*S,S*)-N,N′-bis(6-bromo-2-pyridyl-2-methylene)-1,2-cyclohexanediimine (*S,S*)-L3.3

(*S,S*)-L3.3 was synthesised following the same procedure as for **(*S,S*)-L3.1**, employing 6-bromo-2-pyridinecarboxaldehyde (1.61 mmol). White solid (173.0 mg, 47.74% yield).

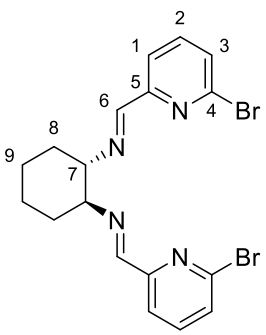

^{1}H NMR (600MHz, $CDCl_3$) δ 8.19 (s, 2H, H^6, CH=N), 7.87 – 7.86 (d, 2H, J_{H-H}=7.68, H^3), 7.51 – 7.49 (t, 2H, J_{H-H}=7.80, H^2), 7.41 – 7.40 (d, 2H, J_{H-H}=7.91, H^1), 3.47 – 3.43 (m, 2H, H^7), 1.85 – 1.70 (m, 6H, H^8, H^9), 1.47 – 1.45 (m, 2H, H^9); ^{13}C NMR (150MHz, $CDCl_3$) δ 160.15 (C^6), 155.83 (C^2), 141.35 (C^3), 138.90 (C^1), 129.03 (C^4), 119.83 (C^5), 73.57 (C^7), 32.59 (C^8), 24.29 (C^9). FT-IR ν (cm^{-1}) 2929, 2855, 1649, 1576, 1546, 1439, 1158, 1119, 1032, 983, 936, 860, 791, 730, 706, 642, 476, 446.

(*S,S*)-N,N′-bis(1-methyl-2-imidazole-2-methylene)-1,2-cyclohexanediimine (*S,S*)-L3.4

(*S,S*)-L3.4 was synthesised following the same procedure as for **(*S,S*)-L3.1**, employing 1-methyl-2-imidazolecarboxaldehyde (2.76 mmol). The product did not precipitate and was extracted with DCM. The solvent was removed to afford the product. Yellow oil (287.0 mg, 69.78% yield).

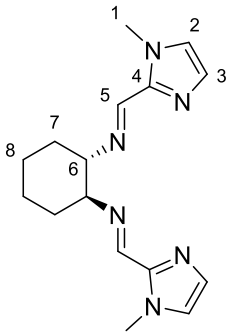

^{1}H NMR (600MHz, $CDCl_3$) δ 8.19 (s, 2H, H^5, CH=N), 7.00 (s, 2H, H^3), 6.83 (s, 2H, H^2), 3.85 (s, 6H, H^1), 3.25 – 3.24 (m, 2H, H^6) 1.83 – 1.67 (m, 6H, H^7, H^8), 1.46 – 1.42 (m, 2H, H^8); ^{13}C NMR (150MHz, $CDCl_3$) δ 152.11 (C^5), 143.11 (C^4), 128.82 (C^3), 124.68 (C^2), 74.74 (C^1), 35.45 (C^6), 32.85 (C^7), 24.27 (C^8). FT-IR ν (cm^{-1}) 2928, 2858, 1646, 1475, 1437, 1369, 1284, 935, 862, 812, 752, 706.

(*S,S*)-N,N′-bis(pyridyl-2-methyl)-1,2-cyclohexanediamine (*S,S*)-L3.6

(*S,S*)-L3.1 (0.484 mmol) was dissolved in 3 mL methanol (MeOH) at 0°C and $NaBH_4$ (1.94 mmol) was added portion wise. The mixture was stirred for 1 hour at room temperature and refluxed for 1 hour. The reaction mixture was cooled to room temperature and extracted with 3 × 10 mL DCM. The organic phase washed with 2 × 10 mL dH_2O and 10 mL saturated NaCl mixture and dried with anhydrous $MgSO_4$. The solvent was removed to afford the product. Yellow oil (139.9 mg, 97.47% yield).

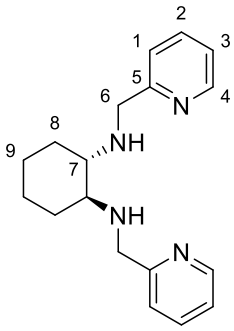

^{1}H NMR (600MHz, $CDCl_3$) δ 8.49 – 8.48 (d, 2H, $J_{H\text{-}H}$=4.84, H^4), 7.61 – 7.58 (t, 2H, $J_{H\text{-}H}$=7.66, H^3), 7.35 – 7.36 (d, 2H, $J_{H\text{-}H}$=7.73, H^1), 7.12 – 7.10 (t, 2H, $J_{H\text{-}H}$=6.28, H^2), 4.02 – 4.00 (d, 2H, $J_{H\text{-}H}$=14.14, H^6), 3.83 – 3.81 (d, 2H, $J_{H\text{-}H}$=14.11, H^6), 2.32 – 2.30 (m, 2H, H^7), 2.12 – 2.10 (m, 2H, H^8), 1.70 – 1.68 (m, 2H, H^8), 1.21 – 1.18 (m, 2H, H^9), 1.09 – 1.06 (m, 2H, H^9); ^{13}C NMR (150MHz, $CDCl_3$) δ 160.20 (C^4), 149.00 (C^3), 136.45 (C^1), 122.37 (C^5), 121.82 (C^2), 61.23 (C^6), 52.25 (C^7), 31.40 (C^8), 24.91 (C^9). FT-IR ν (cm^{-1}) 2926, 2853, 1592, 1569, 1432, 1118, 996, 755.

(*S,S*)-N,N′-bis(6-methyl-2-pyridyl-2-methyl)-1,2-cyclohexanediamine (*S,S*)-L3.7

(*S,S*)-L3.7 was synthesised following the same procedure as for **(*S,S*)-L3.6**, employing **(*S,S*)-L3.2** (0.696 mmol). Yellow oil (221.3 mg, 98.01% yield).

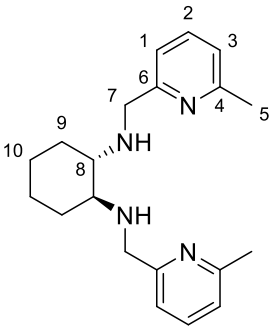

^{1}H NMR (600MHz, $CDCl_3$) δ 7.49 – 7.47 (t, 2H, $J_{H\text{-}H}$=7.60, H^2), 7.18 – 7.17 (d, 2H, $J_{H\text{-}H}$=7.66, H^3), 6.97 – 6.96 (d, 2H, $J_{H\text{-}H}$=7.58, H^1), 4.00 – 3.97 (d, 2H, $J_{H\text{-}H}$=14.11, H^7), 3.78 – 3.76 (d, 2H, $J_{H\text{-}H}$=14.07, H^7), 2.53 – 2.49 (m, 2H, H^8), 2.48 (s, 6H, H^5), 2.32 – 2.31 (m, 2H, H^9), 2.14 – 2.11 (m, 2H, H^9), 1.70 – 1.68 (m, 2H, H^{10}), 1.21 – 1.18 (m, 2H, H^{10}); ^{13}C NMR (150MHz, $CDCl_3$) δ 159.51 (C^2), 157.61 (C^3), 136.66 (C^1), 121.33 (C^6), 119.18 (C^4), 61.25 (C^7), 52.24 (C^5), 31.43 (C^8), 24.92 (C^9), 24.34 (C^{10}). FT-IR ν (cm^{-1}) 2925, 2854, 1593, 1577, 1450, 1120, 779.

(*S,S*)-N,N′-bis(6-bromo-2-pyridyl-2-methyl)-1,2-cyclohexanediamine (*S,S*)-L3.8

(*S,S*)-L3.8 was synthesised following the same procedure as for **(*S,S*)-L3.6**, employing **(*S,S*)-L3.3** (0.336 mmol). White/ Light yellow solid (128.9 mg, 85.45% yield).

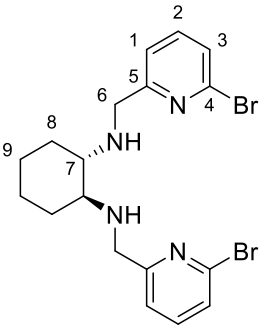

^{1}H NMR (600MHz, $CDCl_3$) δ 7.52 – 7.49 (t, 2H, $J_{H\text{-}H}$=7.67, H^2), 7.43 – 7.41 (d, 2H, $J_{H\text{-}H}$=7.50, H^3), 7.32 – 7.31 (d, 2H, $J_{H\text{-}H}$=7.81, H^1), 4.02 – 3.99 (d, 2H, $J_{H\text{-}H}$=14.77, H^6), 3.80 – 3.78 (d, 2H, $J_{H\text{-}H}$=14.72, H^6), 2.27 – 2.25 (m, 2H, H^7), 2.12 – 2.10 (m, 2H, H^8), 1.71 – 1.69 (m, 2H, H^8), 1.12 – 1.18 (m, 2H, H^9), 1.05 – 1.00 (m, 2H, H^9); ^{13}C NMR (150MHz, $CDCl_3$) δ 162.34 (C^2), 141.35 (C^3), 138.94 (C^1), 126.08 (C^4), 121.16 (C^5), 61.32 (C^6), 51.76 (C^7), 31.55 (C^8), 24.89 (C^9). FT-IR ν (cm^{-1}) 2932, 2849, 1583, 1552, 1435, 1402, 1203, 1157, 1124, 980, 857, 780, 732, 676, 555.

(*S,S*)-N,N′-bis(1-methyl-2-imidazole-2-methyl)-1,2-cyclohexanediamine (*S,S*)-L3.9

(*S,S*)-L3.9 was synthesised following the same procedure as for **(*S,S*)-L3.6**, employing **(*S,S*)-L3.4** (0.814 mmol). Yellow oil (233.0 mg, 94.60% yield).

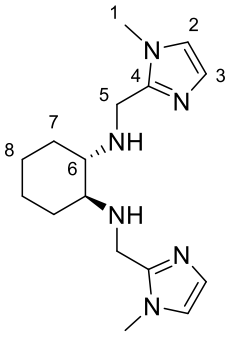

^{1}H NMR (600MHz, $CDCl_3$) δ 6.85 (s, 2H, H^3), 6.75 (s, 2H, H^2), 3.91 – 3.88 (d, 2H, $J_{H\text{-}H}$=13.52, H^5), 3.70 – 3.67 (d, 2H, $J_{H\text{-}H}$=16.52, H^5), 3.59 (s, 6H, H^1), 2.23 – 2.21 (m, 2H, H^6), 2.14 – 2.10 (m, 2H, H^7), 1.70 – 1.69 (m, 2H, H^7), 1.23 – 1.19 (m, 2H, H^8), 1.02 – 1.01 (m, 2H, H^8); ^{13}C NMR (150MHz, $CDCl_3$) δ 146.70 (C^4), 128.34 (C^3), 126.52 (C^2), 61.06 (C^1), 42.85 (C^5), 32.73 (C^6), 31.15 (C^7), 24.81 (C^8). FT-IR ν (cm^{-1}) 2927, 2854, 1498, 1449, 1282, 1108, 977, 733, 702.

(*S,S*)-N,N′-dimethyl-N,N′-bis(pyridyl-2-methyl)-1,2-cyclohexanediamine (*S,S*)-L4.1

(*S,S*)-L3.6 (0.179 mmol) was dissolved in a CH_3CN/AcOH mixture (2.75 mL CH_3CN + 0.37 mL AcOH). 32% aqueous formaldehyde was added and the mixture stirred for 20 minutes at room temperature. $NaBH_4$ was added portion wise and the mixture stirred for 72 hours at room temperature. CH_3CN was removed *in vacuo* and 2N KOH was added till pH > 10. The aqueous phase was extracted with 3 × 10 mL DCM. The organic phase was washed with 2 × 10 mL dH_2O water and 1 × 10 mL saturated NaCl mixture and dried with anhydrous $MgSO_4$. The solvent was removed to afford the product. Yellow oil (52.0 mg, 89.63% yield).

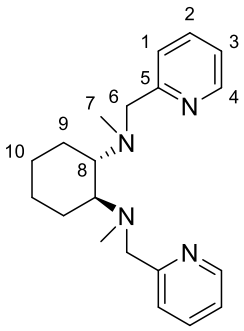

^{1}H NMR (600MHz, $CDCl_3$) δ 8.47 – 8.45 (d, 2H, $J_{H\text{-}H}$=4.88, H^4), 7.59 – 7.54 (m, 4H, H^3, H^1), 7.11 – 7.09 (t, 2H, $J_{H\text{-}H}$=6.03, H^2), 3.93 – 3.91 (d, 2H, $J_{H\text{-}H}$=14.50, H^6), 3.81 – 3.78 (d, 2H, $J_{H\text{-}H}$=14.60, H^6), 2.67 – 2.66 (m, 2H, H^8), 2.27 (s, 6H, H^7), 1.99 – 1.97 (m, 2H, H^9), 1.75 – 1.73 (m, 2H, H^9), 1.28 – 1.24 (m, 2H, H^{10}), 1.16 – 1.12 (m, 2H, H^{10}); ^{13}C NMR (150MHz, $CDCl_3$) δ 160.73, 148.53, 136.41, 123.03, 121.73, 64.37, 60.08, 36.67, 25.67, 25.64. FT-IR ν (cm^{-1}) 2927, 2853, 1589, 1568, 1432, 1144, 1046, 880, 757, 620.

(*S,S*)-N,N′-dimethyl-N,N′-bis(6-methyl-2-pyridyl-2-methyl)-1,2-cyclohexanediamine (*S,S*)-L4.2

(*S,S*)-L4.2 was synthesised following the same procedure as for **(*S,S*)-L4.1**, employing **(*S,S*)-L3.7** (0.203 mmol). Yellow oil (56.0 mg, 78.16% yield).

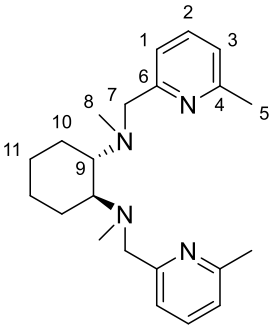

^{1}H NMR (600MHz, $CDCl_3$) δ 7.46 – 7.43 (t, 2H, $J_{H\text{-}H}$=7.61, H^2), 7.37 – 7.36 (d, 2H, $J_{H\text{-}H}$=7.67, H^3), 6.95 – 6.94 (d, 2H, $J_{H\text{-}H}$=7.47, H^2), 3.88 – 3.85 (d, 2H, $J_{H\text{-}H}$=14.83, H^7), 3.74 – 3.72 (d, 2H $J_{H\text{-}H}$=14.69, H^7), 2.63 – 2.62 (m, 2H, H^9), 2.49 (s, 6H, H^5), 2.26 (s, 6H, H^8), 1.96 – 1.94 (m, 2H, H^{10}), 1.74 – 1.72 (m, 2H, H^{10}), 1.26 – 1.22 (m, 2H, H^{11}), 1.14 – 1.11 (m, 2H, H^{11}); ^{13}C NMR (150MHz, $CDCl_3$) δ 157.07, 136.49, 128.42, 126.52, 120.99, 119.61, 64.63, 36.65, 25.79, 25.61, 24.38. FT-IR ν (cm^{-1}) 2926, 2853, 1590, 1577, 1452, 1341, 1151, 1053, 876, 779, 651.

(*S,S*)-N,N′-dimethyl-N,N′-bis(6-bromo-2-pyridyl-2-methyl)-1,2-cyclohexanediamine (*S,S*)-L4.3

(*S,S*)-L4.3 was synthesised following the same procedure as for **(*S,S*)-L4.1**, employing **(*S,S*)-L3.8** (0.084 mmol). Yellow oil (35.0 mg, 86.71% yield).

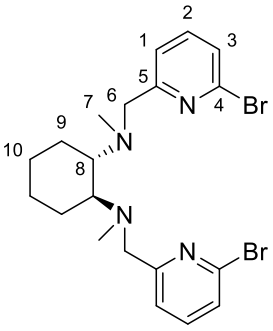

^{1}H NMR (600MHz, $CDCl_3$) δ 7.51 – 7.50 (d, 2H, $J_{H\text{-}H}$=7.43, H^3), 7.45 – 7.43 (t, 2H, $J_{H\text{-}H}$=7.71, H^2), 7.30 – 7.29 (d, 2H, $J_{H\text{-}H}$=7.69, H^1), 3.90 – 3.87 (d, 2H, $J_{H\text{-}H}$=15.20, H^6), 3.77 – 3.75 (d, 2H, $J_{H\text{-}H}$=15.14, H^6), 2.65 – 2.64 (m, 2H, H^8), 2.28 (s, 6H, H^7), 2.00 – 1.95 (m, 2H, H^9), 1.76 – 1.75 (m, 2H, H^9), 1.27 – 1.22 (m, 2H, H^{10}), 1.16 – 1.13 (m, 2H, H^{10}); ^{13}C NMR (150MHz, $CDCl_3$) δ 162.69, 140.98, 138.73, 125.91, 121.54, 64.72, 59.39, 36.91, 25.68, 25.60. FT-IR ν (cm^{-1}) 2927, 2854, 1580, 1554, 1428, 1403, 1259, 1152, 1052, 984, 849, 783, 734, 685, 448.

(*S,S*)-N,N′-dimethyl-N,N′-bis(1-methyl-2-imidazole-2-methyl)-1,2-cyclohexanediamine (*S,S*)-L4.4

(*S,S*)-L4.4 was synthesised following the same procedure as for **(*S,S*)-L4.1**, employing **(*S,S*)-L3.9** (0.198 mmol). Yellow oil (49.0 mg, 74.73% yield).

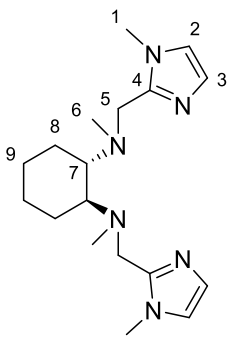

^{1}H NMR (600MHz, $CDCl_3$) δ 6.86 – 6.85 (d, 2H, $J_{H\text{-}H}$=1.19, H^3), 6.77 – 6.76 (d, 2H, $J_{H\text{-}H}$=1.12, H^2), 3.73 – 3.70 (d, 2H, $J_{H\text{-}H}$=13.39, H^5), 3.67 – 3.65 (d, 2H, $J_{H\text{-}H}$=13.39, H^5), 3.65 (s, 6H, H^1), 2.55 – 2.54 (m, 2H, H^7), 2.01 (s, 6H, H^6), 1.90 – 1.88 (m, 2H, H^8), 1.72 – 1.71 (m, 2H, H^8), 1.17 – 1.15 (m, 2H, H^9), 1.13 – 1.11 (m, 2H, H^9); ^{13}C NMR (150MHz, $CDCl_3$) δ 146.13, 126.79, 121.33, 61.95, 50.85, 35.36, 32.66, 25.57, 24.38. FT-IR ν (cm^{-1}) 2928, 2855, 1499, 1450, 1284, 1116, 1039, 732, 702, 665.

[Fe(CF_3SO_3)$_2$-(*S,S*)-N,N′-dimethyl-N,N′-bis(pyridyl-2-methyl)-1,2-cyclohexanediamine] (*S,S*)-C4.1

Under an Argon atmosphere, 2 mL dry DCM was added to $Fe(OTf)_2$ (140.0 mg, 0.431 mmol). **(*S,S*)-L4.1** (0.431 mmol), dissolved in 2 mL dry DCM, was added dropwise to the $Fe(OTf)_2$ mixture. The reaction mixture was stirred for 1 hour at room temperature. After one hour, ~15 mL of dry Et_2O was added. Upon addition of the Et_2O, a precipitate formed. The reaction mixture was stirred for 15 min and then washed twice with 10 mL Et_2O. The precipitate was dried under vacuum to yield the product. Light yellow powder (250.0 mg, 87.30% yield).

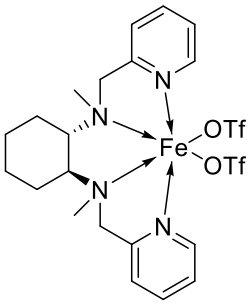

MS (MALDI) *m/z* (%): $[M–OTf]^+$: calcd 529.38, found 529.14 Elemental Analysis $C_{22}H_{28}N_4FeF_6O_6S_2$ (MW = 678.44 g/mol) Calc. (%) C 38.95, H 4.16, N 8.26, S 9.45; Found (%) C 38.77, H 3.99, N 8.20, S 9.39.

[Fe(CF_3SO_3)$_2$-(*S,S*)-N,N′-dimethyl-N,N′-bis(6-methyl-2-pyridyl-2-methyl)-1,2-cyclohexanediamine] (*S,S*)-C4.2

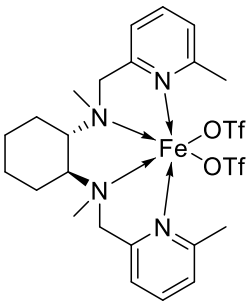

(*S,S*)-C3.2 was synthesised following the same procedure as for **(*S,S*)-C4.1**, employing **(*S,S*)-L4.2** (166.0 mg, 0.471 mmol) as ligand. Light yellow powder (152.8 mg, 45.92% yield).

MS (MALDI) *m/z* (%): $[M–OTf]^+$: calcd 557.43, found 557.16 Elemental Analysis $C_{24}H_{32}N_4FeF_6O_6S_2$ (MW = 706.50 g/mol) Calc. (%) C 40.80, H 4.57, N 7.93, S 9.05; Found (%) C 40.70, H 4.41, N 7.80, S 9.00.

[Fe(CF_3SO_3)$_2$-(*S,S*)-N,N′-dimethyl-N,N′-bis(6-bromo-2-pyridyl-2-methyl)-1,2-cyclohexanediamine] (*S,S*)-C4.3

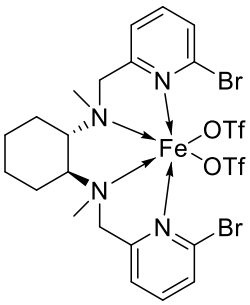

(*S,S*)-C4.3 was synthesised following the same procedure as for **(*S,S*)-C4.1**, employing **(*S,S*)-L4.3** (86.0 mg, 0.178 mmol) as ligand. Light yellow powder (104.0 mg, 69.37% yield).

MS (MALDI) *m/z* (%): $[M–OTf]^+$: calcd 687.17, found 686.56 Elemental Analysis $C_{22}H_{26}Br_2N_4FeF_6O_6S_2$ (MW = 836.24 g/mol) Calc. (%) C 31.60, H 3.13, N 6.70, S 7.67; Found (%) C 29.75, H 3.92, N 6.60, S 7.15.

[Fe(CF_3SO_3)$_2$-(*S,S*)-N,N′-dimethyl-N,N′-bis(1-methyl-2-imidazole-2-methyl)-1,2-cyclohexanediamine] (*S,S*)-C4.4

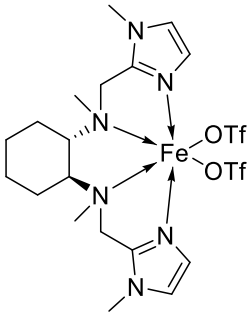

(*S,S*)-C4.4 was synthesised following the same procedure as for **(*S,S*)-C4.1**, employing **(*S,S*)-L4.4** (62.0 mg, 0.188 mmol) as ligand. Light yellow powder (47.3 mg, 36.76% yield).

MS (MALDI) *m/z* (%): $[M–OTf]^+$: calcd 535.39, found 535.16 Elemental Analysis $C_{20}H_{30}N_6FeF_6O_6S_2$ (MW = 684.45 g/mol) Calc. (%) C 35.10, H 4.42, N 12.28, S 9.37; Found (%) C 34.47, H 4.36, N 11.91, S 9.10.

Conditions for oxidation reactions

All the catalytic oxidations were conducted at room temperature. GC analysis was used to analyse the reaction products. The catalytic data shown is the average of at least two runs. Products were identified by comparison to the GC retention time of authentic samples.

Substrate-limiting conditions

The complex (25 µmol) was dissolved in 2 mL acetonitrile and the substrate (1 mmol) was added. The reaction mixture was stirred vigorously while H_2O_2 (1.8 mmol) was added with a syringe pump over a period of 25 minutes. After addition, the reaction mixture was stirred for a further 15 minutes. The reaction mixture was filtered through a syringe packed with silica, celite and a syringe filter. For GC-analysis, 0.2 mL of the filtered reaction mixture was used together with 50 µL of biphenyl (internal standard).

Oxidant-limiting conditions

The complex (2.5 µmol) was dissolved in 2 mL acetonitrile and the substrate (2500 µmol) was added. The reaction mixture was stirred vigorously while 0.36 mL of a 70mM stock solution of H_2O_2 (25 µmol) was delivered with a syringe pump over a period of 25 minutes. After addition, the reaction mixture was stirred for a further 15 minutes. The reaction mixture was filtered through a syringe packed with silica, celite and a syringe filter. For GC-analysis, 0.2 mL of the filtered reaction mixture was used together with 50 µL of biphenyl (internal standard).

Catalytic oxidation with AcOH as additive

The substrate (1 mmol) and AcOH (0.25 mmol) was added to the complex (12.5 µmol) dissolved in 2 mL acetonitrile. H_2O_2 (1.8 mmol) was added with a syringe pump over a period of 25 minutes and the reaction mixture stirred for a further 15 minutes. The reaction mixture was filtered through a syringe packed with silica, celite and a syringe filter. For GC-analysis, 0.2 mL of the filtered reaction mixture was used together with 50 µL of biphenyl (internal standard).

4.6 References

1. Tanase, S.; Reedijk, J.; Hage, R.; Rothenberg, G., *Top. Catal.*, **2010,** *53* (15-18), 1039-1044.
2. Wang, X.; Miao, C.; Wang, S.; Xia, C.; Sun, W., *ChemCatChem*, **2013,** *5* (8), 2489-2494.
3. Olivo, G.; Cussó, O.; Borrell, M.; Costas, M., *J. Biol. Inorg. Chem.*, **2017,** *22* (2-3), 425-452.
4. Prat, I.; Company, A.; Corona, T.; Parella, T.; Ribas, X.; Costas, M., *Inorg. Chem.*, **2013,** *52* (16), 9229-9244.
5. England, J.; Gondhia, R.; Bigorra-Lopez, L.; Petersen, A. R.; White, A. J.; Britovsek, G. J., *Dalton Trans.*, **2009,** (27), 5319-5334.
6. Cussó, O.; Garcia-Bosch, I.; Ribas, X.; Lloret-Fillol, J.; Costas, M., *J. Am. Chem. Soc.*, **2013,** *135* (39), 14871-14878.
7. Hong, S.; Lee, Y. M.; Cho, K. B.; Sundaravel, K.; Cho, J.; Kim, M. J.; Shin, W.; Nam, W., *J. Am. Chem. Soc.*, **2011,** *133* (31), 11876-11879.
8. Mas-Ballesté, R.; Costas, M.; van den Berg, T.; Que, L., *Chem. Eur. J.*, **2006,** *12* (28), 7489-7500.
9. Sasano, Y.; Nagasawa, S.; Yamazaki, M.; Shibuya, M.; Park, J.; Iwabuchi, Y., *Angew. Chem. Int. Ed.*, **2014,** *53* (12), 3236-3240.
10. Hosseini-Monfared, H.; Näther, C.; Winkler, H.; Janiak, C., *Inorg. Chim. Acta*, **2012,** *391*, 75-82.
11. Shi, F.; Tse, M. K.; Pohl, M. M.; Radnik, J.; Brückner, A.; Zhang, S.; Beller, M., *J. Mol. Catal. A: Chem.*, **2008,** *292* (1), 28-35.
12. Al-Hunaiti, A.; Niemi, T.; Sibaouih, A.; Pihko, P.; Leskelä, M.; Repo, T., *Chem. Commun.*, **2010,** *46* (48), 9250-9252.
13. Balogh-Hergovich, É.; Speier, G., *J. Mol. Catal. A: Chem.*, **2005,** *230* (1), 79-83.
14. Zhang, S.; Miao, C.; Xu, D.; Sun, W.; Xia, C., *Chin. J. Cat.*, **2014,** *35* (11), 1864-1870.
15. England, J.; Britovsek, G. J.; Rabadia, N.; White, A. J., *Inorg. Chem.*, **2007,** *46* (9), 3752-3767.
16. Gavrilova, A. L.; Bosnich, B., *Chem. Rev.*, **2004,** *104* (2), 349-384.
17. Oddon, F.; Girgenti, E.; Lebrun, C.; Marchi-Delapierre, C.; Pécaut, J.; Ménage, S., *Eur. J. Inorg. Chem.*, **2012,** (1), 85-96.
18. Britovsek, G. J.; England, J.; White, A. J., *Inorg. Chem.*, **2005,** *44* (22), 8125-8134.
19. Wu, M.; Miao, C. X.; Wang, S.; Hu, X.; Xia, C.; Kühn, F. E.; Sun, W., *Adv. Synth. Catal.*, **2011,** *353* (16), 3014-3022.

20. England, J.; Davies, C. R.; Banaru, M.; White, A. J.; Britovsek, G. J., *Adv. Synth. Catal.*, **2008,** *350* (6), 883-897.
21. Balland, V.; Banse, F.; Anxolabéhère-Mallart, E.; Nierlich, M.; Girerd, J. J., *Eur. J. Inorg. Chem.*, **2003,** (13), 2529-2535.
22. Mialane, P.; Nivorojkine, A.; Pratviel, G.; Azema, L.; Slany, M.; Godde, F.; Simaan, A.; Banse, F.; Kargar-Grisel, T.; Bouchoux, G., *Inorg. Chem.*, **1999,** *38* (6), 1085-1092.
23. Gütlich, P.; Garcia, Y.; Goodwin, H. A., *Chem. Soc. Rev.*, **2000,** *29* (6), 419-427.
24. Costas, M.; Tipton, A. K.; Chen, K.; Jo, D. H.; Que, L., *J. Am. Chem. Soc.*, **2001,** *123* (27), 6722-6723.
25. Costas, M.; Que Jr, L., *Angew. Chem.*, **2002,** *114* (12), 2283-2285.
26. Chen, K.; Que, L., *J. Am. Chem. Soc.*, **2001,** *123* (26), 6327-6337.
27. Zang, Y.; Kim, J.; Dong, Y.; Wilkinson, E. C.; Appelman, E. H.; Que, L., *J. Am. Chem. Soc.*, **1997,** *119* (18), 4197-4205.
28. Chen, M. S.; White, M. C., *Science*, **2007,** *318* (5851), 783-787.
29. Lyakin, O. Y.; Ottenbacher, R. V.; Bryliakov, K. P.; Talsi, E. P., *ACS Catal.*, **2012,** *2* (6), 1196-1202.
30. White, M. C.; Doyle, A. G.; Jacobsen, E. N., *J. Am. Chem. Soc.*, **2001,** *123* (29), 7194-7195.
31. Mas-Ballesté, R.; Que, L., *J. Am. Chem. Soc.*, **2007,** *129* (51), 15964-15972.
32. Tanaka, S.; Kon, Y.; Nakashima, T.; Sato, K., *RSC Adv.*, **2014,** *4* (71), 37674-37678.
33. Ligtenbarg, A. G.; Oosting, P.; Roelfes, G.; La Crois, R. M.; Lutz, M.; Spek, A. L.; Hage, R.; Feringa, B. L., *Chem. Commun.*, **2001,** (4), 385-386.
34. Marais, L.; Burés, J.; Jordaan, J. H.; Mapolie, S.; Swarts, A. J., *Org. Biomol. Chem*, **2017,** *15* (33), 6926-6933.

Chapter 5

Conclusions and recommendations for future work

5.1 Conclusions

The aim of this project was the development of a catalyst system capable of oxidising olefinic and alcohol substrates under ambient air and at room temperature. This catalyst system combined an iron(II) precursor and bis-heterocyclic diamine ligands. We sought to determine the effect of varying steric and electronic properties of the ligands and the corresponding complexes as well as the effect of the ligand topology on the catalytic activity. This would be accomplished by synthesising the (*R,R*) and (*S,S*) configurations of the complexes.

The first objective of this project was the synthesis of the ligand sets, with both secondary and tertiary diamines. The ligands have different steric and electronic properties by i) varying the *N*-heterocycle, and ii) varying the substituents on the pyridine ring.

The focus then shifted to the development of iron(II) complexes with the bis-heterocyclic diamine ligands. The ligands and corresponding complexes were fully characterised with a range of spectroscopic and analytical techniques.

The next objective was to evaluate the iron(II) complexes in the oxidation of alkenes and alcohols. Various parameters of the alkene and alcohol oxidation reactions would be optimised. These include oxidant concentration, substrate concentration and acetic acid additives. The way in which the steric and electronic effects influence the catalysis was also evaluated. In the case of alcohol oxidation, the efficiency of this catalyst system was investigated by extending the alcohol substrate scope.

A set of (*R,R*) diimine ligands was synthesised and the structure confirmed with ^{1}H and ^{13}C NMR spectroscopy as well as FT-IR spectroscopy. These diimine ligands were reduced to form the corresponding secondary diamine ligands. Characterisation was done with ^{1}H and ^{13}C NMR spectroscopy and FT-IR spectroscopy. The iron(II) complexes were synthesised employing $Fe(OTf)_2$ as metal precursor. Characterisation of the complexes by mass spectrometry, elemental analysis and UV-Vis spectroscopy confirmed the correct structure and composition of the iron(II) complexes. These complexes were applied as catalysts in the oxidation of *cis*-cyclooctene with H_2O_2 as oxidant and a reaction time of 40 min at room temperature. The catalysis data (% conversion, turnover number and oxidation efficiency) showed that all the complexes have similar catalytic activity. This data led us to believe that the complexes have low stability. The stability of the complexes were investigated by reacting the secondary diamine ligands with H_2O_2. The amine bond was oxidised to form the imine bond and confirmed with FT-IR spectroscopy. An ESI-MS experiment was conducted and samples taken at 0, 5, 15 and 25 minutes. At t = 25 minutes, the fragment visible in the ESI-MS spectrum corresponded to the oxidised complex and deactivation of the complex proceeded *via* oxidative degradation. This leads to a lower stability and lifetime of the catalysts

and therefore the secondary diamines are not a good option for the harsh oxidising environment.

Due to the secondary diamine ligands exhibiting poor stability, the ligands were methylated to form the corresponding tertiary diamine ligands. The (*R,R*) and (*S,S*) configuration of these ligand sets was synthesised. The structures were confirmed with ^{1}H and ^{13}C NMR and FT-IR. $Fe(OTf)_2$ was used as precursor to synthesise the corresponding iron(II) complexes, **(*R,R*)** and **(*S,S*)-C4.1** to **C4.4**. A variety of analytical techniques was used to determine the structure of the complexes, including mass spectrometry, elemental analysis, UV-Vis spectroscopy and magnetic susceptibility. In all cases, MS analysis displayed the $[M\text{-}OTf]^+$ ion, which is characteristic for this class of complexes. Complexes with the desired composition were synthesised as confirmed by elemental analysis, which shows a good correlation between the experimental and calculated data. Small differences in the experimentally determined composition values could be attributed to trace amounts of solvent. The UV-Vis and magnetic susceptibility measurements showed that **(*R,R*)** and **(*S,S*)-C4.1** interchange between the high- and low-spin configuration and that these complexes also have the strongest ligand field. From these measurements, it is evident that the rest of the complexes are in the high-spin configuration.

These iron(II) complexes were investigated as catalysts for alkene and alcohol oxidation. *Cis*-cyclooctene was oxidised to cyclooctene epoxide with 100% selectivity seen for all the complexes. **(*R,R*)-C4.1** showed the best activity and was able to convert 96% of *cis*-cyclooctene. A significant decrease in the catalytic activity was seen through the addition of the 6-methyl and 6-bromo substituents on the pyridine ring. The observed catalytic activity also decreased when the pyridine donor was replaced with an imidazole donor. This confirms that pyridine donors are necessary for high catalytic activity. When adding acetic acid to the system, an increase of up to 30% in the catalytic activity was seen. The influence of the ligand topology as well as the steric and electronic properties of the ligands was investigated. This indicated that the steric effect is more notable than the electronic effect. Adding substituents on the pyridine ring has a pronounced steric effect, which limits the pyridyl ring from getting too close to the metal centre. These complexes then favour the more unstable high-spin configuration. A steric effect is also visible when the pyridine donor is replaced with an imidazole donor and results in the weakening of the Fe-N(Me-Im) bond. This results in a weaker ligand field with lower catalytic activity. When comparing the catalytic activity of the (*R,R*) and (*S,S*) complexes, it is evident that there is not a big difference between the catalytic activity for the two configurations. This is a result of the complexes interchanging between the two configurations when in solution.

The oxidation of benzyl alcohol was evaluated with these complexes and they were active catalysts for oxidising benzyl alcohol to benzaldehyde. Benzyl alcohol was used as model substrate to optimise different parameters of the oxidation reaction. When increasing the catalyst loading, the catalytic activity increased due to an increase in the number of available active sites. When increasing the oxidant concentration, trace amounts of benzoic acid were observed, which is characteristic of over-oxidation and did not necessarily result in higher catalytic activity. The highest conversion of 73% was seen for **(*S,S*)-C4.1** with 25 µmol of catalyst and 1.8 mmol of H_2O_2. The substrate scope was extended to determine the functional group tolerance and limitations of the iron(II) system. This system was able to oxidise a range of alcohol substrates which, included allylic, benzylic and aliphatic alcohols. Another advantage of this system is that it is able to oxidise primary as well as secondary alcohols to the respective aldehyde and ketone products.

5.2 Recommendations for future work

5.2.1 Synthesis of ligands and iron(II) complexes

Further work can be done on the synthesis of the ligands and corresponding iron(II) complexes. This includes attempting to isolate the *cis*-α and *cis*-β topologies of the complexes. Que and co-workers found distinctly different catalytic activity for the two topologies.[1] Further investigation can be done on the structure of the iron(II) complexes by attempting to recrystallise the complexes and employ single-crystal X-ray diffraction analysis to determine the crystal structure. This will give more information about the topology as well as high- or low-spin configuration of the complexes.[2] The electronic effects of substituents can be further investigated by synthesising complexes with substituents on the *meta*- or *para*-position of the pyridine ring. Substituents on these positions may have more of an electronic than steric effect and possibly enhance the catalytic activity.[3, 4]

5.2.2 Alkene and alkane oxidation

Different parameters of the oxidation reaction can still be optimised. These include the rate of addition of H_2O_2, the temperature at which the oxidation reaction is conducted, the solvent used as well as the reaction time. Studies have shown that performing the reactions at 0°C or at -30°C can result in yields of 99 to 100% while the catalyst loading can be decreased to 0.1 mol%. There is also a difference in the yield when comparing all-at-once addition of H_2O_2 and addition with a syringe pump.[5, 6] The mechanism of the alkene oxidation reaction can be investigated by mass spectrometry and UV-Vis spectroscopy to determine the different active species formed. There have been studies that have isolated the reactive intermediates and characterised these species with UV-Vis and ESI-MS.[7, 8, 9]

The efficiency and limitations of this specific iron(II) oxidation system can be further investigated by extending the alkene substrate scope to include benzylic as well as aromatic and aliphatic alkenes.[6, 10, 11] This iron(II) system can also be evaluated in the oxidation of alkanes, which are more difficult to oxidise than alkenes and alcohols. There are various studies that show that iron(II) complexes with polydentate pyridine-based ligands and H_2O_2 are capable of oxidising alkanes.[12, 13, 14]

5.2.3 Alcohol oxidation

The use of non-heme iron(II) complexes in combination with H_2O_2 for the oxidation of alcohols has not been extensively investigated. For the alcohol oxidation reaction, there are still a few aspects that can be investigated. The product yields obtained for the alcohol oxidation substrate scope could be improved by increasing the reaction time.[15] Different parameters of the oxidation reaction can be optimised, such as temperature, rate of H_2O_2 addition and solvent. The reaction mechanism of alcohol oxidation can also be investigated by various spectroscopic techniques in an attempt to determine the reactive species that are involved in this reaction. This is of particular importance since the key step differs for alkene/alkane and alcohol oxidation, respectively. In the case of the former, the key step is oxygen atom transfer, whereas alcohol oxidation is envisaged to proceed via hydrogen atom abstraction. Key high-valent iron intermediates have been identified for hydrocarbon oxidation. An important contribution would be to establish whether these intermediates are formed during alcohol oxidation.

5.3 References

1. Costas, M.; Que Jr, L., *Angew. Chem.*, **2002,** *114* (12), 2283-2285.
2. England, J.; Davies, C. R.; Banaru, M.; White, A. J.; Britovsek, G. J., *Adv. Synth. Catal.*, **2008,** *350* (6), 883-897.
3. Cussó, O.; Garcia-Bosch, I.; Ribas, X.; Lloret-Fillol, J.; Costas, M., *J. Am. Chem. Soc.*, **2013,** *135* (39), 14871-14878.
4. Olivo, G.; Lanzalunga, O.; Mandolini, L.; Di Stefano, S., *J. Org. Chem.*, **2013,** *78* (22), 11508-11512.
5. Mas-Ballesté, R.; Que, L., *J. Am. Chem. Soc.*, **2007,** *129* (51), 15964-15972.
6. Lyakin, O. Y.; Ottenbacher, R. V.; Bryliakov, K. P.; Talsi, E. P., *ACS Catal.*, **2012,** *2* (6), 1196-1202.
7. Chen, K.; Que, L., *J. Am. Chem. Soc.*, **2001,** *123* (26), 6327-6337.
8. Zang, Y.; Kim, J.; Dong, Y.; Wilkinson, E. C.; Appelman, E. H.; Que, L., *J. Am. Chem. Soc.*, **1997,** *119* (18), 4197-4205.
9. Roelfes, G.; Lubben, M.; Hage, R.; Que Jr, L.; Feringa, B. L., *Chem. Eur. J.*, **2000,** *6* (12), 2152-2159.
10. Costas, M.; Tipton, A. K.; Chen, K.; Jo, D. H.; Que, L., *J. Am. Chem. Soc.*, **2001,** *123* (27), 6722-6723.
11. White, M. C.; Doyle, A. G.; Jacobsen, E. N., *J. Am. Chem. Soc.*, **2001,** *123* (29), 7194-7195.
12. Tanase, S.; Reedijk, J.; Hage, R.; Rothenberg, G., *Top. Catal.*, **2010,** *53* (15-18), 1039-1044.
13. He, Y.; Gorden, J. D.; Goldsmith, C. R., *Inorg. Chem.*, **2011,** *50* (24), 12651-12660.
14. Olivo, G.; Cussó, O.; Borrell, M.; Costas, M., *J. Biol. Inorg. Chem.*, **2017,** *22* (2-3), 425-452.
15. Zhang, S.; Miao, C.; Xu, D.; Sun, W.; Xia, C., *Chin. J. Cat.*, **2014,** *35* (11), 1864-1870.